Engineering Nanomaterials to Overcome

Barriers in Cancer Therapy

Christine Erline Wang

A dissertation
submitted in partial fulfillment of the
requirements for the degree of

Doctor of Philosophy

University of Washington

2016

Reading Committee:
Suzie H. Pun, Chair
Anthony J. Convertine
André Lieber

Program Authorized to Offer Degree:
Bioengineering

University of Washington

Abstract

Engineering Nanomaterials to Overcome Barriers in Cancer Therapy

Christine Erline Wang

Chair of the Supervisory Committee:
Professor Suzie H. Pun
Bioengineering

Cytotoxic chemotherapy is used for the frontline treatment of most types of cancer but is associated with significant toxicity due to the lack of cell specificity of these drugs. Newer treatment strategies, such as polymeric drug delivery vehicles that preferentially accumulate in tumors via the EPR effect and oncolytic adenoviruses that replicate conditionally in tumor cells, can reduce the adverse side effects associated with systemic anti-cancer treatments. However, there remain numerous barriers to the successful clinical translation of these therapeutics. Part I focuses on the diffusional barriers to drug delivery to solid tumors. In Chapter 1, we investigate tight junction-opening proteins as a means to enhance nanoparticle penetration into tumors. Part II describes the development of polymer nanostructures for anti-cancer drug delivery. Chapter 2 summarizes the major design parameters for drug delivery to tumors and introduces controlled living polymerization as a synthetic tool. Chapters 3 and 4 describe the synthesis of polymeric drug carriers with a novel sunflower-like architecture. Part III focuses on methods to improve the safety of adenoviruses for cancer gene therapy. Chapter 5 provides an overview of adenovirus pharmacology and current modification strategies, while Chapter 6 describes a new approach to developing materials that can shield adenoviruses against immune recognition. Finally, Chapter 7 summarizes the major findings of this work and concludes with recommendations for future directions.

TABLE OF CONTENTS

iii

iv

Part IV. Future perspectives

LIST OF FIGURES

LIST OF TABLES

ACKNOWLEDGEMENTS

This thesis would not have been possible without the contributions and support of many people over the years. Words cannot express how grateful I am to my family, friends, mentors, coworkers, and collaborators who have helped me during this journey.

First and foremost, I would like to thank my advisor, Suzie Pun, for the opportunity to work in her lab and for her guidance and scientific insight over the seven years I have known her. She has always served as a positive role model, challenging me to do more than I knew I could and providing encouragement in the face of numerous setbacks. I feel incredibly fortunate to have found a mentor who cares so deeply about my personal well being in addition to my professional development.

I would also like to thank the members of my supervisory committee, André Lieber, Tony Convertine, Pat Stayton, and Christine Luscombe, who have given generously of their intellect, time, and lab resources. Your scientific input has been invaluable in the completion of this work.

I would like to acknowledge many of my labmates, past and present, for their scientific and non-scientific contributions:

- Hua Wei, who taught me about the practical aspects of polymer chemistry. When I began working with Hua on sunflower polymers, I never would have guessed what a big part they would play in my graduate work, and this thesis would not have been possible without him.
- Kat Wang, who mentored me as a rotation student, for always being supportive and down-to-earth.
- Julie Shi and honorary lab member Sergio Haro, who have been my best friends and surrogate big siblings for the past five years. I will always remember the food adventures, bike rides around Greenlake, late night talks at the kitchen table about lab and life, and eye-opening lessons in parenthood (which will eventually come in handy).
- Dave Chu, my officemate and first friend in grad school, for always being so generous with his time and expertise in the lab, and for the countless pep talks and chicken and wine Tuesdays outside of the lab.

x

- Leslie Chan and Maryelise Cieslewicz, for being great friends, and for continually impressing me with their hard work and baking skills.

- Kevin Tan, my cohort-mate, for commiserating with me through grad school, and for providing fashion advice and endless entertainment in the form of random Facebook videos, pop culture trivia, and deep interrogations of fellow labmates.

- Chayanon Ngambenjawong, whose work ethic and creativity in the lab are inspiring, and who provided comic relief at the most unexpected moments.

- Bob Lamm, for being an extremely caring friend and lab citizen, and for encouraging me to be social while also recognizing when I wanted to introvert.

- Gary Liu, for his positive attitude and for putting up with my incessant teasing.

- Joan Go Schellinger, Drew Sellers, and Heather Gustafson, for their mentorship and guidance in the lab.

I would also like to acknowledge my friends Austin Day, Tom Long, and Joe Phan, for providing an outlet from lab with karaoke nights, board games, and hiking.

I would especially like to thank my family – my older sister, Melissa, for being the "guinea pig" child and paving the way for me in everything I've done, including the Ph.D. My parents, James and Huei-Ching, have always emphasized the importance of education and hard work. This work is truly the culmination of the love and support they have always shown me.

Finally, I would like to thank my husband, Jonathan Lin, for his unwavering love, encouragement, and proofreading. I am continually amazed by his intense curiosity and commitment to doing good science, and these have made me a better scientist in turn. I could not ask for a better collaborator in life.

DEDICATION

To my husband, Jonathan,

my parents, James and Huei-Ching,

and my sister, Melissa.

Part I.

Overcoming Physical Barriers to
Drug Delivery in Solid Tumors

1

<p style="text-align:center">Chapter 1.</p>

INVESTIGATING THE SIZE LIMITATIONS OF JO PROTEIN-MEDIATED NANOPARTICLE DELIVERY

Christine E. Wang, Roma Yumul, Jonathan Lin, André Lieber, and Suzie H. Pun

Abstract

JO is a recombinant protein that transiently opens intercellular junctions in epithelial tumors by cleaving the junction protein DSG2. Co-administration of JO has been shown to significantly increase the efficacy of various monoclonal antibodies and chemotherapy drugs in murine tumor models by allowing for increased intratumoral penetration of the drugs. To investigate the size-dependent effect of JO on nanocarriers, we used PEGylated gold nanoparticles (AuNPs) of two different sizes as model drugs and investigated their biodistribution following JO protein treatment. JO was found to significantly increase tumor accumulation of AuNPs in a manner dependent on particle size and tumor volume. Preliminary analysis of intratumoral nanoparticle distribution also indicates that AuNPs can be observed at increased distances from tumor blood vessels following JO treatment.

1.1   Introduction

Nanoparticle-based drug carriers are attractive because of their ability to exploit the enhanced permeability and retention (EPR) effect for selective accumulation in tumors.[1] However, the ability of these carriers to penetrate into solid tumors is another important consideration, especially because many small molecule anticancer drugs are diffusion-limited, and the incomplete distribution of drugs in the tumor tissue can lead to chemotherapy resistance.[2,3] In particular, epithelial tumors are characterized by the presence of intercellular junctions which restrict the penetration of molecules.[4,5] One such epithelial junction protein is desmoglein-2 (DSG2), which has been found to be upregulated in a number of malignant cell types including gastric cancer,[6] ovarian cancer,[7] and breast cancer.[8]

<p style="text-align:center">3</p>

Recently, DSG2 was identified as the receptor used by several human adenoviruses (Ad), including Ad serotype 3, for cellular infection.[7] In subsequent studies, a recombinant protein derived from the Ad3 fiber knob was produced.[9] This protein, named junction opener-1 (JO-1), was found to trigger the transient opening of intercellular junctions through binding and cleavage of the DSG2 dimers between epithelial cells.[9,10] This effect was observed in mice with epithelial tumors within one hour of intravenous injection of JO-1.[10] Co-administration of JO-1 has been shown to facilitate intratumoral penetration and therapeutic efficacy of monoclonal antibodies (mAbs) such as the anti-Her2/neu mAb trastuzumab (Herceptin) and the EGFR inhibitor cetuximab (Erbitux).[10] Furthermore, JO-1 was tested in combination with several chemotherapeutic drugs including paclitaxel (Taxol), irinotecan (Camptosar), nanoparticle albumin-bound paclitaxel (Abraxane), and liposomal doxorubicin (Doxil). JO-1 co-therapy enhanced the efficacy of these drugs and overcame drug resistance in several models, while reducing the drug doses necessary for therapeutic effect.[8] JO-1 and variants of this protein (such as the affinity-enhanced version, JO-4[11]) are therefore interesting for clinical application.

To develop a better understanding of the size limitations of JO protein-mediated disruption of tight junctions, we sought to investigate the effect of JO pre-treatment on the *in vivo* biodistribution of gold nanoparticles of different sizes. Gold nanoparticles were selected as a surrogate for nano-sized drug carriers (*e.g.*, liposomes, micelles, polymer-drug conjugates, etc.) because they can be synthesized with defined sizes and over a wide size range, surface-modified through reactions with thiol groups, quantified by inductively coupled plasma mass spectrometry (ICP-MS) with excellent sensitivity, and visualized by light and electron microscopy. Herein, we synthesize polyethylene glycol (PEG)-modified gold nanoparticles and quantify their biodistribution in JO-treated and untreated mice by ICP-MS. We also demonstrate a technique to investigate the intratumoral distribution of nanoparticles using microscopy and quantitative image analysis.

1.2 Materials and methods

1.2.1 AuNP surface modification

Gold nanoparticles (AuNPs) with diameters of 5 and 100 nm were purchased from Ted Pella (Redding, CA) and Nanopartz (Loveland, CO), respectively (actual diameters: 5.5 and

4

103 nm as determined by the manufacturers). AuNPs were surface-modified by reaction with PEG$_{5000}$-thiol (Laysan Bio, Arab, AL); PEG-SH was added in excess (4 PEG molecules per nm^2 gold surface area,[12] assuming spherical particles) and allowed to react for 30 min at room temperature prior to characterization or use.

1.2.2   Particle characterization

The effective diameters of AuNPs were measured by dynamic light scattering (DLS) with a ZetaPlus analyzer (Brookhaven Instruments, Holtsville, NY) at a detection angle of 90°. Unmodified or PEGylated AuNPs with initial diameters of 5 or 100 nm were first measured in nanopure water. Particle size measurements were acquired for 6 independent samples, using 5 1-minute runs for each sample.

To confirm particle stability in the presence of physiological salt concentrations, unmodified or PEGylated AuNPs were diluted with an equal volume of 2× PBS (or nanopure water as a negative control) immediately before sizing. Size was measured again after 2 h and 24 h; measurements were completed using 3 independent samples. Similarly, particle stability in serum was assessed by diluting AuNPs with an equal volume of 2× PBS containing 20% fetal bovine serum (FBS), for a final serum concentration of 10%. Serum stability was monitored by DLS or by measuring absorbance spectra for the samples from 400-800 nm using a Tecan Safire2 plate reader (Männedorf, Switzerland).

1.2.3   Animals

Male Scid-beige (CB17) mice (8-10 weeks) were obtained from The Jackson Laboratory (strain name: NOD.CB17-*Prkdc*^{scid}298/J). All experimental procedures were performed in accordance with protocols approved by the University of Washington Institutional Animal Care and Use Committee.

1.2.4   Cell culture

A549 cells (ATCC CCL-185) were maintained in F-12K medium (Corning cellgro) supplemented with 10% fetal bovine serum (FBS, HyClone) and 1% penicillin/streptomycin

(HyClone). Cells were cultured as a monolayer in a 37°C, 5% CO_2 environment. Medium was replaced every 2-3 days. Cells were passaged at ~70-80% confluence by incubation with Trypsin-EDTA, followed by resuspension in complete growth medium.

1.2.5   Biodistribution of AuNPs

To develop xenograft tumors, mice were inoculated subcutaneously in the right flank with 5×10^6 A549 cells in 100 µL of F-12K medium without serum.

After tumor inoculation, mice were randomly distributed into groups of 5-6 mice each. Biodistribution studies were initiated when the tumors reached the specified volumes (200-300 mm³ or 500-600 mm³). Mice receiving JO-4 pretreatment were first injected with 2 mg JO-4 protein/kg mouse in PBS via tail vein injection. One hour later, mice were injected with 35 or 120 nm PEGylated AuNPs in PBS at a dose of 100 µg gold/kg mouse via tail vein injection. After 6 hours, mice were anesthesized by intraperitoneal injection with 2.5% Avertin solution (300 µL/20 g mouse). Mice were then perfused with PBS, and tumors and organs were harvested. Gold content in the tumor and liver was analyzed for all mice. Gold content in the brain, colon, heart, intestine, kidney, lung, and spleen was analyzed for a subset of 3 mice per group, selecting for mice with tumor weights closest to the average overall tumor weight (~240 mg).

Gold content in tissue samples was measured by ICP-MS at the Environmental Health Laboratory & Trace Organics Analysis Center at the University of Washington. The gold content of each sample was normalized to sample mass. Statistical significance was assessed using a Student's two-tailed t-test.

1.2.6   Light and fluorescence microscopy

For imaging studies, JO-4 and AuNP injections were completed as described above, with the tumors harvested following perfusion. Tumors were embedded in optimal cutting temperature (OCT) compound (Tissue-Tek, Sakura Finetek USA, Torrance, CA) in cryomolds, flash frozen, and cryosectioned into 8 µm-thick sections.

Tumor sections were post-fixed in 4% paraformaldehyde (PFA) in PBS for 15 min at room temperature and stained for blood vessels with rat anti-mouse CD31 antibody (clone

6

MEC 13.3, BD Pharmingen) and Alexa Fluor 488 donkey anti-rat IgG secondary antibody. After immunofluorescence staining, sections were stained for AuNPs by incubating with silver enhancement solution (Ted Pella) for 20 min at room temperature. Finally, sections were washed, coverslipped using Fluoromount-G (eBioscience), and imaged on a Nikon E800 upright microscope with a 60x objective.

1.2.7   Image analysis

A total of 9 image pairs (brightfield for AuNPs, fluorescence for CD31) were obtained of each tumor section. Images were thresholded using Fiji image processing software. MATLAB was then used to overlay the thresholded brightfield and fluorescence images, perform particle detection, and calculate the penetration distance for each AuNP, defined as the distance from the particle to the nearest CD31-stained pixel. Distance data were aggregated from all images of a tumor section and binned in MATLAB. Sample MATLAB code can be found in the Appendix of this dissertation.

1.3   Results and discussion

1.3.1   AuNP sizing and stability

AuNPs were surface modified by reaction with PEG-thiol; PEGylation of nanoparticles is commonly employed to reduce aggregation and protein adsorption, thereby increasing circulation half-life *in vivo*. Particle sizing by DLS was performed for AuNPs of 2 different diameters before and after PEGylation (Figure 1.1). The diameters of the unmodified particles were generally consistent with those reported by the manufacturers (experimental: 10.8 and 103.9 nm; reported: 5.5 and 103 nm). The discrepancy in the smaller particles likely results from inaccuracies in DLS sizing given the relatively small size and low count rate of these particles (whereas the manufacturer's specifications are determined using a combination of DLS, TEM, and UV-Vis spectroscopy). The final diameters of the PEGylated AuNPs were measured to be 33.2 ± 1.4 nm and 121.1 ± 1.2 nm, demonstrating a moderate size increase after PEG modification consistent with previous reports.[13,14] These particle sizes were selected based on the sizes of other nanocarriers that

7

have been clinically approved or are in late-stage clinical trials, such as Genexol-PM (~24 nm)[15] and similar polymeric micelles (20-40 nm)[16] at the lower size range and Doxil (80-100 nm)[17] and BIND-014 (~100 nm)[18] at the higher range.
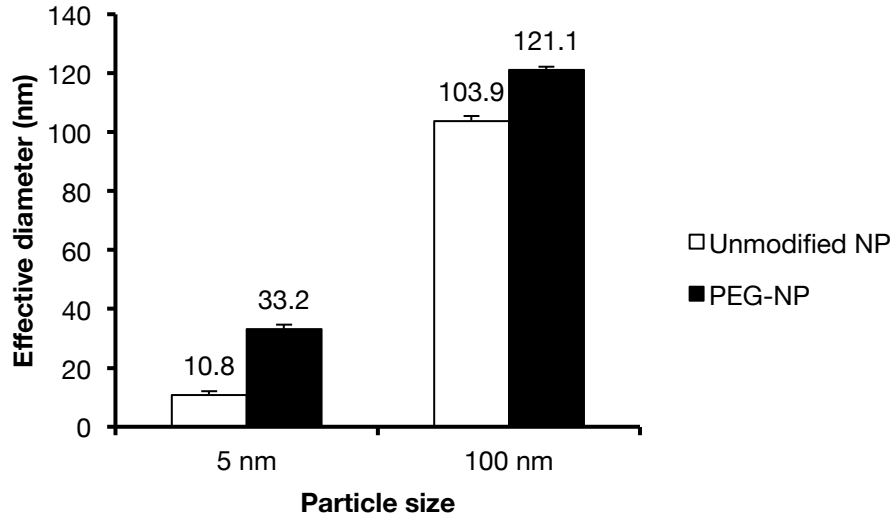
Figure 1.1 Particle sizing of unmodified and PEGylated AuNPs as determined by DLS. Data are reported as the mean ± S.D., $n = 6$.

Nanoparticles were then evaluated for stability in salt and serum. In the presence of physiological salt concentrations, unmodified AuNPs were shown to aggregate rapidly (Figure 1.2 and Figure 1.3a), whereas PEGylated AuNPs remained stable in PBS even after 24 h. Serum stability was also assessed by suspending particles in PBS containing 10% FBS. The addition of serum conferred increased stability on unmodified AuNPs; particle sizing indicated that unmodified 100 nm AuNPs did not form large aggregates over 24 h, although the slight increase in effective diameter suggests that some aggregation behavior or protein adsorption to the nanoparticles may be occurring (Figure 1.2). Meanwhile, no change in particle size was observed for PEGylated AuNPs incubated in serum.

8
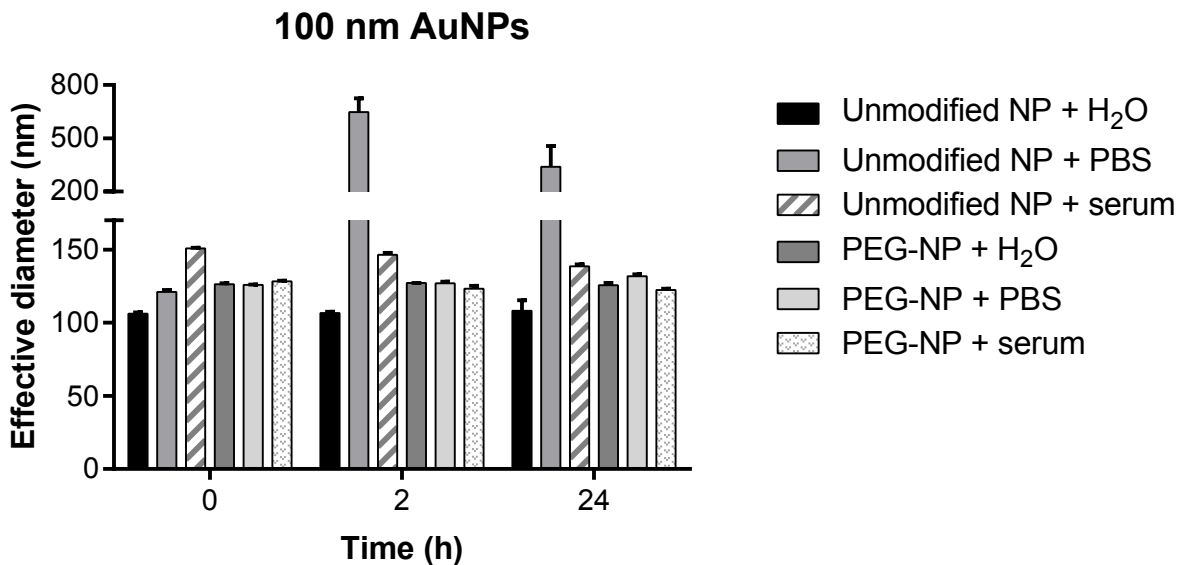
100 nm AuNPs

Figure 1.2 Stability of unmodified and PEGylated 100 nm AuNPs incubated in PBS or PBS containing 10% serum as monitored by DLS. Data are reported as the mean ± S.D., $n = 3$.

Due to the low count rate of the smaller AuNPs on DLS and the presence of protein aggregates in serum solutions, the serum stability of 5 nm AuNPs was confirmed by an alternative method. Because aggregation of AuNPs results in a red shift in their absorbance spectra, serum stability was assessed by monitoring absorbance over the range 400-800 nm.[12] Similar to the larger particle size, PEGylated 5 nm AuNPs in serum displayed stable absorbance spectra over 2 h (Figure 1.3b). Significant aggregation behavior was observed only for unmodified 5 nm AuNPs in PBS, as indicated by a noticeable shift in this spectrum toward longer wavelengths, corroborating the results obtained by DLS (Figure 1.3a). Overall, these results indicate that PEG coating yields AuNPs that are sterically stabilized in the presence of salt and serum.

9
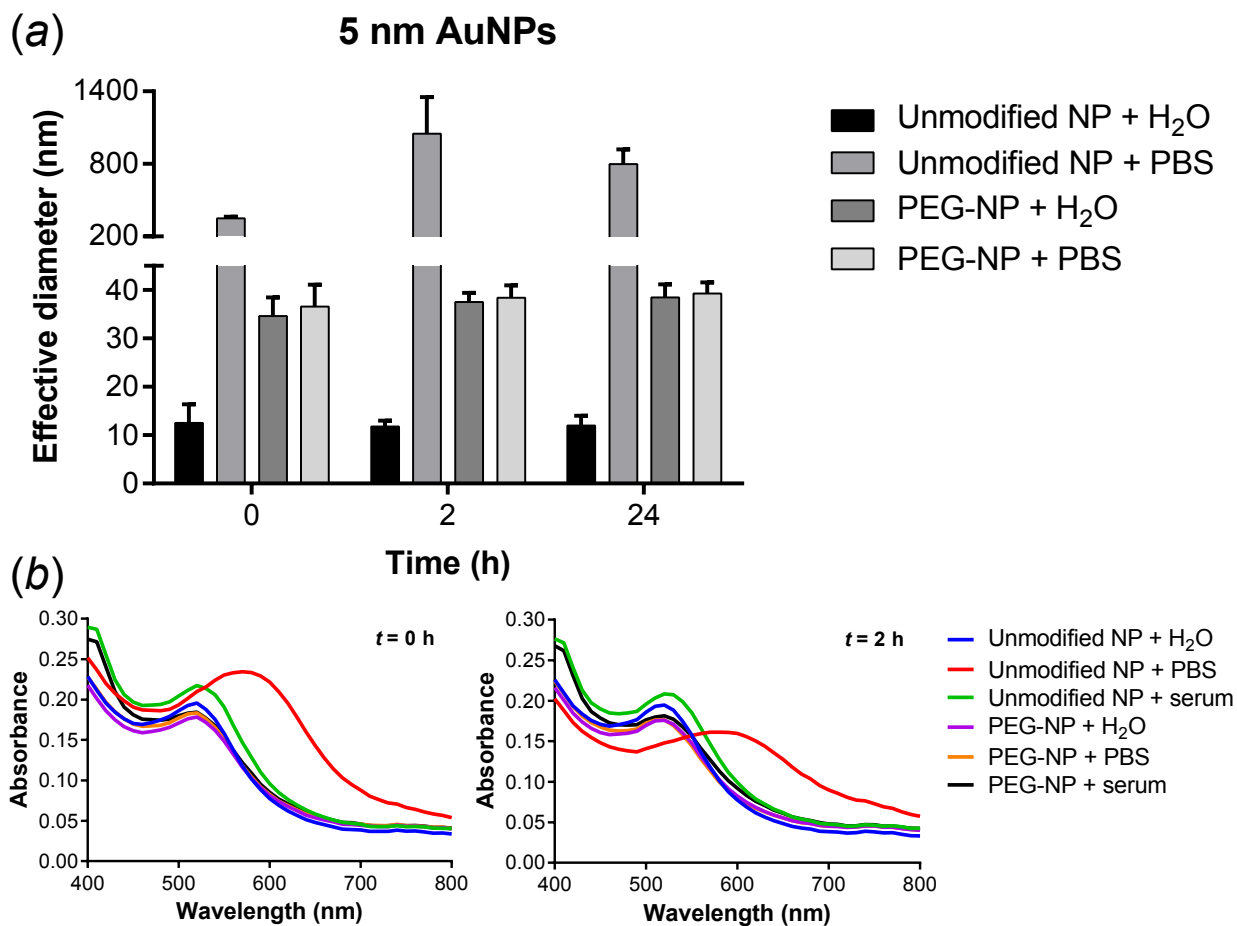
Figure 1.3 Stability of unmodified and PEGylated 5 nm AuNPs incubated in PBS or PBS containing 10% serum as monitored by (a) DLS and (b) red shift in absorbance. Data are reported as the mean ± S.D., $n = 3$.

1.3.2   *Biodistribution of AuNPs with JO-4 pretreatment*

PEGylated AuNPs are referred to by their hydrodynamic sizes after PEG modification, 35 nm and 120 nm. The A549 lung cancer model was used to assess the *in vivo* biodistribution of nanoparticles administered alone or in conjunction with JO-4 pretreatment. AuNP biodistribution was initially analyzed for the tumor and the liver (the primary site of nanoparticle clearance);[19,20] studies were conducted in mice bearing two different sizes of tumors (tumor volumes of 200-300 mm³ or 500-600 mm³) to represent changes in extracellular matrix and tight junction development with tumor progression.[21,22]
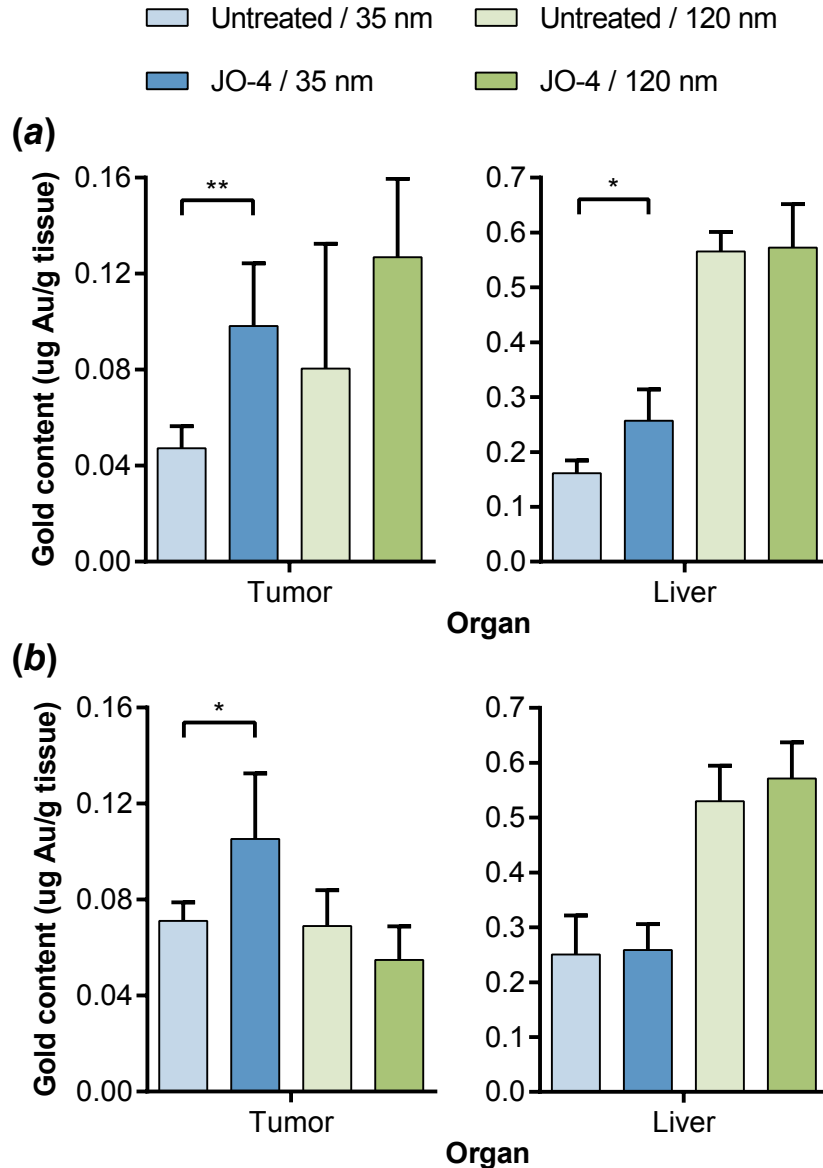
Figure 1.4 Tumor and liver accumulation of two different sizes of AuNPs 6 h post-NP injection in control or JO-4 pretreated mice bearing (a) 200-300 mm^3 or (b) 500-600 mm^3 tumors. Data are reported as the mean ± S.D., $n = 5$ or 6. *$p < 0.05$, **$p < 0.01$

Biodistribution results (as normalized to tissue weight) indicated that JO-4 pretreatment significantly increased tumor accumulation of the smaller 35 nm AuNPs (Figure 1.4). This result is unsurprising given that the A549 tumor model was previously used to demonstrate increased efficacy of cetuximab,[10] irinotecan (586.7 Da),[8] and Doxil (~90 nm)[8] with JO-1 co-therapy. Interestingly, although the increase was observed with both tumor volumes, the magnitude of the JO-mediated increase was less pronounced for

the larger 500-600 mm^3 tumors. This is in good agreement with recent work by Chan and coworkers demonstrating that AuNP accumulation increases with tumor volume due to the higher porosity and decreased rigidity of the extracellular matrix in larger tumors.[22] Meanwhile, JO-4 pretreatment did not significantly affect tumor accumulation of 120 nm AuNPs regardless of tumor size (Figure 1.4), suggesting that this particle size may be just above the threshold of junction opening for this particular tumor model. However, given the previous success of this strategy for the delivery of Doxil, differences in particle rigidity are also likely to influence JO-facilitated transport through epithelial junctions, as Doxil comprises a deformable lipid bilayer.

Surprisingly, a significant increase in liver accumulation of 35 nm AuNPs was also observed for the JO-4 pretreated group with smaller tumors (Figure 1.4a), although DSG2 is not broadly accessible in the liver (DSG2 is not found on hepatocytes but is detectable in the intrahepatic bile duct epithelium).[23] This trend was not present in the mice bearing larger tumors, which demonstrate higher liver accumulation of 35 nm AuNPs even in the absence of JO-4 (Figure 1.4b). One possible explanation is that interstitial fluid pressure (IFP) increases with tumor growth[24] and could transiently exceed the microvascular fluid pressure, leading to intravasation of nanoparticles back into the blood supply[25] and ultimately clearance by the liver.

To establish a complete picture of AuNP biodistribution, gold content in the colon, heart, intestine, kidney, lung, brain, and spleen was analyzed for a subset of mice bearing 500-600 mm^3 tumors. JO-4 pretreatment had no significant effect on AuNP accumulation in any of the organs examined (Figure 1.5), suggesting that the protein acts specifically on the DSG2-expressing tumor cells. Accumulation of 120 nm AuNPs was particularly high in the spleen, likely due to size-dependent uptake by splenic macrophages.[26]
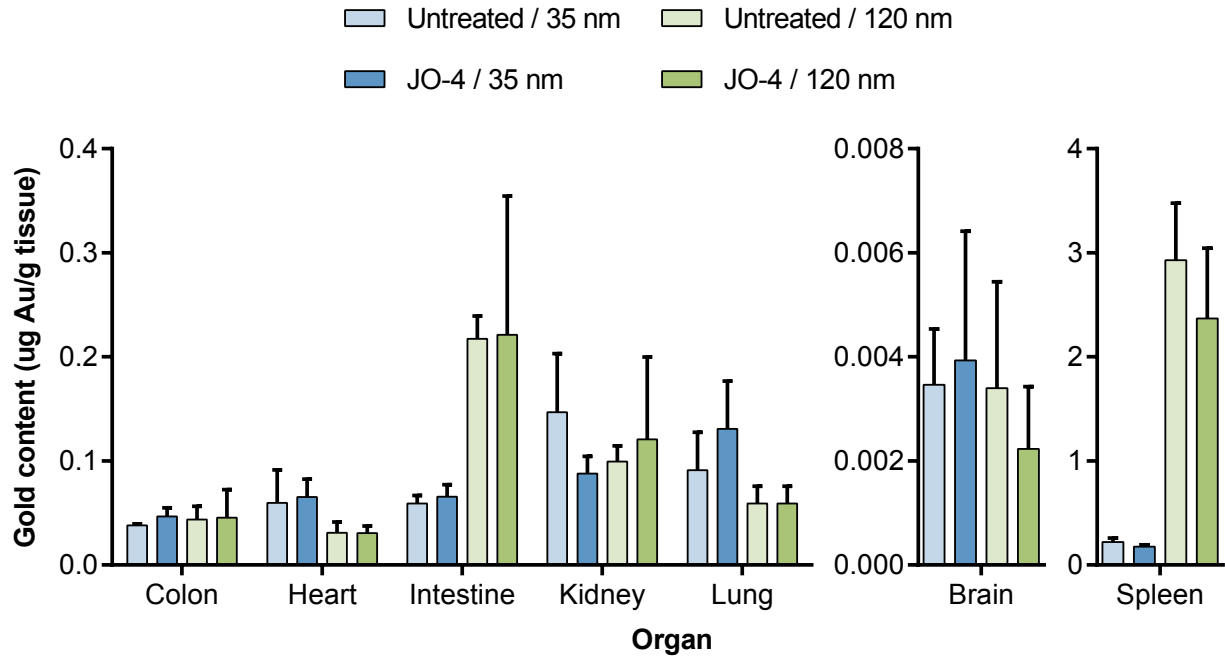
Figure 1.5 Biodistribution of two different sizes of AuNPs 6 h post-NP injection in control or JO-4 pretreated mice bearing 500-600 mm^3 tumors. Data are reported as the mean ± S.D., $n = 3$.
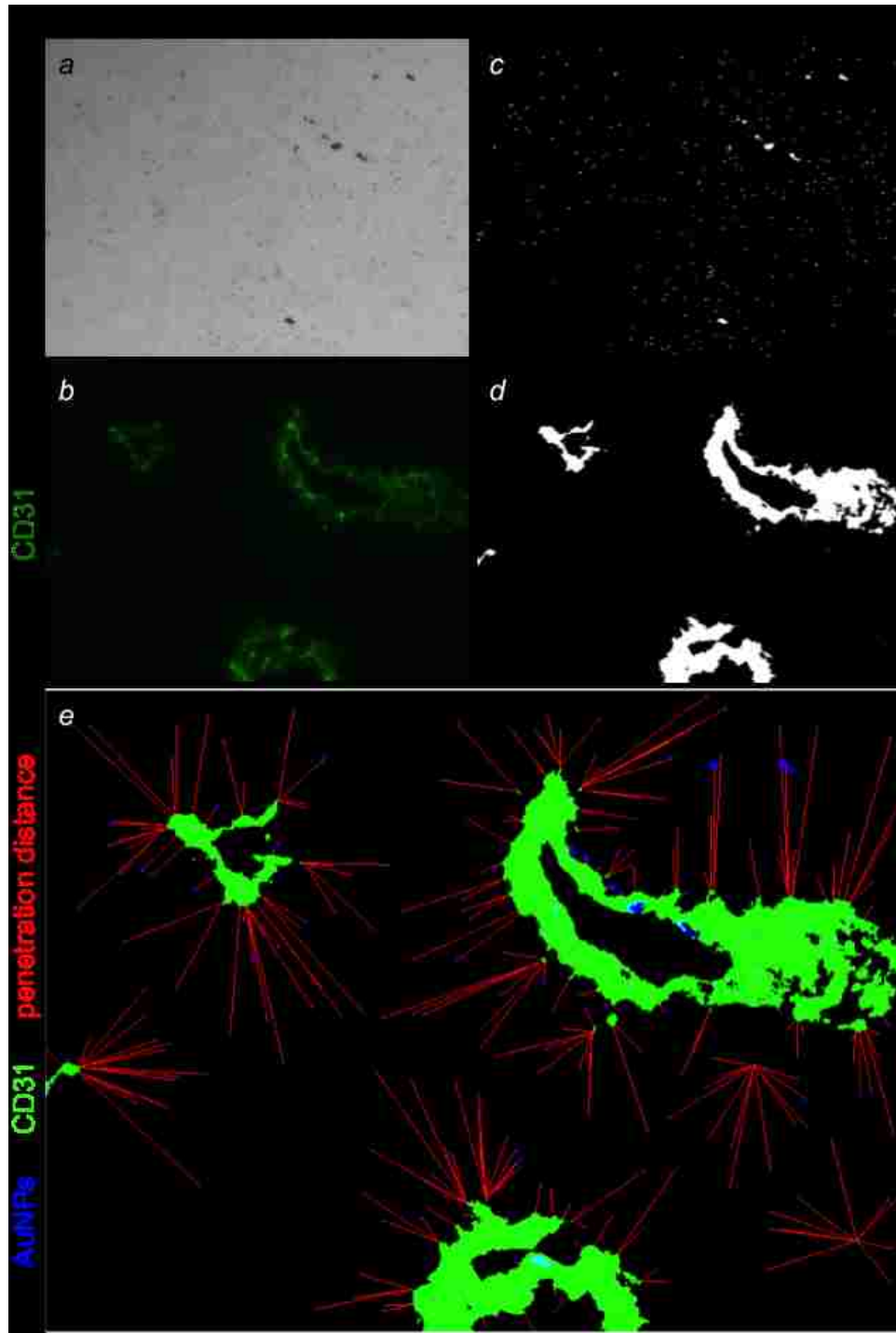
Figure 1.6 Representative images of a tumor section and image analysis strategy. (a) 35 nm AuNPs (black) were visualized by silver enhancement and brightfield microscopy. (b) Blood vessels were stained with anti-CD31 antibody (green) and imaged by fluorescence microscopy for the same field of view. Images are shown before (a,b) and after (c,d) thresholding. (e) Composite image showing relative locations of AuNPs (blue) and blood vessels (green) in a tumor section, with red lines indicating the shortest distance from each AuNP to a blood vessel.

14

1.3.3   *Intratumoral penetration of AuNPs*

Because ICP-MS provides only a bulk measurement of gold content in tissue and not spatial information, we sought to develop an imaging technique to enable quantification of AuNP penetration into tumors. The tumors of mice injected with 35 nm AuNPs were subjected to this image analysis because they were significantly affected by JO-4 pretreatment. AuNPs and CD31 (a marker for blood vessels) were imaged by brightfield microscopy and fluorescence microscopy, respectively, and images were analyzed to determine the penetration distance for each AuNP, defined as the distance from the particle to the nearest CD31-stained pixel (Figure 1.6). This process was repeated for 9 different fields of view of a single tumor section per mouse, and penetration distances for thousands of individual AuNPs were aggregated into histograms.

Interestingly, more than 3 times as many AuNPs were detected in the images of JO-4 treated tumors compared to untreated tumors (Table 1.1), a greater difference than indicated by the ICP-MS data (Figure 1.4). In addition, a large fraction of AuNPs in all mice had penetration distances close to 0, indicating that these particles remained colocalized with the vasculature; however, these blood vessel-associated AuNPs accounted for a greater fraction of the total in the untreated mice (Table 1.1). Analysis of the subset of AuNPs penetrating farther than 5 µm from a blood vessel reveals that AuNPs were found at greater distances from the tumor vasculature in the JO-treated mice as compared to the untreated mice (Figure 1.7). Overall, the median penetration distance for these nanoparticles was increased from approximately 17 µm to over 20 µm with JO-4 pretreatment (Table 1.1). Analysis of tumors from additional mice and of additional sections per tumor is ongoing.

Table 1.1 Statistics for AuNP penetration analysis.

Treatment	Mouse ID	Average # of AuNPs per image	% of AuNPs ≤5 µm from blood vessel	% of AuNPs >5 µm from blood vessel	Median penetration distance (µm)
Untreated / 35 nm	593	372 ± 94	31.5	68.5	17.3
	594	203 ± 125	33.0	67.0	17.4
JO-4 / 35 nm	583	1381 ± 660	27.6	72.4	22.4
	584	1630 ± 725	21.5	78.5	20.7

15
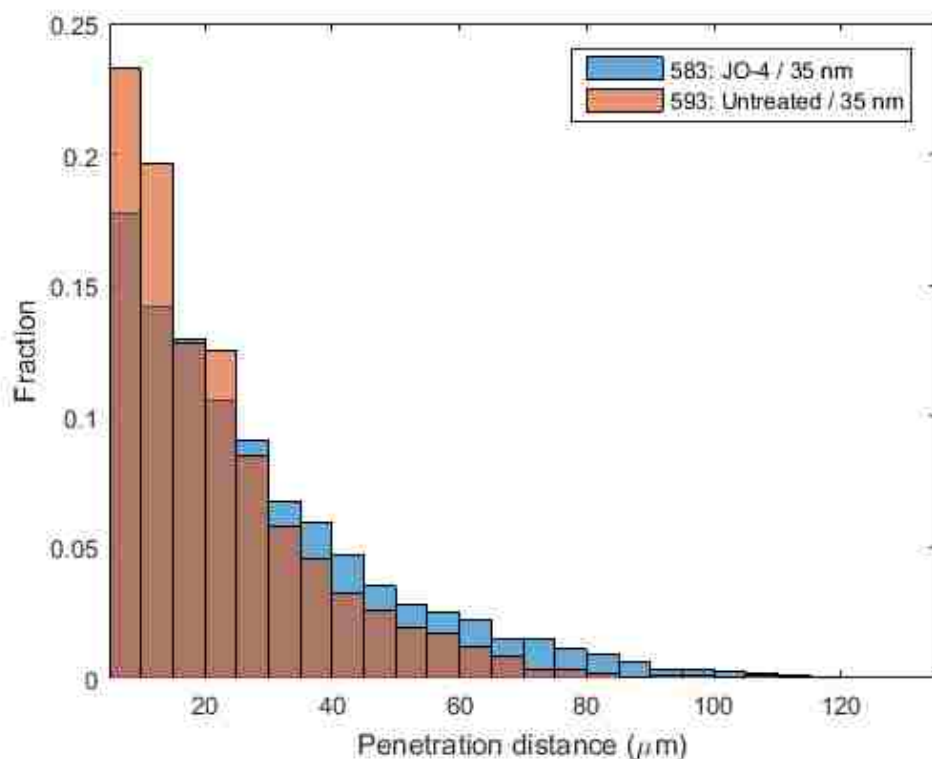
Figure 1.7 Normalized histograms of AuNP penetration distances. Data were aggregated from 9 different fields of view of a single tumor section per mouse, $n = 1$.

1.4 Conclusions and future work

The limited penetration of small molecule drugs or nanoparticulate drug carriers into solid tumors poses a critical barrier for chemotherapy efficacy, as exposure to subtoxic drug concentrations can give rise to resistance in distal tumor cells. In this work, JO-4 was found to increase tumor delivery of 35 nm AuNPs, but not of 120 nm AuNPs, in two different sizes of tumors. Importantly, junction opening appeared to be specific to tumor tissue without off-target effects in other organs. In addition, preliminary image analysis indicates that AuNPs penetrate to greater distances from the tumor vasculature in JO-treated mice. Additional work is underway to increase the sample size for this analysis. The methods described here can also be applied to study a variety of tumor and animal models or evaluate other strategies for altering drug penetration into solid tumors. Overall, a mechanistic understanding of the size limitations of junction opening *in vivo* could elucidate design criteria for novel drug carriers that can best exploit this delivery mechanism.

16

1.5 Acknowledgements

References

1. Matsumura, Y. & Maeda, H. A new concept for macromolecular therapeutics in cancer chemotherapy: mechanism of tumoritropic accumulation of proteins and the antitumor agent smancs. *Cancer Res.* **46,** 6387–6392 (1986).
2. Tannock, I. F., Lee, C. M., Tunggal, J. K., Cowan, D. S. M. & Egorin, M. J. Limited penetration of anticancer drugs through tumor tissue: a potential cause of resistance of solid tumors to chemotherapy. *Clin. Cancer Res.* **8,** 878–884 (2002).
3. Minchinton, A. I. & Tannock, I. F. Drug penetration in solid tumours. *Nat. Rev. Cancer* **6,** 583–592 (2006).
4. Christiansen, J. & Rajasekaran, A. K. Biological impediments to monoclonal antibody-based cancer immunotherapy. *Mol. Cancer Ther.* **3,** 1493–1501 (2004).
5. Green, S. K., Karlsson, M. C. I., Ravetch, J. V. & Kerbel, R. S. Disruption of cell-cell adhesion enhances antibody-dependent cellular cytotoxicity: implications for antibody-based therapeutics of cancer. *Cancer Res.* **62,** 6891–6900 (2002).
6. Biedermann, K., Vogelsang, H., Becker, I., Plaschke, S., Siewert, J. R., Höfler, H. & Keller, G. Desmoglein 2 is expressed abnormally rather than mutated in familial and sporadic gastric cancer. *J. Pathol.* **207,** 199–206 (2005).
7. Wang, H., Li, Z.-Y., Liu, Y., Persson, J., Beyer, I., Möller, T., Koyuncu, D., Drescher, M. R., Strauss, R., Zhang, X.-B., Wahl, J. K., Urban, N., Drescher, C., Hemminki, A., Fender, P. & Lieber, A. Desmoglein 2 is a receptor for adenovirus serotypes 3, 7, 11 and 14. *Nat. Med.* **17,** 96–104 (2011).
8. Beyer, I., Cao, H., Persson, J., Song, H., Richter, M., Feng, Q., Yumul, R., van Rensburg, R., Li, Z., Berenson, R., Carter, D., Roffler, S., Drescher, C. & Lieber, A. Coadministration of epithelial junction opener JO-1 improves the efficacy and safety of chemotherapeutic drugs. *Clin. Cancer Res.* **18,** 3340–3351 (2012).
9. Wang, H., Li, Z., Yumul, R., Lara, S., Hemminki, A., Fender, P. & Lieber, A. Multimerization of adenovirus serotype 3 fiber knob domains is required for efficient binding of virus to desmoglein 2 and subsequent opening of epithelial junctions. *J. Virol.* **85,** 6390–6402 (2011).
10. Beyer, I., van Rensburg, R., Strauss, R., Li, Z., Wang, H., Persson, J., Yumul, R., Feng, Q., Song, H., Bartek, J., Fender, P. & Lieber, A. Epithelial junction opener JO-1 improves monoclonal antibody therapy of cancer. *Cancer Res.* **71,** 7080–7090 (2011).
11. Richter, M., Yumul, R., Wang, H., Saydaminova, K., Ho, M., May, D., Baldessari, A., Gough, M., Drescher, C., Urban, N., Roffler, S., Zubieta, C., Carter, D., Fender, P. & Lieber, A. Preclinical safety and efficacy studies with an affinity-enhanced epithelial junction opener and PEGylated liposomal doxorubicin. *Mol Ther Methods Clin Dev* **2,**

15005 (2015).

12. Bergen, J. M., Recum, von, H. A., Goodman, T. T., Massey, A. P. & Pun, S. H. Gold nanoparticles as a versatile platform for optimizing physicochemical parameters for targeted drug delivery. *Macromol Biosci* **6,** 506–516 (2006).

13. Ghosn, B., van de Ven, A. L., Tam, J., Gillenwater, A., Sokolov, K. V., Richards-Kortum, R. & Roy, K. Efficient mucosal delivery of optical contrast agents using imidazole-modified chitosan. *J Biomed Opt* **15,** 015003 (2010).

14. Qian, X., Peng, X.-H., Ansari, D. O., Yin-Goen, Q., Chen, G. Z., Shin, D. M., Yang, L., Young, A. N., Wang, M. D. & Nie, S. In vivo tumor targeting and spectroscopic detection with surface-enhanced Raman nanoparticle tags. *Nat. Biotechnol.* **26,** 83–90 (2008).

15. Werner, M. E., Cummings, N. D., Sethi, M., Wang, E. C., Sukumar, R., Moore, D. T. & Wang, A. Z. Preclinical Evaluation of Genexol-PM, a Nanoparticle Formulation of Paclitaxel, as a Novel Radiosensitizer for the Treatment of Non-Small Cell Lung Cancer. *Int J Radiat Oncol Biol Phys* **86,** 463–468 (2013).

16. Cabral, H. & Kataoka, K. Progress of drug-loaded polymeric micelles into clinical studies. *J Control Release* **190,** 465–476 (2014).

17. Soundararajan, A., Bao, A., Phillips, W. T. & Perez, R. [186 Re] Liposomal doxorubicin (Doxil): in vitro stability, pharmacokinetics, imaging and biodistribution in a head and neck squamous cell carcinoma xenograft model. *Nuclear medicine and …* (2009).

18. Hoff, Von, D. D., Mita, M. M., Ramanathan, R. K., Weiss, G. J., Mita, A. C., LoRusso, P. M., Burris, H. A., Hart, L. L., Low, S. C., Parsons, D. M., Zale, S. E., Summa, J. M., Youssoufian, H. & Sachdev, J. C. Phase I Study of PSMA-Targeted Docetaxel-Containing Nanoparticle BIND-014 in Patients with Advanced Solid Tumors. *Clin. Cancer Res.* **22,** 3157–3163 (2016).

19. Alexis, F., Pridgen, E., Molnar, L. K. & Farokhzad, O. C. Factors affecting the clearance and biodistribution of polymeric nanoparticles. *Mol. Pharm.* **5,** 505–515 (2008).

20. Tsoi, K. M., MacParland, S. A., Ma, X.-Z., Spetzler, V. N., Echeverri, J., Ouyang, B., Fadel, S. M., Sykes, E. A., Goldaracena, N., Kaths, J. M., Conneely, J. B., Alman, B. A., Selzner, M., Ostrowski, M. A., Adeyi, O. A., Zilman, A., McGilvray, I. D. & Chan, W. C. W. Mechanism of hard-nanomaterial clearance by the liver. *Nature Materials* **15,** 1212–1221 (2016).

21. Pitteri, S. J., Kelly-Spratt, K. S., Gurley, K. E., Kennedy, J., Buson, T. B., Chin, A., Wang, H., Zhang, Q., Wong, C.-H., Chodosh, L. A., Nelson, P. S., Hanash, S. M. & Kemp, C. J. Tumor microenvironment-derived proteins dominate the plasma proteome response during breast cancer induction and progression. *Cancer Res.* **71,** 5090–5100 (2011).

22. Sykes, E. A., Dai, Q., Sarsons, C. D., Chen, J., Rocheleau, J. V., Hwang, D. M., Zheng, G., Cramb, D. T., Rinker, K. D. & Chan, W. C. W. Tailoring nanoparticle designs to target cancer based on tumor pathophysiology. *Proc. Natl. Acad. Sci. U.S.A.* **113,** E1142–51 (2016).

23. Wang, H., Beyer, I., Persson, J., Song, H., Li, Z., Richter, M., Cao, H., van Rensburg, R., Yao, X., Hudkins, K., Yumul, R., Zhang, X.-B., Yu, M., Fender, P., Hemminki, A. & Lieber, A. A new human DSG2-transgenic mouse model for studying the tropism and pathology of human adenoviruses. *J. Virol.* **86,** 6286–6302 (2012).

24. Boucher, Y., Baxter, L. T. & Jain, R. K. Interstitial pressure gradients in tissue-isolated and subcutaneous tumors: implications for therapy. *Cancer Res.* **50,** 4478–

4484 (1990).

25.   Rofstad, E. K., Tunheim, S. H., Mathiesen, B., Graff, B. A., Halsør, E. F., Nilsen, K. &
       Galappathi, K. Pulmonary and lymph node metastasis is associated with primary
       tumor interstitial fluid pressure in human melanoma xenografts. *Cancer Res.* **62,**
       661–664 (2002).

26.   Storm, G., Belliot, S. O., Daemen, T. & Lasic, D. D. Surface modification of
       nanoparticles to oppose uptake by the mononuclear phagocyte system. *Advanced
       Drug Delivery Reviews* **17,** 31–48 (1995).

20

Part II.

Polymer Nanostructures for
Tumor-Targeted Drug Delivery

22

Chapter 2.

POLYMER NANOSTRUCTURES FOR TUMOR-TARGETED DRUG DELIVERY: DESIGN PARAMETERS AND SYNTHETIC APPROACHES†

2.1   Introduction

In recent years, polymeric nanoparticles have joined established liposome technology (e.g. Doxil) as clinically approved anticancer drug delivery vehicles. The first approved formulation, Genexol-PM, a polyethylene glycol-*b*-poly(*D,L*-lactide) (PEG-PDLLA) micelle encapsulating paclitaxel, is available in Korea and is undergoing Phase II clinical trials in the US.[1] Several PEG-polypeptide micelle formulations are also in mid- to late-stage clinical trials for delivery of cisplatin, paclitaxel, and doxorubicin,[1] and a targeted micelle formulation for docetaxel delivery (BIND-014) is currently in Phase II trials. These aforementioned micelles are self-assembled structures that mitigate the toxicity profiles and improve solubility of highly hydrophobic drugs. However, ongoing challenges with such systems include the need for a formulation step during manufacturing and incomplete control of drug release profiles. For example, studies with fluorescent dye-loaded PEG-PDLLA micelles showed that the micelles were destabilized and their cargo rapidly released as early as 15 minutes post-injection due interactions with α- and β-globulins in the blood.[2] Other polymeric formulations, including linear polymer-drug conjugates such as CRLX101 (a camptothecin-cyclodextrin polymer conjugate), are progressing in clinical trials.[3-5]

Advances in controlled polymerization techniques have led to the development of new polymers with well-defined and controllable nanoscale size, morphology, and composition. These materials, here referred to as "polymer nanostructures," are well suited for drug delivery applications. Polymers with advanced architectures synthesized by controlled polymerization can approach the size of micellar systems without the need for self-

---

† Adapted from Wang, C. E., Stayton, P. S., Pun, S. H., and Convertine, A. J. *Journal of Controlled Release* (2015). doi:10.1016/j.jconrel.2015.08.054.

23

assembly. Drugs and targeting ligands can be readily conjugated to the polymers via both reversible and stable bonds, respectively. Here, we review design guidelines for nano-sized, tumor drug delivery systems that have been defined by experimental reports from the literature and discuss controlled polymerization techniques that are being applied to the synthesis of novel drug and gene delivery vehicles.

2.2   Designing polymer carriers with desired pharmacokinetics and biodistribution for anticancer drug delivery

2.2.1   EPR and tumor penetration

The "enhanced permeability and retention" (EPR) effect, first reported by Maeda and colleagues in 1986, has been widely exploited for drug delivery to solid tumors.[6] The EPR effect results from the unique pathophysiology of the tumor, particularly the tumor vasculature, and comprises several factors (Figure 2.1).[7] First, tumor cells induce angiogenesis as a means of supplying oxygen and other nutrients to the growing tumor, leading to hypervascularization within tumors. However, this neovasculature is often abnormal in morphology or leaky, with large fenestrations in the endothelium that allow for increased permeation of macromolecules. In addition, solid tumors have impaired lymphatic drainage, leading to prolonged retention of macromolecules in the tumor tissue or tumor interstitium.[8]

To use the EPR effect for preferential tumor delivery, the concentration of drug in plasma must remain high for >6 h.[7,9] This can be achieved with anticancer drugs or drug carriers with sizes above the renal clearance threshold (>40 kDa, or diameter >5 nm).[10] Another factor in prolonged drug circulation is avoidance of the reticuloendothelial system (RES, also known as the mononuclear phagocyte system, or MPS) in the liver and spleen. Larger particle sizes as well as greater surface charges (either positive or negative) are subject to increased surface opsonization, complement activation, and ultimately scavenging by Kupffer and liver endothelial cells, along with other phagocytic cells of the RES. In addition, cell membranes and blood vessel lumens are highly anionic; cationic drug formulations that interact strongly with these surfaces are therefore expected to have poor stability and short plasma half-lives.[9] A common strategy to reduce opsonization and increase circulation half-life is modification with poly(ethylene glycol) (PEG).[10-12] PEGs with

24
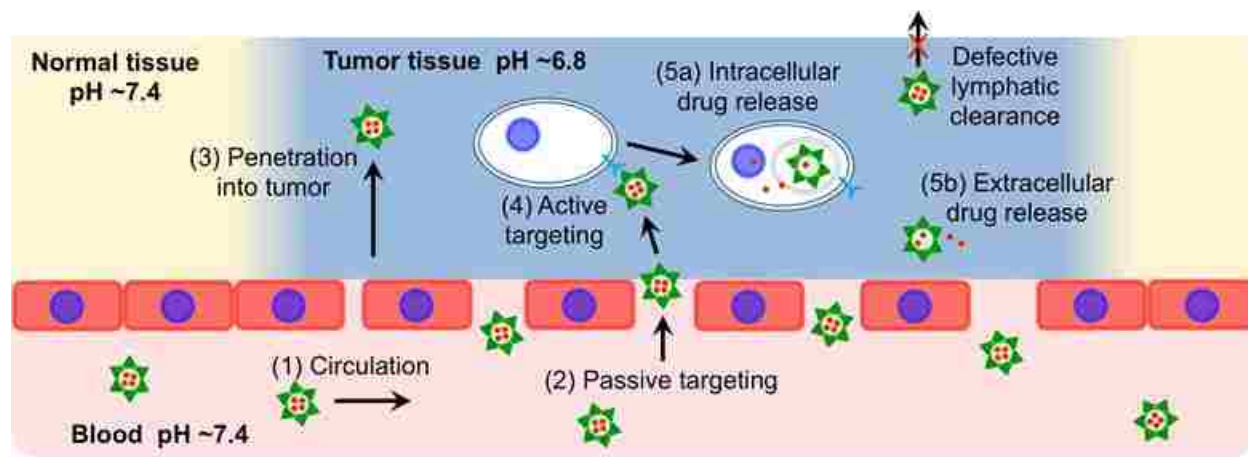
	Property	Design parameter
1	Prolonged circulation	>40 kDa or >5 nm; near neutral, hydrophilic shield
2	Passive targeting/ extravasation into tumor	Diameter between 6 and 400 nm
3	Tumor penetration	Diameter <50 nm; neutral or slightly negative charge
4	Active targeting/cellular uptake	Decoration with targeting ligands
5	Drug release	Drug stable in circulation; release triggered intracellularly or in tumor microenvironment

Figure 2.1 Design parameters for drug delivery to solid tumors. Drug carriers in circulation *(1)* are passively targeted to the tumor site by the "enhanced permeability and retention" effect, which encompasses extravasation of the carrier into the tissue via leaky tumor vasculature *(2)* and prolonged residence due to defective lymphatic clearance. Diffusional barriers often prevent vehicles from penetrating into the tumor tissue *(3)*. Carrier functionalization with "active" targeting ligands can facilitate uptake of drug carriers by cancer cells *(4)*. Finally, release of drug cargo can occur intracellularly or in the extracellular space in response to stimuli such as pH or protease activity *(5)*.

molecular weights of 2,000 to 10,000 Da and at a high grafting density (such that the PEG chains adopt a "brush" conformation rather than a low density "mushroom" conformation) are typically used to prevent protein adsorption and prolong circulation.[13]

The first step in cancer drug delivery is extravasation of the drug or drug carrier out of the vasculature and into the tumor. At the lower bound, drugs should be >2-6 nm in diameter to avoid extravasation into normal tissue[14]. As mentioned previously, the leaky vasculature of the tumor can allow for the extravasation of large macromolecules (diameters up to 400 nm[15] or even >1 μm[16] in some models), although it should also be noted that the extent of this effect has been found to be highly heterogeneous both within a

single tumor as well as between different tumor models and patients.[17-19] In addition, tumors are often characterized by elevated interstitial fluid pressure, which reduces convective transport across the vessel wall, particularly for large particles.[11] Therefore, the upper size limit must be balanced against the requirements for effective transvascular transport and drug penetration into the tumor tissue.

After initial accumulation due to the leaky vasculature, large macromolecules can have prolonged residence time in tumor tissues. This results from the defective lymphatic drainage system within tumors and the difference in clearance rate between solid tumors and normal tissues.[8] Gradual accumulation of drug at the tumor results in a form of passive localized drug delivery. However, a key limitation in nanoparticle-based drug delivery to solid tumors is poor penetration into the tumor due to limited diffusion past cell-cell junctions and the extracellular matrix. This is an important consideration because many small molecule anticancer drugs exhibit limited tissue penetration, and the resulting drug concentration gradient likely plays a role in drug resistance and tumor recurrence.[20-22] Tumor penetration has been shown to be highly dependent on vehicle size. Vehicles smaller than ~50 nm in diameter are generally most effective for tumor penetration, while larger vehicles may be restricted to the perivascular space.[23-25] Vehicle charge is an additional consideration; neutral or slightly negatively charged particles may have improved penetration as compared to their slightly positive counterparts[26], due to the negative charge of the extracellular matrix.

2.2.2   Active targeting

While the EPR effect forms the basis of "passive targeting" to tumors, "active targeting" using various targeting moieties has also been widely investigated. Targeting ligands can include small molecules, peptides, proteins, or aptamers that bind specifically to receptors expressed (or overexpressed) on the cells or tissues of interest. Ligands that have been commonly used for anticancer targeting include the small molecule folate[27], the protein transferrin[28], and antibodies to tumor markers such as HER2[29].

Selection of an appropriate targeting ligand requires the consideration of several parameters:

a. Binding affinity. The binding affinity between targeting ligand and receptor should be high enough to permit ligand recognition at therapeutically-relevant doses and in the possible presence of natural ligands, while being reversible enough so that tumor penetration can occur.[30] Studies with single-chain variable fragments (scFvs) of antibodies found that tumor retention required a minimum binding affinity (K_d) of $\sim 10^{-8}$ M but plateaued at affinities $>10^{-9}$ M, and that scFv with $\sim 10^{-11}$ M affinity was only able to penetrate 2-3 cell diameters into a solid tumor.[31,32] One strategy to enhance targeting by low affinity ligands is by using multivalent display of targeting ligands to increase avidity.

b. Size. The size of the targeting ligand impacts the final size of the targeted construct as well as the ligand density that can be achieved. For example, full antibodies are ~10 nm, relatively large in the context of the requirements for tumor penetration (sub-50 nm). Antibody derivatives such as scFvs have reduced size while retaining antibody specificity. Small molecules and peptide ligands have minimal effect on overall vehicle size and can therefore be conjugated at greater densities.

c. Ease of synthesis, modification, and conjugation. Small molecules can be chemically synthesized with varying functional groups and at relatively low cost. At the other extreme, proteins and antibodies require recombinant expression, which adds to cost, and have a limited range of site-specific conjugation chemistries and reaction conditions. Peptides and aptamers typically offer a compromise between small molecules and proteins in terms of manufacture cost, storage stability, and binding affinity.

d. Receptor-mediated endocytosis. Targeting ligands can often mediate internalization of drug carriers into the target cells via receptor-mediated endocytosis. Effective internalization is dependent on nanoparticle size, shape, as well as the target receptor.

2.3   Considerations in integrating drugs with polymeric carriers

2.3.1   Drug loading

The drug loading capacity and efficiency of potential carriers are important parameters in determining clinical relevance. Low drug loading necessarily increases the amount of

material required to achieve a therapeutic dose of drug. This problem is further exacerbated by the fact that delivery formulations are often less effective than free drug, due to incomplete drug release or inactivation of the drug. Methods for drug loading in polymer carriers vary based on the structure of the drug carrier and the physicochemical properties of the drug, such as size and solubility. The three most common methods rely on hydrophobic interactions, ionic attraction, and covalent conjugation.

Micelles, formed from assemblies of amphiphilic block copolymers or other polymers with hydrophobic domains, can be particularly useful as carriers of poorly water-soluble drugs. Many anticancer agents, including camptothecin and paclitaxel, contain multiple aromatic rings and are hydrophobic, a property that intrinsically contributes to their efficacy by facilitating penetration across the cell membrane.[33] Hydrophobic drugs can be physically entrapped within the micelle core; drug loading capacity and efficiency depends on the miscibility of polymer and drug, as well as the length of the hydrophobic block.[34,35]

Polymer-drug conjugates based on hydrophilic polymers are another class of drug carriers. Drugs can be conjugated to the polymer termini (although loading is limited with this approach) or to pendant groups along the polymer backbone. Drug content is dependent on the molecular weight of the polymer itself and the number of functional groups incorporated for drug attachment. A high density of hydrophobic drugs can lead to polymer aggregation into micelles or other supramolecular assemblies[36]; this should be taken into account when designing polymer nanostructures, e.g. by shielding hydrophobic drugs within a polymeric brush.

2.3.2   Drug release

Ideally, a drug delivery vehicle should protect its payload during circulation and allow for drug release only upon reaching the target site. For delivery formulations such as polymeric micelles in which drug is physically but not covalently encapsulated, drug release can occur due either to premature vehicle disassembly or via passive diffusion, leading to drug leakage in circulation. The structural stability of micelles has been improved by introducing covalent crosslinks in the hydrophilic shell, hydrophobic core, or core-shell interface.[37] Stimuli-responsiveness must then be introduced to allow for particle destabilization in response to pH, temperature, or reducing conditions. For example, polymeric micelles have

been reported that destabilize under acidic pH (e.g. poly(*L*-histidine)-containing polymers) or increased temperature (e.g. poly(*N*-isopropylacrylamide) (pNIPAAm)-containing polymers).[38,39] In addition, micelles that are based on disulfide-containing polymers or that contain reducible crosslinks can exploit the highly reducing environment of the cytosol for triggered intracellular degradation.[40,41]

Covalent drug attachment can reduce drug leakage during circulation. However, drugs often have limited potency while attached to their polymeric carriers, so release of the active drug at the target site is necessary. Various conjugation chemistries have been employed for triggered drug release in tumor tissue or intracellularly. The pH-sensitive hydrazone linkage is often used because it hydrolyzes under acidic conditions.[42,43] This allows for intracellular drug release primarily in the late endosomes and lysosomes (pH ~5.5). Some extracellular release may also occur as the tumor microenvironment is known to be mildly acidic (pH ~6.8)[44], although hydrolysis of the hydrazone bond is slower at this pH. Enzyme-cleavable linkages are also attractive because *in vivo* degradation occurs in very specific environments. Efficient intracellular drug release has been demonstrated using peptide-based linkers that are substrates for the lysosomal protease cathepsin B; these linkers are stable in circulation but are rapidly cleaved following endocytosis.[45-47] As another example, matrix metalloproteinases (MMPs) are often overexpressed in tumors due to their role in extracellular remodeling and tumor progression[48]; consequently, MMP-sensitive peptide linkers have also been used for triggered drug release within the tumor microenvironment.[49]

2.4   Controlled polymerization techniques

Natural polymers such as albumin, chitosan, and heparin have been used in FDA-approved drug delivery formulations. Despite this precedence, the heterogeneity, cost, and difficulty of working with biopolymers has generated interest in developing synthetic polymers with enhanced drug delivery potential.[50] Historically, the preparation of monodisperse polymers with controlled, spatially-defined functional groups for drug delivery applications has been quite challenging. Conventional addition and chain growth polymerization techniques typically yield polymers with broad molecular weight distributions ($M_w/M_n \sim 2$)[51] and cannot

29

be used to prepare advanced polymer architectures such as block copolymers and polymeric stars.

With the advent of controlled "living" polymerization methods such as atom transfer radical polymerization (ATRP), reversible addition-fragmentation chain-transfer (RAFT) polymerization, and ring opening metathesis polymerization (ROMP), the preparation of synthetic polymers for drug delivery applications has been greatly simplified.[52,53] These methods are applicable to a wide range of functional monomers and can be conducted in most solvents, including water, using commercially available reagents. This unprecedented synthetic latitude is for the first time allowing for the preparation of water-soluble or amphiphilic architectures with precise dimensions and appropriate functionality for the attachment and targeted delivery of diagnostic and therapeutic agents. These techniques can be roughly divided into controlled radical polymerization (CRP, e.g. ATRP and RAFT) and metathesis polymerization (e.g. ROMP and REMP) (Figure 2.2).
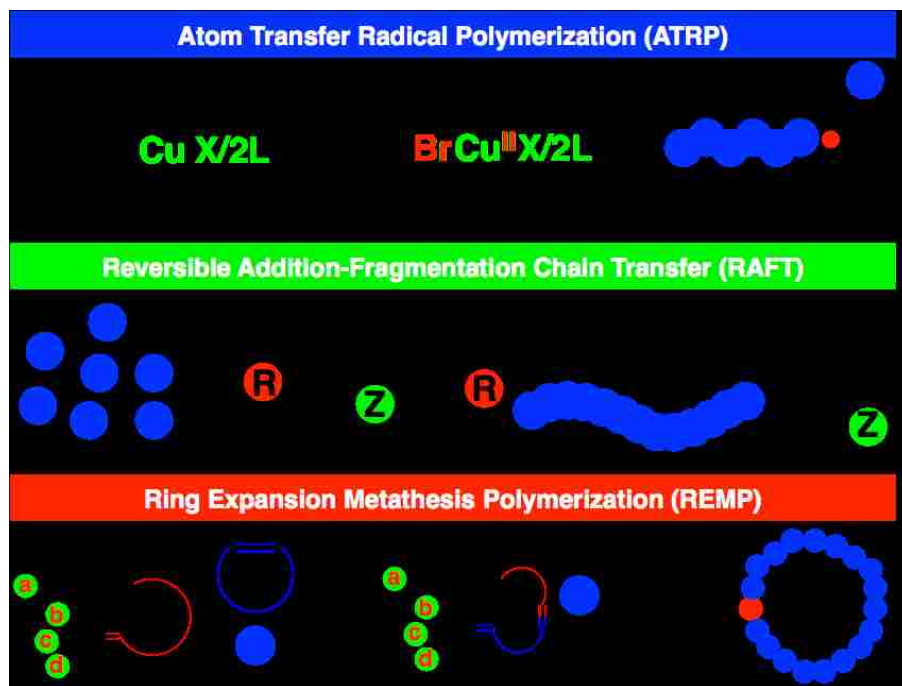
Figure 2.2 Schematic representation of controlled polymerization methods that have been widely employed to prepare sophisticated polymer architectures for drug delivery.

30

2.4.1   Atom transfer radical polymerization (ATRP)

ATRP, first reported by Matyjaszewski and coworkers in 1995, is an extremely versatile technique for preparing sophisticated polymer nanostructures with dense multivalent polymer structures.[54] In ATRP, the active-dormant equilibrium is established between non-propagating alkyl halide initiators (R-X) and radicals that are produced by the homolytic cleavage of the R–X bond. This cleavage is accomplished with the use of a redox-active transition metal complex, which is raised to a higher oxidation state with the transfer of a coordinated (pseudo) halide ligand. The transition metal catalyst is generally copper but other metals have also been reported.[55] The resultant radicals ($P_n\cdot$) can then react with monomer (M) to produce polymeric radicals ($P_n\cdot$) before undergoing deactivation with the higher oxidation state metal halide complex, regenerating the original catalyst and reversibly terminating the growing polymer chain. Because ATRP is a radical process, the activation-deactivation equilibrium must be shifted to yield predominately dormant chains in order to minimize radical termination events. This equilibrium is determined by a number of factors including the solvent polarity, ligand composition, temperature, solvent polarity, alkyl halide, and catalyst. Especially careful control is required when conducting ATRP in polar solvents such as water where excessive radical formation can lead to a loss of "livingness."

2.4.2   Reversible addition-fragmentation chain-transfer (RAFT) polymerization

Another CRP technique that has been widely employed to prepare sophisticated polymer nanostructures for drug delivery applications is RAFT. This technique was first reported by Commonwealth Scientific and Industrial Research Organization (CSIRO) in 1998.[56] Since that time RAFT has become one of the premier methods to prepare sophisticated polymers for biotechnology applications because of its broad chemical compatibility and ease of use. RAFT employs a thiocarbonyl thio compound as a degenerate chain transfer agent (CTA), which is most commonly a dithioester or trithiocarbonate.[56] By simple manipulation of the initial monomer, CTA, and radical initiator stoichiometry, it is possible to prepare near monodisperse materials over a range of predefined molecular weights. These agents contain the general structure shown in Figure 2.2, where R is a radical initiating group and Z stabilizes the thiocarbonyl towards radical addition. Through a series of chain transfer

31

steps, polymerizations proceed in a controlled process with most polymer chains containing R and Z groups at their α and ω chain termini, respectively. Following polymerization of a given monomer or monomers, the resultant macroCTA can be isolated for use in subsequent block (co)polymerization steps. Because this methodology does not require the use of any metal catalysts, it is particularly well suited for use in biotechnology applications. RAFT polymerizations are also well-controlled in water, assuming appropriate pH conditions are maintained, making them ideal for many bioconjugation applications.[57,58]

2.4.3 *Metathesis polymerization*

Similar to ATRP and RAFT, ring-opening metathesis polymerization (ROMP) is a chain growth polymerization process that can be used to yield well-controlled polymers with narrow molecular weight distributions.[59] In ROMP, cyclic olefins are converted to polymers via a metal-mediated double bond exchange process. Unlike radical initiated polymerizations, where the thermodynamic driving force for propagation is the conversion of double to single bonds, the driving force in ROMP is the relief of ring strain and associated steric considerations. Cyclic olefin monomers commonly employed in ROMP usually possess considerable ring strain and include cyclobutenes, cyclopentenes, cis-cyclooctenes, and norbornenes. A variation of ROMP is ring expansion metathesis polymerization (REMP), which can be employed to prepare macrocyclic polymers. In REMP, the catalyst contains a short tether that forms a cyclic structure with the alkylidene. Ring opening reactions with the cyclic catalyst leads to the formation of larger macrocyclic structures.

2.5 *Polymer architectures for drug delivery*

Controlled polymerization can be used to synthesize sophisticated new polymeric materials that retain the desirable properties of traditional nanoparticle therapies (e.g improving drug solubility and increasing therapeutic indices) while substantially reducing or eliminating the need for complex formulations. This section summarizes the impact of controlled polymerization techniques on the synthesis of advanced polymeric architectures:

star polymers, polymer brushes, hyperbranched polymers, and macrocyclic polymers (Figure 2.3).
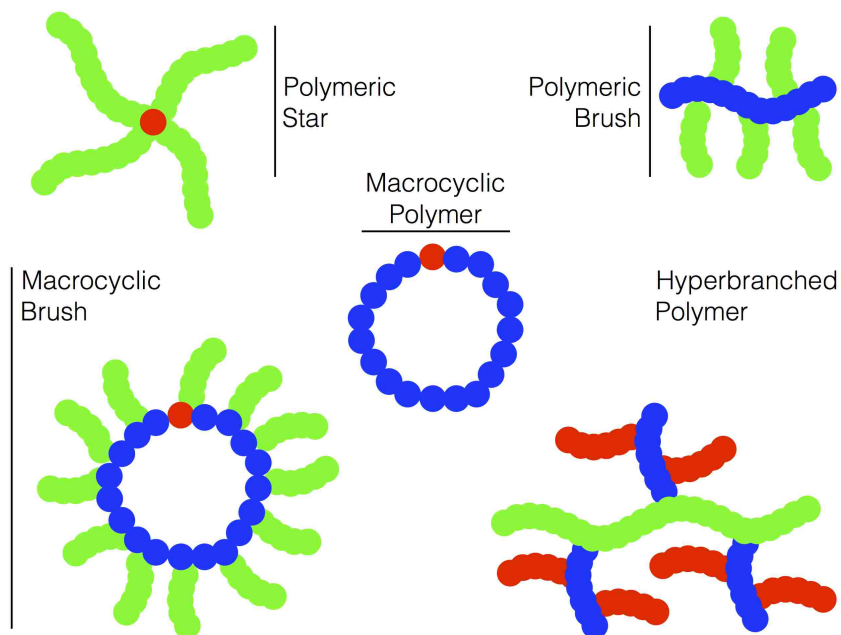
Figure 2.3 Schematic representations of advanced macromolecular architectures being investigated for drug delivery.

2.5.1 Star polymers

Star polymers have been investigated for biomedical and pharmaceutical applications because of their well-defined globular structures, low solution viscosities, and core-shell architectures.[60] Star polymers consist of at least three linear macromolecular segments radiating from a single central core.

Star polymers are generally prepared using one of three synthetic strategies: the grafting-onto approach, the core-first approach, and the arm-first approach.[61] In the core-first approach, a multifunctional ATRP initiator or chain transfer agent is attached to a central scaffold from which polymerization of the arms proceed. Star polymers can also be synthesized using the arm-first crosslinking method; in this approach, linear copolymers with "living" chain ends are linked together by conducting a subsequent copolymerization in the presence of divinyl monomers to form a crosslinked core.[62,63]

Star polymers are an attractive architecture because they can be prepared in a single step with good control over segment length and number. However, only a limited number of

arms are possible before star-star coupling becomes significant. Additionally, the small number of polymeric arms limits the overall molecular weights that can be achieved.

2.5.2   Polymer brushes

Cylindrical polymer brushes generally consist of a linear macromolecular scaffold from which polymeric segments radiate. Because of the large amount of steric repulsion between the polymeric arms, the scaffold adopts an elongated anisotropic confirmation.[64] This unique conformation, which has a large directional persistence length similar to DNA, may provide substantially enhanced *in vivo* circulation times and cellular uptake.[65] Polymer brushes can be synthesized with high number of arms and large molecular weights.

Brush copolymers are prepared using some of the same general approaches as star polymers. However, the large number of arm segments can lead to high levels of brush-brush coupling when using radical-based polymerization techniques. For this reason, low instantaneous radical concentrations in combination with limiting the overall monomer conversion are commonly employed to mitigate termination. ATRP is well-suited for preparing dense polymer brushes via the core-first approach because macromolecular scaffolds can be easily functionalized using commercially available α-haloesters or benzyl halides, and because the instantaneous radical concentration can be carefully controlled to minimize brush-brush coupling.[66] ROMP has also been widely employed to prepare brush copolymers because of its ability to polymerize large macromonomers with controllable molecular weights and low molar mass dispersities.[67,68]

2.5.3   Hyperbranched polymers

Dendrimers and dendrimer-like polymers have attracted considerable interest as potential platforms for drug delivery. These materials have a high degree of branching and can incorporate a large number of functional groups at spatially-defined positions within the globular structure. Dendritic materials can also be designed to be hydrolytically or enzymatically degradable by incorporating degradable linkages at branch junctions. Traditionally, dendrimers have been prepared via stepwise synthesis from a central core to generate materials with a highly regular branching pattern, low molar mass dispersities,

34

and controllable functional group density.[69]. The high cost and limited selection of commercially available dendrimers has led to the development of hyperbranched polymers with many of the same properties as dendrimers but with simpler preparation methods.[70]

Hyperbranched polymers can be conveniently prepared via the use of initiator-monomers (inimers). Polymers synthesized via this method have larger molar mass dispersities; however, their constituent segments are still somewhat controlled.[71] Inimers such as acrylic-substituted ATRP initiators and acrylic-substituted RAFT agents can be incorporated into CRPs where they serve as branch points along the growing polymer chains. The average degree of branching/crosslinking can then be controlled by simple manipulation of the inimer to monomer ratio and overall monomer conversion. For example, inimers have been employed to prepare architecturally distinct antigen carriers with pH-responsive endosomal-releasing segments.[72] In these studies, dendritically branched copolymers were synthesized using a methacrylate-functionalized RAFT CTA. Antigen delivery with the hyperbranched and cross-linked polymer architecture enhanced *in vitro* MHC-I antigen presentation relative to free antigen, whereas the linear construct did not have a discernible effect.

2.5.4   *Macrocyclic polymers*

Macrocyclic polymers are an interesting polymer structure due to their lack of chain ends, smaller hydrodynamic diameters, and lower radii of gyration compared to their linear analogs. These polymers have been shown to have increased circulation time *in vivo* compared to their linear analogs, leading to higher tumor accumulation.[73,74] The smaller hydrodynamic sizes of macrocyclic polymers may also be advantageous for improved tumor penetration.

The synthesis of macrocyclic polymers can be achieved by the ring closure (RC) or ring expansion (RE) methods. In the RC method, linear polymers containing telechelic functional groups undergo intramolecular coupling to form the macrocyclic polymers.[75] A major advantage of this strategy is that the backbone can be prepared by CRP, using a wide range of commercially available functional monomers and functional chain transfer agents (CTAs) or ATRP initiators. Following polymerization, the chain end is modified to introduce the appropriate complementary functional group at the ω chain terminus for end-to-end

www.manaraa.com

cyclization. However, the RC method is limited by the need for dilute cyclization conditions and/or the need for preparative size exclusion chromatography to purify the final cyclic polymers.

Ring-expansion metathesis polymerization (REMP), which was first reported by Grubbs and coworkers in 2002, provides an attractive alternative to ring closing methods for producing cyclic polymers.[76] In this technique, initiation occurs via insertion of cyclic olefin monomers into a Ru-alkyl-indene bond, expanding the cyclic catalyst ring. REMP can be used to prepare large quantities of pure cyclic polymer with high molecular weights even at high polymer concentrations. However, this technique is applicable to a more limited range of monomers and can show some broadening of the molar mass dispersity as a result of competing intramolecular chain transfer reactions.[77]

2.6   Conclusions and future perspectives

Recent advances in controlled living polymerization have made it possible to synthesize polymers with increasingly sophisticated architectures. ATRP and RAFT in particular are powerful techniques for synthesizing polymers with defined chemical compositions, low molar mass dispersities, engineered three-dimensional structures, and spatially defined functional segments. Additionally, the high valency of these systems allows for the creation of drug delivery vehicles with high loading capacity without the need for complex formulations. Although relatively few of these nanostructures have been investigated for drug delivery applications thus far, materials that can be synthesized reproducibly and with well-defined properties will be highly attractive for clinical translation.

References

1.   Cabral, H. & Kataoka, K. Progress of drug-loaded polymeric micelles into clinical studies. *J Control Release* **190,** 465–476 (2014).
2.   Chen, H., Kim, S., He, W., Wang, H., Low, P. S., Park, K. & Cheng, J.-X. Fast release of lipophilic agents from circulating PEG-PDLLA micelles revealed by in vivo forster resonance energy transfer imaging. *Langmuir* **24,** 5213–5217 (2008).
3.   Sanna, V., Pala, N. & Sechi, M. Targeted therapy using nanotechnology: focus on cancer. *Int J Nanomedicine* **9,** 467–483 (2014).
4.   Eblan, M. J. & Wang, A. Z. Improving chemoradiotherapy with nanoparticle therapeutics. *Transl Cancer Res* **2,** 320–329 (2013).

5. Hu, C.-M. J., Fang, R. H., Luk, B. T. & Zhang, L. Polymeric nanotherapeutics: clinical development and advances in stealth functionalization strategies. *Nanoscale* **6,** 65–75 (2014).

6. Matsumura, Y. & Maeda, H. A new concept for macromolecular therapeutics in cancer chemotherapy: mechanism of tumoritropic accumulation of proteins and the antitumor agent smancs. *Cancer Res.* **46,** 6387–6392 (1986).

7. Iyer, A. K., Khaled, G., Fang, J. & Maeda, H. Exploiting the enhanced permeability and retention effect for tumor targeting. *Drug Discov. Today* **11,** 812–818 (2006).

8. Noguchi, Y., Wu, J., Duncan, R., Strohalm, J., Ulbrich, K., Akaike, T. & Maeda, H. Early phase tumor accumulation of macromolecules: a great difference in clearance rate between tumor and normal tissues. *Jpn. J. Cancer Res.* **89,** 307–314 (1998).

9. Maeda, H. The enhanced permeability and retention (EPR) effect in tumor vasculature: the key role of tumor-selective macromolecular drug targeting. *Adv Enzyme Regul* **41,** 189–207 (2001).

10. Longmire, M., Choyke, P. L. & Kobayashi, H. Clearance properties of nano-sized particles and molecules as imaging agents: considerations and caveats. *Nanomedicine* **3,** 703–717 (2008).

11. Jain, R. K. & Stylianopoulos, T. Delivering nanomedicine to solid tumors. *Nat Rev Clin Oncol* **7,** 653–664 (2010).

12. Moghimi, S. M., Hunter, A. C. & Murray, J. C. Long-circulating and target-specific nanoparticles: theory to practice. *Pharmacol. Rev.* **53,** 283–318 (2001).

13. Perry, J. L., Reuter, K. G., Kai, M. P., Herlihy, K. P., Jones, S. W., Luft, J. C., Napier, M., Bear, J. E. & DeSimone, J. M. PEGylated PRINT nanoparticles: the impact of PEG density on protein binding, macrophage association, biodistribution, and pharmacokinetics. *Nano Lett* **12,** 5304–5310 (2012).

14. Jain, R. K. Transport of molecules across tumor vasculature. *Cancer Metastasis Rev* **6,** 559–593 (1987).

15. Yuan, F., Dellian, M., Fukumura, D., Leunig, M., Berk, D. A., Torchilin, V. P. & Jain, R. K. Vascular permeability in a human tumor xenograft: molecular size dependence and cutoff size. *Cancer Res.* **55,** 3752–3756 (1995).

16. Hashizume, H., Baluk, P., Morikawa, S., McLean, J. W., Thurston, G., Roberge, S., Jain, R. K. & McDonald, D. M. Openings between defective endothelial cells explain tumor vessel leakiness. *Am J Pathol* **156,** 1363–1380 (2000).

17. Lammers, T., Kiessling, F., Hennink, W. E. & Storm, G. Drug targeting to tumors: principles, pitfalls and (pre-) clinical progress. *J Control Release* **161,** 175–187 (2012).

18. Bertrand, N., Wu, J., Xu, X., Kamaly, N. & Farokhzad, O. C. Cancer nanotechnology: the impact of passive and active targeting in the era of modern cancer biology. *Advanced Drug Delivery Reviews* **66,** 2–25 (2014).

19. Prabhakar, U., Maeda, H., Jain, R. K., Sevick-Muraca, E. M., Zamboni, W., Farokhzad, O. C., Barry, S. T., Gabizon, A., Grodzinski, P. & Blakey, D. C. Challenges and key considerations of the enhanced permeability and retention effect for nanomedicine drug delivery in oncology. in *Cancer Res.* **73,** 2412–2417 (2013).

20. Tannock, I. F., Lee, C. M., Tunggal, J. K., Cowan, D. S. M. & Egorin, M. J. Limited penetration of anticancer drugs through tumor tissue: a potential cause of resistance of solid tumors to chemotherapy. *Clin. Cancer Res.* **8,** 878–884 (2002).

21. Minchinton, A. I. & Tannock, I. F. Drug penetration in solid tumours. *Nat. Rev. Cancer* **6,** 583–592 (2006).

22. Beyer, I., Cao, H., Persson, J., Song, H., Richter, M., Feng, Q., Yumul, R., van Rensburg, R., Li, Z., Berenson, R., Carter, D., Roffler, S., Drescher, C. & Lieber, A.

37

Coadministration of epithelial junction opener JO-1 improves the efficacy and safety of chemotherapeutic drugs. *Clin. Cancer Res.* **18,** 3340–3351 (2012).

23. Goodman, T. T., Olive, P. L. & Pun, S. H. Increased nanoparticle penetration in collagenase-treated multicellular spheroids. *Int J Nanomedicine* **2,** 265–274 (2007).

24. Ng, C. P. & Pun, S. H. A perfusable 3D cell-matrix tissue culture chamber for in situ evaluation of nanoparticle vehicle penetration and transport. *Biotechnol. Bioeng.* **99,** 1490–1501 (2008).

25. Perrault, S. D., Walkey, C., Jennings, T., Fischer, H. C. & Chan, W. C. W. Mediating tumor targeting efficiency of nanoparticles through design. *Nano Lett* **9,** 1909–1915 (2009).

26. Davis, M. E., Chen, Z. G. & Shin, D. M. Nanoparticle therapeutics: an emerging treatment modality for cancer. *Nat Rev Drug Discov* **7,** 771–782 (2008).

27. Lu, Y. & Low, P. S. Folate-mediated delivery of macromolecular anticancer therapeutic agents. *Advanced Drug Delivery Reviews* **54,** 675–693 (2002).

28. Daniels, T. R., Bernabeu, E., Rodríguez, J. A., Patel, S., Kozman, M., Chiappetta, D. A., Holler, E., Ljubimova, J. Y., Helguera, G. & Penichet, M. L. The transferrin receptor and the targeted delivery of therapeutic agents against cancer. *Biochim. Biophys. Acta* **1820,** 291–317 (2012).

29. Sadat, S. M. A., Saeidnia, S., Nazarali, A. J. & Haddadi, A. Nano-pharmaceutical Formulations for Targeted Drug Delivery against HER2 in Breast Cancer. *Curr Cancer Drug Targets* **15,** 71–86 (2015).

30. Fujimori, K., Covell, D. G., Fletcher, J. E. & Weinstein, J. N. Modeling analysis of the global and microscopic distribution of immunoglobulin G, F(ab')2, and Fab in tumors. *Cancer Res.* **49,** 5656–5663 (1989).

31. Adams, G. P., Schier, R., Marshall, K., Wolf, E. J., McCall, A. M., Marks, J. D. & Weiner, L. M. Increased affinity leads to improved selective tumor delivery of single-chain Fv antibodies. *Cancer Res.* **58,** 485–490 (1998).

32. Adams, G. P., Schier, R., McCall, A. M., Simmons, H. H., Horak, E. M., Alpaugh, R. K., Marks, J. D. & Weiner, L. M. High affinity restricts the localization and tumor penetration of single-chain fv antibody molecules. *Cancer Res.* **61,** 4750–4755 (2001).

33. Torchilin, V. P. Targeted polymeric micelles for delivery of poorly soluble drugs. *Cell. Mol. Life Sci.* **61,** 2549–2559 (2004).

34. Kataoka, K., Harada, A. & Nagasaki, Y. Block copolymer micelles for drug delivery: design, characterization and biological significance. *Advanced Drug Delivery Reviews* **47,** 113–131 (2001).

35. Kim, S., Shi, Y., Kim, J. Y., Park, K. & Cheng, J.-X. Overcoming the barriers in micellar drug delivery: loading efficiency, in vivo stability, and micelle-cell interaction. *Expert Opin Drug Deliv* **7,** 49–62 (2010).

36. Pu, Y., Chang, S., Yuan, H., Wang, G., He, B. & Gu, Z. The anti-tumor efficiency of poly(L-glutamic acid) dendrimers with polyhedral oligomeric silsesquioxane cores. *Biomaterials* **34,** 3658–3666 (2013).

37. Li, Y., Xiao, K., Zhu, W., Deng, W. & Lam, K. S. Stimuli-responsive cross-linked micelles for on-demand drug delivery against cancers. *Advanced Drug Delivery Reviews* **66,** 58–73 (2014).

38. Lee, E. S., Na, K. & Bae, Y. H. Super pH-sensitive multifunctional polymeric micelle. *Nano Lett* **5,** 325–329 (2005).

39. Zhu, X., Chen, S., Luo, Q., Ye, C., Liu, M. & Zhou, X. Body temperature sensitive micelles for MRI enhancement. *Chem. Commun. (Camb.)* **51,** 9085–9088 (2015).

40. Ghosh, S., Irvin, K. & Thayumanavan, S. Tunable disassembly of micelles using a

redox trigger. *Langmuir* **23,** 7916–7919 (2007).

41. Kakizawa, Y., Harada, A. & Kataoka, K. Environment-Sensitive Stabilization of Core−Shell Structured Polyion Complex Micelle by Reversible Cross-Linking of the Core through Disulfide Bond. *J. Am. Chem. Soc.* **121,** 11247–11248 (1999).

42. Bae, Y., Fukushima, S., Harada, A. & Kataoka, K. Design of environment-sensitive supramolecular assemblies for intracellular drug delivery: polymeric micelles that are responsive to intracellular pH change. *Angew. Chem. Int. Ed. Engl.* **42,** 4640–4643 (2003).

43. Padilla De Jesús, O. L., Ihre, H. R., Gagne, L., Fréchet, J. M. J. & Szoka, F. C. Polyester Dendritic Systems for Drug Delivery Applications: In Vitro and In Vivo Evaluation. *Bioconjug. Chem.* **13,** 453–461 (2002).

44. Gerweck, L. E. & Seetharaman, K. Cellular pH gradient in tumor versus normal tissue: potential exploitation for the treatment of cancer. *Cancer Res.* **56,** 1194–1198 (1996).

45. Duncan, R. Polymer conjugates as anticancer nanomedicines. *Nat. Rev. Cancer* **6,** 688–701 (2006).

46. Dubowchik, G. M., Firestone, R. A., Padilla, L., Willner, D., Hofstead, S. J., Mosure, K., Knipe, J. O., Lasch, S. J. & Trail, P. A. Cathepsin B-labile dipeptide linkers for lysosomal release of doxorubicin from internalizing immunoconjugates: model studies of enzymatic drug release and antigen-specific in vitro anticancer activity. *Bioconjug. Chem.* **13,** 855–869 (2002).

47. Doronina, S. O., Toki, B. E., Torgov, M. Y., Mendelsohn, B. A., Cerveny, C. G., Chace, D. F., DeBlanc, R. L., Gearing, R. P., Bovee, T. D., Siegall, C. B., Francisco, J. A., Wahl, A. F., Meyer, D. L. & Senter, P. D. Development of potent monoclonal antibody auristatin conjugates for cancer therapy. *Nat. Biotechnol.* **21,** 778–784 (2003).

48. Choi, K. Y., Swierczewska, M., Lee, S. & Chen, X. Protease-activated drug development. *Theranostics* **2,** 156–178 (2012).

49. Chau, Y., Padera, R. F., Dang, N. M. & Langer, R. Antitumor efficacy of a novel polymer-peptide-drug conjugate in human tumor xenograft models. *Int. J. Cancer* **118,** 1519–1526 (2006).

50. Chan, L. W., Wang, X., Wei, H., Pozzo, L. D., White, N. J. & Pun, S. H. A synthetic fibrin cross-linking polymer for modulating clot properties and inducing hemostasis. *Sci Transl Med* **7,** 277ra29–277ra29 (2015).

51. Braunecker, W. A. & Matyjaszewski, K. Controlled/living radical polymerization: Features, developments, and perspectives. *Progress in Polymer Science* **32,** 93–146 (2007).

52. Boyer, C., Bulmus, V., Davis, T. P., Ladmiral, V., Liu, J. & Perrier, S. Bioapplications of RAFT polymerization. *Chemical Reviews* **109,** 5402–5436 (2009).

53. Matyjaszewski, K. & Xia, J. Atom transfer radical polymerization. *Chemical Reviews* **101,** 2921–2990 (2001).

54. Wang, J.-S. & Matyjaszewski, K. Controlled/'Living' Radical Polymerization. Halogen Atom Transfer Radical Polymerization Promoted by a Cu(I)/Cu(II) Redox Process. *Macromolecules* **28,** 7901–7910 (1995).

55. Zhang, Y., Wang, Y. & Matyjaszewski, K. ATRP of methyl acrylate with metallic zinc, magnesium, and iron as reducing agents and supplemental activators. *Macromolecules* **44,** 683–685 (2011).

56. Chiefari, J., Chong, Y. K., Ercole, F., Krstina, J., Jeffery, J., Le, T. P. T., Mayadunne, R. T. A., Meijs, G. F., Moad, C. L., Moad, G., Rizzardo, E. & Thang, S. H. Living free-radical polymerization by reversible addition-fragmentation chain transfer: the

39

RAFT process. *Macromolecules* 5559–5562 (1998). at <http://pubs.acs.org/doi/pdf/10.1021/ma9804951>

57. Thomas, D. B., Convertine, A. J., Hester, R. D., Lowe, A. B. & McCormick, C. L. Hydrolytic Susceptibility of Dithioester Chain Transfer Agents and Implications in Aqueous RAFT Polymerizations†. *Macromolecules* **37,** 1735–1741 (2004).

58. Thomas, D. B., Convertine, A. J., Myrick, L. J., Scales, C. W., Smith, A. E., Lowe, A. B., Vasilieva, Y. A., Ayres, N. & McCormick, C. L. Kinetics and Molecular Weight Control of the Polymerization of Acrylamide via RAFT †. *Macromolecules* **37,** 8941–8950 (2004).

59. Bielawski, C. W. & Grubbs, R. H. Living ring-opening metathesis polymerization. *Progress in Polymer Science* **32,** 1–29 (2007).

60. Trollsås, M. & Hedrick, J. L. Dendrimer-like Star Polymers. *J. Am. Chem. Soc.* 4644–4651 (1998). doi:10.1021/ja973678w

61. Hawker, C. J. Architectural Control in 'Living' Free Radical Polymerizations: Preparation of Star and Graft Polymers. *Angewandte Chemie International Edition in English* **34,** 1456–1459 (1995).

62. Boyer, C., Teo, J., Phillips, P., Erlich, R. B., Sagnella, S., Sharbeen, G., Dwarte, T., Duong, H. T. T., Goldstein, D., Davis, T. P., Kavallaris, M. & McCarroll, J. Effective Delivery of siRNA into Cancer Cells and Tumors Using Well-Defined Biodegradable Cationic Star Polymers. … *pharmaceutics* **10,** 2435–2444 (2013).

63. Li, Y., Duong, H. T. T., Laurent, S., MacMillan, A., Whan, R. M., Elst, L. V., Muller, R. N., Hu, J., Lowe, A., Boyer, C. & Davis, T. P. Nanoparticles based on star polymers as theranostic vectors: endosomal-triggered drug release combined with MRI sensitivity. *Advanced healthcare materials* **4,** 148–156 (2015).

64. Wintermantel, M., Gerle, M., Fischer, K. & Schmidt, M. Molecular Bottlebrushes†. *Macromolecules* **29,** 978–983 (1996).

65. Hörtz, C., Birke, A., Kaps, L., Decker, S., Wächtersbach, E., Fischer, K., Schuppan, D., Barz, M. & Schmidt, M. Cylindrical Brush Polymers with Polysarcosine Side Chains: A Novel Biocompatible Carrier for Biomedical Applications. *Macromolecules* **48,** 2074–2086 (2015).

66. Pyun, J., Kowalewski, T. & Matyjaszewski, K. Synthesis of Polymer Brushes Using Atom Transfer Radical Polymerization. *Macromolecular Rapid …* **24,** 1043–1059 (2003).

67. Gao, A. X., Liao, L. & Johnson, J. A. Synthesis of Acid-Labile PEG and PEG-Doxorubicin-Conjugate Nanoparticles via Brush-First ROMP. *ACS Macro Lett* **3,** 854–857 (2014).

68. Greenwald, R. B., Pendri, A., Conover, C. D., Zhao, H., Choe, Y. H., Martinez, A., Shum, K. & Guan, S. Drug Delivery Systems Employing 1,4- or 1,6-Elimination: Poly(ethylene glycol) Prodrugs of Amine-Containing Compounds. *J. Med. Chem.* **42,** 3657–3667 (1999).

69. Bugno, J., Hsu, H.-J. & Hong, S. Recent advances in targeted drug delivery approaches using dendritic polymers. *Biomaterials Science* (2015). doi:10.1039/C4BM00351A

70. Smet, M. in *Synthesis, Properties, and Applications* 387–413 (John Wiley & Sons, Inc., 2011). doi:10.1002/9780470929001.ch15

71. Sun, H., Kabb, C. P. & Sumerlin, B. S. Thermally-labile segmented hyperbranched copolymers: using reversible-covalent chemistry to investigate the mechanism of self-condensing vinyl copolymerization. *Chemical Science* **5,** 4646–4655 (2014).

72. Wilson, J. T., Postma, A., Keller, S., Convertine, A. J., Moad, G., Rizzardo, E.,

Meagher, L., Chiefari, J. & Stayton, P. S. Enhancement of MHC-I Antigen Presentation via Architectural Control of pH-Responsive, Endosomolytic Polymer Nanoparticles. *AAPS J* **17,** 358–369–369 (2015).

73. Nasongkla, N., Chen, B., Macaraeg, N., Fox, M. E., Fréchet, J. M. J. & Szoka, F. C. Dependence of Pharmacokinetics and Biodistribution on Polymer Architecture: Effect of Cyclic versus Linear Polymers. *J. Am. Chem. Soc.* **131,** 3842–3843 (2009).

74. Chen, B., Jerger, K., Fréchet, J. M. J. & Szoka, F. C. The influence of polymer topology on pharmacokinetics: differences between cyclic and linear PEGylated poly(acrylic acid) comb polymers. *J Control Release* **140,** 203–209 (2009).

75. Laurent, B. A. & Grayson, S. M. An efficient route to well-defined macrocyclic polymers via 'click' cyclization. *J. Am. Chem. Soc.* **128,** 4238–4239 (2006).

76. Bielawski, C. W., Benitez, D. & Grubbs, R. H. An 'endless' route to cyclic polymers. *Science* **297,** 2041–2044 (2002).

77. Zhang, K. & Tew, G. N. Cyclic polymers as a building block for cyclic brush polymers and gels. *Reactive and Functional Polymers* **80,** 40–47 (2014).

Chapter 3.

ATRP SYNTHESIS OF SUNFLOWER POLYMERS USING CYCLIC MULTIMACROINITIATORS

Hua Wei*, Christine E. Wang*, Nicholas Tan, Andrew J. Boydston, and Suzie H. Pun

Equally contributing authors

Abstract

Polymers with advanced architectures can now be readily and reproducibly synthesized using controlled living polymerization. These materials are attractive as potential drug carriers due to their tunable size, versatile methods of drug incorporation and release, and ease of functionalization with targeting ligands. In this work, we report the design and development of macrocyclic brush, or "sunflower," polymers, synthesized by controlled radical polymerization of hydrophilic "petals" from a cyclic multimacroinitiator "core." These nanostructures can be synthesized with low polydispersity and controlled sizes depending on polymerization time. We further demonstrate that folate-functionalized sunflower polymers facilitate receptor-mediated uptake into cancer cells. These materials therefore show potential as drug carriers for anti-cancer therapies.[†]

3.1   Introduction

Polymeric drug carriers are used to alter the biodistribution and pharmacokinetics of their drug cargo in order to improve therapeutic indices. Desirable characteristics of polymeric carriers that allow for facile adaptation to drug-specific applications include: (i) tunable size and surface charge, (ii) high drug loading capacity, (iii) controllable drug release, (iv) mechanisms for preferential accumulation at the target site based on passive or active targeting strategies, and (v) reproducible synthesis. Polymer nanostructures with advanced architectures (e.g. cyclic polymers,[1-3] polymer brushes,[4,5] star polymers,[6,7] and hyperbranched polymers[8,9]) are a promising class of materials for this application.[10] Indeed,

Szoka and coworkers have demonstrated that cyclic polymers and PEG-grafted cyclic polymers exhibit longer circulation times than their analogous, molecular weight-matched linear polymers.[11,12] Polymer-drug conjugates prepared from polymeric nanostructures offer the additional advantage of being formulation-free; sizes of these constructs can be similar to those of polymeric micelles without the need for additional formulation and characterization steps of the self-assembled structures.

One architecture of interest is the macrocyclic brush, or "jellyfish" polymer,[13] which has not to our knowledge been applied as a drug carrier. Notably, ring expansion metathesis polymerization (REMP) has been used to prepare macrocyclic brush polymers by Grubbs' and Tew's groups independently.[14,15] REMP maximizes the formation of cyclic polymers and avoids interchain reactions at high polymerization concentrations; however, this strategy is limited by the monomer species, and suffers from the relatively complicated synthesis of various norbornene-based monomers with activated functional groups or macromonomers with polymer side-chains. In addition, "grafting from," as compared to "grafting onto" and "grafting through," offers much better control over the generation of uniform polymer brushes by minimizing the effect of steric hindrance and avoiding tedious purification processes. Recently, nitroxide-mediated radical polymerization (NMRP) and ring-opening polymerization (ROP) have been reported to produce macrocyclic brush polymers by the "grafting from" approach,[16] but again only limited monomers can be employed by such approaches.

To develop a more universal platform material based on macrocyclic brush structures for drug delivery applications, we explored herein the preparation of macrocyclic brush polymers using atom transfer radical polymerization (ATRP), which provides access to a broad range of monomers and the ability to control polymer architecture and dimensions due to its "living" characteristics.[17] In this work, we report the development of macrocyclic brush, or "sunflower" polymers (Figure 3.1) as a universal platform for targeted drug delivery. Sunflower polymers are synthesized by controlled radical polymerization (CRP) using a cyclic macroinitiator "core" from which "petals" are polymerized, radiating from the core. As a proof of concept, we further conjugate a commonly used cancer targeting ligand, folate, to the petal termini and a model cargo, fluorescein, to the cyclic core buried within the polymer petals, and demonstrate receptor-mediated delivery to mammalian cells.
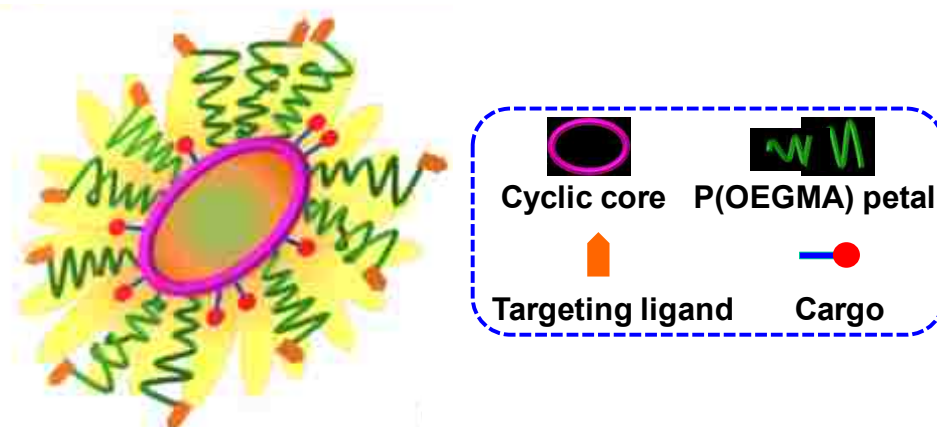
Figure 3.1 Schematic illustration of sunflower polymer containing targeting ligands and cargo.

3.2   Materials and methods

3.2.1   Materials

All chemicals were purchased from Sigma-Aldrich and used without further purification unless otherwise noted.

3.2.2   Polymer synthesis

Synthesis of ethyl glycinate methacrylamide (EGMA) monomer

Ethyl glycinate hydrochloride (10.15 g, 0.072 mol) was dissolved in 100 mL of dry dichloromethane (DCM). Anhydrous TEA (20 mL, 0.144 mol) was then added at room temperature, and the solution was cooled to 0°C in an ice bath. Methacryloyl chloride (7.251 mL, 0.072 mol) was added dropwise via a syringe pump to the cooled ethyl glycinate solution over 2 h. After completion of this addition, the reaction mixture was warmed up to room temperature and was stirred for another 2 h. After the reaction, the solution was filtered to remove the by-product triethylamine hydrochloride precipitate. Subsequently, the solvent was removed by rotary evaporation, and the crude product was purified by column chromatography with an ethyl acetate/hexane mixture (1/2, v/v, R_f = 0.2-0.3 on silica). The product was isolated by evaporation of the solvents and further dried in a vacuum oven to form a colorless oily residue. Yield: 78% (9.55 g).

44

Synthesis of linear P(HEMA-st-EGMA) precursors (Alkyne-P(HEMA-st-EGMA)-N₃)

The linear precursor with Br terminus was prepared by ATRP of 2-hydroxyethyl methacrylate (HEMA) and EGMA in a 2-propanol (IPA)/*N,N*-dimethylformamide (DMF) mixed solution, using propargyl 2-bromoisobutyrate[18] as the initiator and *N,N,N′,N″,N″*-pentamethyldiethylenetriamine (PMDETA)/Cu(I)Br as the catalyst. Typically, a 10 mL round-bottom flask was charged with propargyl 2-bromoisobutyrate (0.041 g, 0.2 mmol), HEMA (1.30 g, 10 mmol), EGMA (0.57 g, 3.33 mmol) to obtain a HEMA and initiator molar ratio ([HEMA]/[Initiator]) of 50. The above mixture was dissolved in a 9:1 % w/w IPA/DMF mixture to obtain a 50% w/w HEMA solution. The flask was degassed using a stream of dry nitrogen gas to remove any trace of oxygen in the system. CuBr catalyst and PMDETA (relative molar ratios of initiator:CuBr:PMDETA = 1:1:1) were then added quickly under a nitrogen flow. Finally, the reaction mixture was sealed, followed by immersing the flask into an oil bath preheated to 65°C to start the polymerization. The reaction mixture turned green and became viscous as the reaction progressed. After 16 h, the reaction mixture was quenched by exposing to air. The reaction mixture was diluted with 2 mL of methanol and then subjected directly to dialysis against distilled water to remove the copper catalyst. The product was harvested by freeze-drying. Yield: 70~80%.

A non-clickable linear analogue was synthesized following the same reaction conditions except using ethyl 2-bromoisobutyrate (EBB) as the initiator.

Afterward, the linear precursor with azide terminus was obtained as follows. Alkyne-P(HEMA-*st*-EGMA)-Br (1.0 g) and NaN₃ in a 20-fold molar excess were dissolved in a 1/4 v/v % water/DMF mixed solvent (10 mL) in a round-bottom flask equipped with a magnetic stirrer. The flask was sealed with a rubber septum and was stirred at 45°C for 48 h. After purification by extensive dialysis to remove residual sodium salts, the linear precursor, alkyne-P(HEMA-*st*-EGMA)-N₃, was obtained by freeze-drying. Yield: 90% (0.9 g).

The bromo-terminus of the non-clickable linear copolymer was also converted to an azide group following the same methods.

Synthesis of cyclic P(HEMA-st-EGMA) copolymer by intra-chain click cyclization

In a typical procedure, 750 mL of DMF was placed in a 1000 mL three-neck flask and degassed by bubbling dry nitrogen gas for 1 h. 20-fold molar equivalents of PMDETA and CuBr were then charged into the flask under the protection of nitrogen flow. A solution of

45

alkyne-P(HEMA-*st*-EGMA)-N₃ linear precursor (0.5 g) in degassed DMF (10 mL) was added to the copper catalyst solution via a syringe pump at the rate of 0.007 mL/min. The reaction was carried out at 100°C in a nitrogen atmosphere for 24 h. At the end of the polymer solution addition, the mixture was allowed to proceed for another 24 h. After the mixture was cooled to room temperature, DMF was removed under reduced pressure, and the concentrated residue was transferred directly to a dialysis tube (MWCO: 3.5 kDa, Fisher Scientific) and dialyzed against distilled water to remove the copper catalyst. The resulting cyclic polymer, cyclic P(HEMA-*st*-EGMA), was harvested by freeze-drying. Yield: 80% (0.4 g).

Preparation of cyclic poly(2-(2-bromoisobutyrnyloxy)ethyl methacrylate-st-EGMA) (P((HEMA-iBuBr)-st-EGMA)) macroinitiator

Cyclic poly(2-(2-bromoisobutyrnyloxy)ethyl methacrylate-*st*-EGMA) (P((HEMA-iBuBr)-*st*-EGMA)) macroinitiator was prepared by esterification of cyclic P(HEMA-*st*-EGMA). Cyclic P(HEMA-*st*-EGMA) (0.2 g, 1.07 mmol of HEMA units) was dissolved in 10 mL of dry DMF, and then anhydrous TEA (581 μL, 4.17 mmol) was added at room temperature. The solution was cooled to 0°C in an ice bath. 2-bromoisobutyryl bromide (404 μL, 3.2 mmol) was added dropwise via a syringe pump to the cooled polymer solution over 30 min. After completion of this addition, the solution was further stirred at 0°C for 1 h and at room temperature for 48 h. After the reaction, the reaction mixture was poured into distilled water to precipitate the product. The product was separated by centrifugation and further purified twice by redissolving/reprecipitating with DMF/water, and finally dried in a vacuum oven for 24 h, yielding a light yellow powdery product. Yield: 58% (0.21 g).

Linear multimacroinitiator for the preparation of comb-like polymer was prepared following the same procedures except using non-clickable linear copolymer, P(HEMA-*st*-EGMA)-N₃.

Preparation of sunflower polymer, P((HEMA-sunflower-oligo(ethylene glycol) monomethyl ether methacrylate-st-EGMA) (P((HEMA-sf-OEGMA)-st-EGMA))

A panel of sunflower polymers, P((HEMA-*sf*-OEGMA)-*st*-EGMA), with OEGMA radiating rays was prepared by ATRP using cyclic P((HEMA-iBuBr)-*st*-EGMA) macroinitiator. Cyclic

46

P((HEMA-iBuBr)-*st*-EGMA) macroinitiator (0.05 g, 0.149 mmol of initiator sites), and OEGMA (M_n = 300 g/mol, 4.46 g, 14.9 mmol) were dissolved in a 1/2 v/v % anisole/DMF mixed solution (30 mL). The solution was split in equal volumes into five 10 mL round-bottom flasks. After putting in a stir bar and sealing with a rubber septum, each solution was thoroughly degassed by nitrogen bubbling for 10 min. Meanwhile, a catalyst stock solution of $CuBr_2$ (3.3 mg, 14.9 μmol) and 2,2'-bipyridine (51.2 mg, 327.8 μmol) was made in DMF (500 μL). The solution was bubbled with nitrogen to deoxygenate the mixture. Solid CuBr (21 mg, 149 μmol) was added to the copper stock solution under nitrogen atmosphere and sonicated to promote dissolution. The resultant copper catalyst stock solution (100 μL) was added quickly to each cyclic initiator-monomer mixture under a nitrogen blanket. Finally, the reaction mixtures were sealed, followed by immersing the flasks into an oil bath preheated to 60°C to start the polymerization. The reactions were subsequently quenched by exposing flasks to air at predetermined time intervals. Each reaction mixture was poured into ethyl ether to precipitate the product. The product was separated by centrifugation and further purified by extensive dialysis against distilled water to remove the copper catalyst. The resulting sunflower polymer was harvested by freeze-drying. The conversion of polymerization and molecular weight of each sunflower polymer were determined by ^{1}H NMR and GPC analyses.

Comb-like polymer was prepared following the same polymerization condition except using the linear multimacroinitiator.

Preparation of folate-conjugated sunflower polymer (FA-sunflower polymer) by click coupling

Similar to the synthesis of alkyne-P(HEMA-st-EGMA)-N_3 linear precursor, sunflower polymer with an azide terminus on each OEGMA radiating ray was prepared by reacting the resultant sunflower polymer with NaN_3 in a 20-fold molar excess in a 1/4 v/v % water/DMF mixed solvent. The reaction was carried out at 45°C for 48 h. After the reaction, the product was purified by extensive dialysis to remove residual sodium salts, and harvested by freeze-drying.

To a round-bottom flask containing thoroughly degassed DMF solution (10 mL) of azide-terminated sunflower polymer (210 mg, 97 μmol of azide terminus) and alkyne-functionalized folate[19] (0.05 g, 106 μmol), PMDETA (20.3 μL, 97 μmol), and CuBr (14 mg, 97

μmol) were added quickly under a nitrogen flow. The reaction mixture was stirred at room temperature for 24 h. After the reaction, the mixture was poured into ethyl ether to precipitate the product and to remove the unreacted propargyl folate. The product was separated by centrifugation and further purified by dialysis against distilled water to remove the copper catalyst. The resulting FA-sunflower polymer was isolated by freeze-drying. Yield: 86% (220 mg). The amount of folate conjugated to each polymer was determined by absorbance at 360 nm based on a standard curve obtained from solutions of free folic acid.

Folate-conjugated comb-like polymer was prepared following the same reaction conditions.

Preparation of P((HEMA-sf-OEGMA-folate)-st-(GMA-hydrazide))

A 50 mL falcon tube equipped with a magnetic stirrer was charged with FA-sunflower polymer (220 mg, 32.3 μmol of EGMA units), hydrazine hydrate (18 μL, 370 μmol), and anhydrous methanol (6 mL). The reaction was performed at room temperature for 10 h. After the reaction, the resultant polymer precursor, P((HEMA-*sf*-OEGMA-folate)-*st*-(GMA-hydrazide)), was purified by extensive dialysis against distilled water and collected by freeze-drying. Yield: 82% (180 mg). The content of hydrazide was determined by modified TNBSA assays.[20,21]

Preparation of P((HEMA-sf-OEGMA-folate)-st-(GMA-fluorescein))

A 50 mL falcon tube equipped with a magnetic stirrer was charged with the polymer precursor P((HEMA-sf-OEGMA-folate)-st-(GMA-hydrazide)) (90.0 mg, 14.6 μmol of hydrazide), NHS-Fluorescein (PI-46410, Thermo Scientific, MW = 473.4 g/mol, 13.8 mg, 29.2 μmol), and anhydrous methanol (4 mL). The tube was sealed, and the reaction was allowed to proceed in the dark at room temperature for 48 h. The resultant fluorescein-labeled sunflower polymer, P((HEMA-sf-OEGMA-folate)-st-(GMA-fluorescein)), was purified by extensive dialysis against distilled water (4L) for 24 h and collected by freeze-drying. Yield: 75.1% (67.6 mg). The amount of fluorescein conjugated to each polymer was determined by ^{1}H NMR spectroscopy.

Folate-comb polymer-fluorescein was prepared following the same reaction conditions.

3.2.3 Polymer characterization

^{1}H NMR spectra were recorded on a Bruker AV 500 nuclear magnetic resonance (NMR) instrument using DMSO-d_6, CDCl$_3$, and D$_2$O as the solvents.

Fourier transform infrared (FT-IR) spectra were recorded on a Bruker Vector 33 FT-IR spectrometer. Samples were pressed into potassium bromide (KBr) pellets for measurements.

Gel permeation chromatography (GPC) was used to determine molecular weight and polydispersity (M_w/M_n, PDI) of polymer samples prepared. SEC Tosoh TSK-GEL R-3000 and R-4000 columns (Tosoh Bioscience, Montgomeryville, PA) were connected in series to a Agilent 1200 series (Agilent Technologies, Santa Clara, CA), Optilab-rEX refractometer, and miniDAWN TREOS triple-angle static light scattering detector (Wyatt Technology, Santa Barbara, CA). HPLC-grade DMF containing 0.1 wt% LiBr at 60°C was used as the mobile phase at a flow rate of 1 mL/min. Absolute molecular weight averages and dn/dc were calculated using ASTRA software (Wyatt).

Average dimensions of sunflower polymers in an aqueous phase were measured by dynamic light scattering (DLS) with a ZetaPALS (Brookhaven Instruments Corp.) at a detection angle of 90°. The measurements were performed in triplicate. The aqueous solution was passed through a 0.22 μm pore-sized syringe filter before measurements.

3.2.4 Cell culture

KB cells (ATCC CCL-17, a derivative of the HeLa human cervical adenocarcinoma line) and A549 cells (ATCC CCL-185, lung epithelial carcinoma) were maintained in folate-free RPMI 1640 (Life Technologies) and F-12K (Corning cellgro) media, respectively. Media was supplemented with 10% fetal bovine serum (HyClone) and 1% penicillin/streptomycin (HyClone). Cells were cultured as a monolayer in a 37°C, 5% CO$_2$ environment. Medium was replaced every 2-3 days. Cells were passaged at ~70-80% confluence by incubation with Trypsin-EDTA, followed by resuspension in complete growth medium.

3.2.5   *In vitro uptake and competition studies*

Cells were seeded in 24-well plates at a density of 40,000 cells per well in 1 mL of complete growth medium and incubated in a 37°C, 5% CO_2 environment for 24 h. Cells were rinsed once with PBS and incubated in 1 mL of supplemented folate-free RPMI 1640 medium +/- 2 mM folate competition for 1 h at room temperature. Polymer samples at varying concentrations were prepared in serial dilutions in water and then diluted 10-fold in supplemented folate-free RPMI 1640 medium +/- 2 mM folate. The media was aspirated from each well, and cells were incubated with 200 µL of polymer solution for 20 min at 37°C. After incubation, the polymer solutions were aspirated, and the cells were rinsed twice with PBS/1% BSA. Cells were then harvested by incubation with 200 µL of Trypsin-EDTA, followed by resuspension with 1 mL of complete growth medium. Cells were transferred to 1.5 mL microcentrifuge tubes and pelleted at 300 *g* for 5 min at 4°C. The supernatant was aspirated, and the cell pellets were resuspended in 200 µL of PBS/1% BSA containing 2 µg/mL propidium iodide (PI) as a marker for cell viability. Cells were analyzed for uptake of fluorescent polymer using a MACSQuant Analyzer flow cytometer (Miltenyi).

3.2.6   *In vitro cytotoxicity studies*

The cytotoxicities of various polymers were evaluated *in vitro* using the MTS assay. The cells were seeded in 96-well plates at a density of 2500 cells per well in 100 µL of complete growth medium and incubated in a 37°C, 5% CO_2 environment for 24 h. Samples were prepared in serial dilutions in water and then diluted 10-fold in Opti-MEM medium (Invitrogen). The cells were rinsed once with PBS and incubated with 40 µL of the sample solutions with different polymer concentrations at 37°C for 4 h. Cells were then rinsed with PBS and the medium was replaced with 100 µL of culture medium. At 48 h, 20 µL of 3-(4,5-dimethylthiazol-2-yl)-5-(3-carboxymethoxyphenyl)-2-(4-sulfophenyl)-2H-tetrazolium (MTS, Promega) reagent was added to each well. Cells were then incubated at 37°C, 5% CO_2 for 3 h. The absorbance of each well was measured at 490 nm on a Tecan Safire2 plate reader (Maïnnedorf, Switzerland). Cell viability (%) for each concentration was determined by normalizing to the cells only signal.
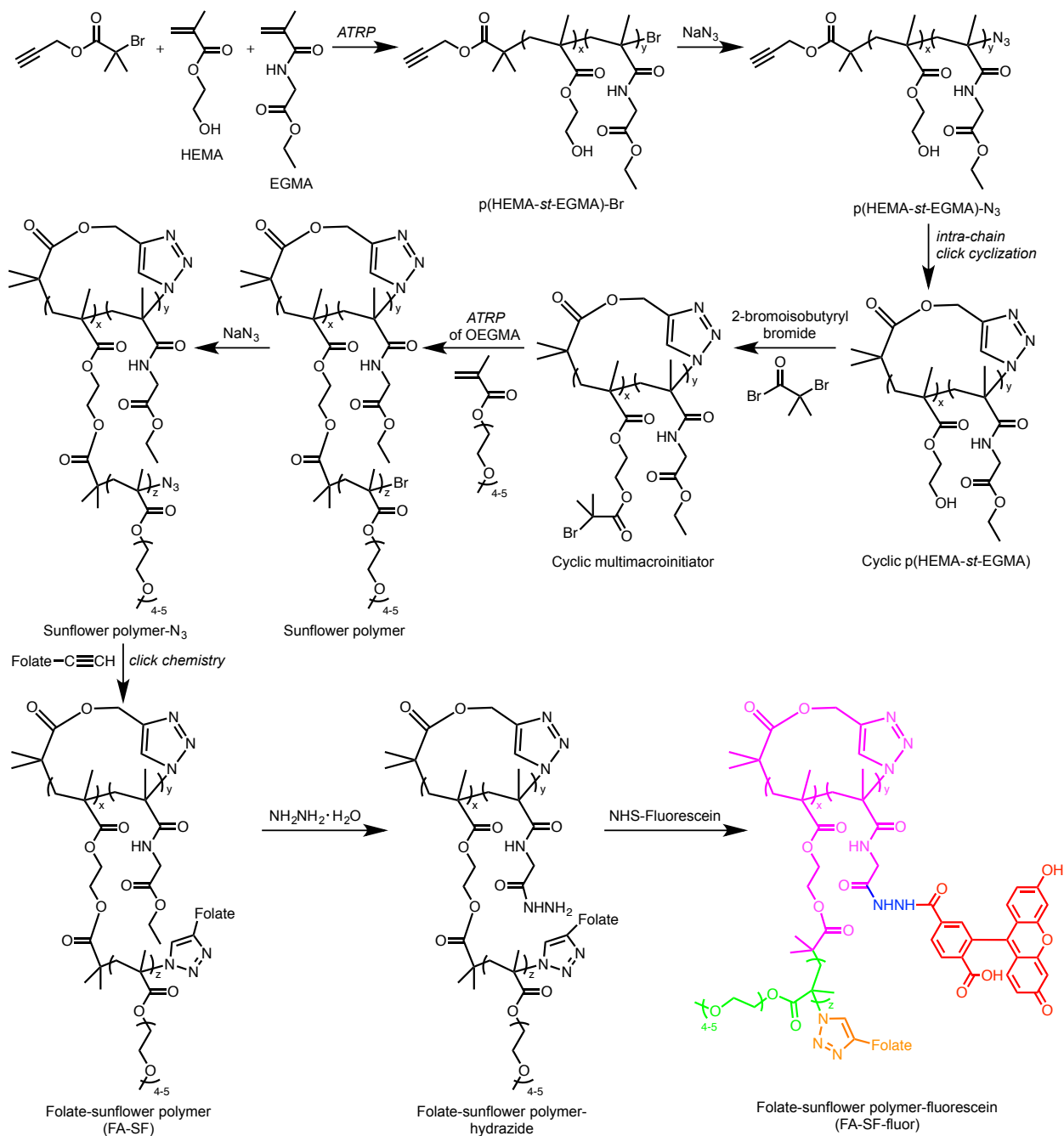
Figure 3.2 Synthesis of folate-sunflower polymer-fluorescein.

3.3   Results and discussion

3.3.1   Synthesis and characterization of sunflower polymers

The two main steps in sunflower polymer synthesis are (i) synthesis of the cyclic multimacroinitiator and (ii) polymerization of "petals" from the cyclized core (Figure 3.2).

51

The cyclic multimacroinitiator was first synthesized by (i) atom transfer radical copolymerization of ethyl glycinate methacrylamide (EGMA) and hydroxyethylmethacrylate (HEMA) using an alkyne-terminated initiator, (ii) conversion of the terminal bromine to an azide and intrachain click cyclization of the α-alkyne-ω-azide linear polymers, and (iii) conversion of HEMA monomers to alkyl halide ATRP initiators.

The ATRP conditions for the synthesis of P(HEMA-*st*-EGMA) copolymer were adapted from reported procedures[22] with some modifications considering that ATRP of acrylamide-type monomers remains challenging,[23] and more active ligands, such as 1,1,4,7,10,10-hexamethyltriethyllenetetramine (HMTETA),[24] *N,N,N',N'',N''*-pentamethyldiethylene-triamine (PMDETA),[25] and Tris[2-(dimethylamino)ethyl]amine (Me$_6$TREN),[26] can offer improved control over the polymerization. Linear P(HEMA-*st*-EGMA) was first synthesized using the CuBr/PMDETA catalyst in isopropanol/*N,N'*-dimethylformamide (IPA/DMF) (9/1, w/w) at 65°C for 16 h. The benefits of this current polymerization condition are confirmed by a kinetics study. The statistical copolymer panel showed a clear shift of the gel permeation chromatography (GPC) elution trace toward higher molecular weight with polymerization time (Figure 3.3). The living characteristics were reflected by the pseudo-first-order kinetics and narrow PDI during the whole polymerization process (Figure 3.3). A high conversion (~82%) of monomers was achieved after polymerization for 16 h, affording polymer of DP ~41, close to the target value of 50. Moreover, there was no obvious high molecular weight "shoulder" recorded in the GPC elution trace (Figure 3.3 and Figure 3.4a), indicating minimal coupling termination of polymer chains during polymerization and retention of chain end functionalities for further azidonation.
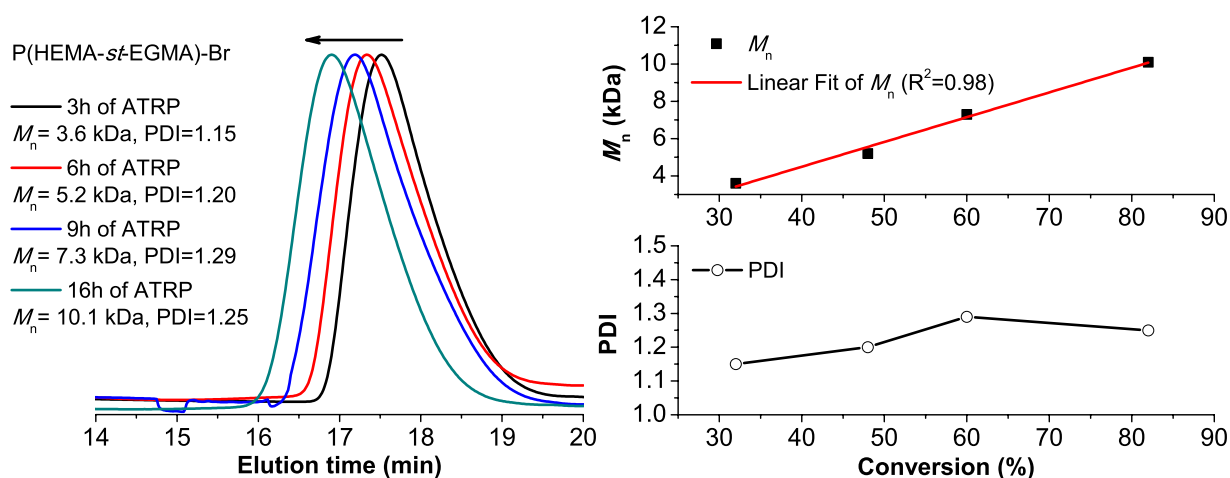
Figure 3.3 ATRP kinetics for the synthesis of P(HEMA-*st*-EGMA) copolymer.

The molar ratio of HEMA and EGMA in the resulting copolymers was determined to be 3.3:1 by ^{1}H NMR spectroscopy, close to the feed molar ratio (3:1), indicating good control of the copolymer composition by ATRP. The resulting copolymer was thus denoted P(HEMA$_{41}$-st-EGMA$_{12}$). GPC shows that the copolymers have molecular weight (M_n) of 4.86 kDa and relatively low polydispersity (PDI) of 1.27, indicating controlled synthesis of copolymers (Figure 3.4a).
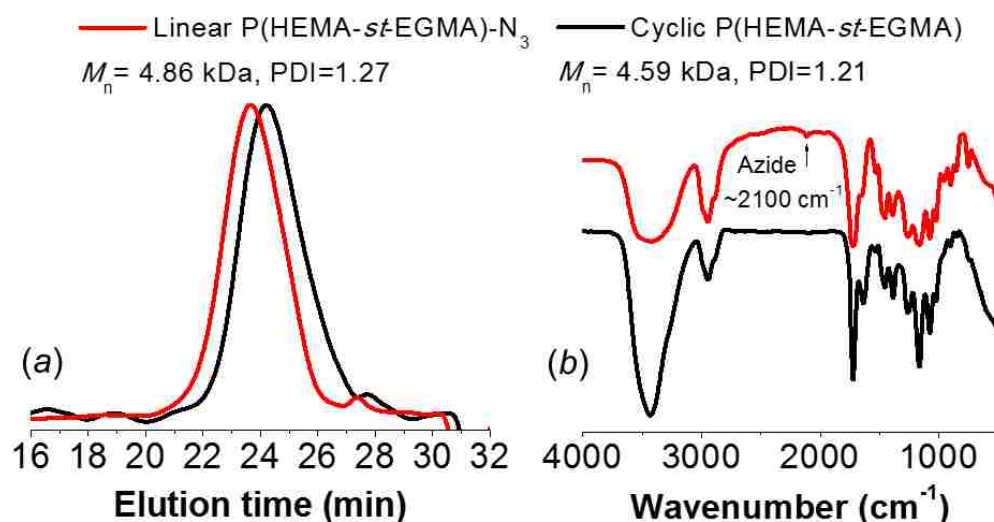
Figure 3.4   (a) GPC elution traces and (b) FT-IR spectra of linear and cyclic P(HEMA$_{41}$-st-EGMA$_{12}$).

A survey of the literature showed that a large excess of sodium azide (10-40 fold molar excess compared to bromo-termini)[27-30] is usually used for chain end azidonation to achieve complete conversion of the chain termini. Therefore, the linear precursor, P(HEMA-st-EGMA)-N$_3$, was prepared by substitution with a 20-fold molar excess of sodium azide. Cyclic polymers were then prepared by intra-chain Cu(I)-catalyzed azide-alkyne cycloaddition (CuAAc) of linear precursors following reported procedures.[31,32] Successful cyclization was confirmed by FT-IR and GPC analyses, which show absence of the azide group (~2100 cm^{-1}) after polymer cyclization and a clear shift toward longer retention times for the cyclic polymer compared to the linear precursor (Figure 3.4).

Cyclic poly(2-(2-bromoisobutyrnyloxy)ethyl methacrylate-st-EGMA) (P((HEMA-iBuBr)-st-EGMA)) multimacroinitiator was then prepared by esterification of cyclic P(HEMA-st-EGMA) with 2-bromoisobutyryl bromide. The disappearance of the characteristic signal at 4.8 ppm, assigned to the hydroxyl group of HEMA units, in the ^{1}H NMR spectrum of cyclic

53

multimacroinitiator compared to the parent cyclic polymer (Figure S3.1) confirms complete conjugation of ATRP initiating sites to the pendant hydroxyl groups of the cyclic polymer.

The cyclic multimacroinitiator and its linear analogue were used for ATRP of oligoethylene glycol methacrylate (OEGMA) to prepare sunflower and comb polymers, respectively. ATRP was performed using the catalyst CuBr/2,2'-bipyridine (bpy) in anisole/DMF (1/2, v/v) at 60°C for different lengths of time. Three important parameters were optimized to minimize the generation of cross-linked structures and free polymer chains in the ATRP process due to the use of multimacroinitiators: (i) the feed concentration of OEGMA monomer was kept at 0.5 M; (ii) the monomer conversion was controlled to a low level (below 25%); and (iii) a small amount of $CuBr_2$ ([$CuBr_2$] = 0.1[CuBr]) was added to slow down the polymerization kinetics. A kinetic study was carried out using cyclic multimacroinitiator with a target DP of 100 for each radiating petal. The sunflower polymer panel showed a clear shift of the GPC elution trace toward higher molecular weight with polymerization time (Figure 3.5). The living characteristics were reflected by the pseudo-first-order kinetics and narrow PDI (around 1.3) during the whole polymerization process (Figure 3.5). Furthermore, the difference in topology of sunflower versus comb-like polymers was confirmed by GPC analyses. Sunflower polymers eluted at later times than comb polymers, indicating more compact structure and smaller effective molecular weight (Figure 3.6).
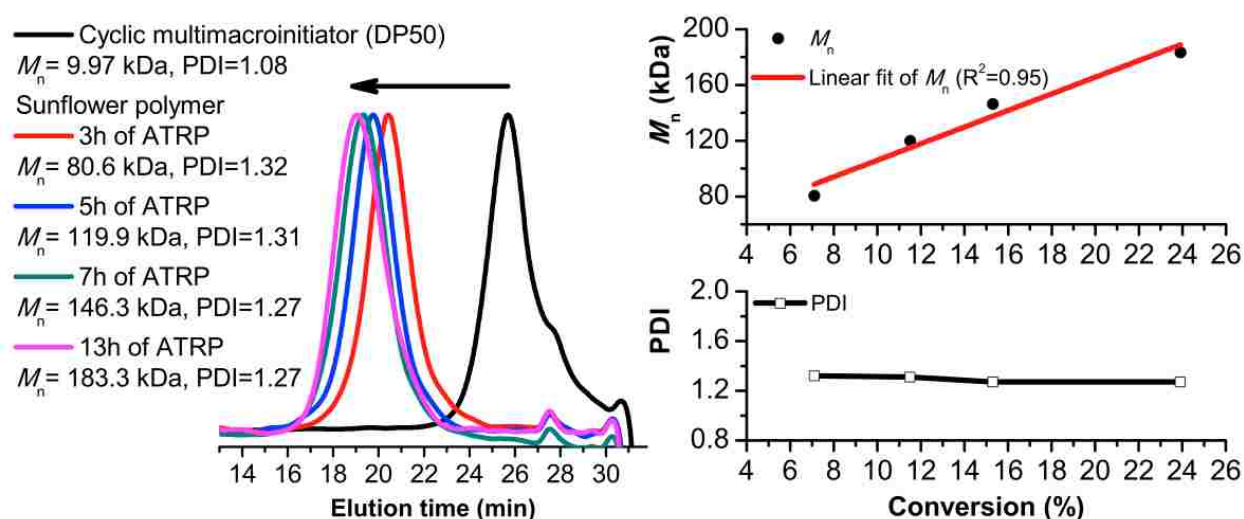
Figure 3.5 ATRP kinetics of sunflower polymer prepared from cyclic multimacroinitiator, with a target DP of 100 for each petal.

54
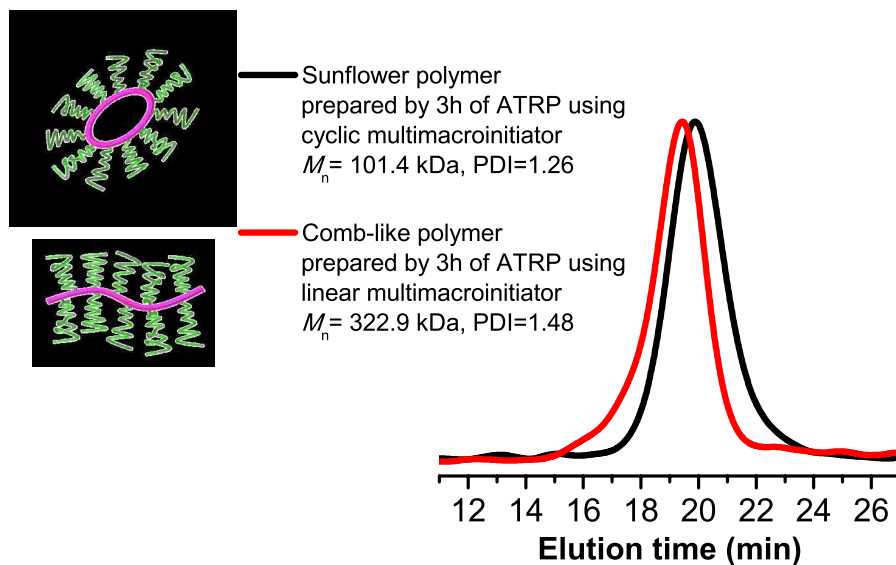
Figure 3.6 GPC elution traces of sunflower polymer and comb-like polymer prepared with the same polymerization time using cyclic and linear multimacroinitiators.

Finally, the hydrodynamic Z-average diameters of sunflower polymers were determined by dynamic light scattering (DLS). Particle size increased with increasing P(OEGMA) petal polymerization time, ranging from 13.5 to 16.8 nm for the panel (Figure 3.7). The ability to control particle size is a particular advantage of using this polymerization strategy for synthesizing drug carriers.
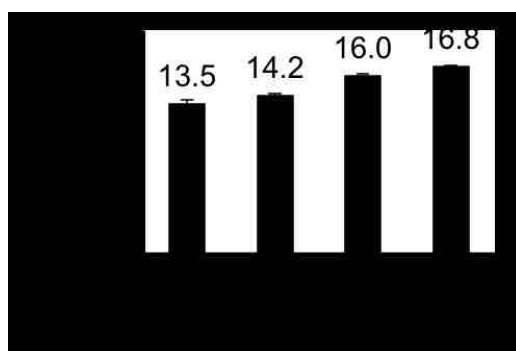
Figure 3.7 Summary of Z-average sizes of sunflower polymers with petals polymerized for different lengths of time.

3.3.2   *Synthesis of folate-targeted sunflower polymers and evaluation of uptake in FR+ cells*

The sunflower polymer with petals synthesized by 3 h ATRP of OEGMA (M_n = 101 kDa, PDI = 1.26, R_h = 14 nm) was selected for further biological evaluation. Targeted polymer

constructs were prepared by conjugation of alkyne-functionalized folate (FA) to the P(OEGMA) petal termini via CuAAC "click" coupling. FA was selected for targeting due to significant literature precedence establishing drug carrier targeting to cancer cells via the folate receptor (FR).[33-36] FA conjugation was confirmed by ^{1}H NMR analysis, which shows the appearance of characteristic signals at 6.7-8.7 ppm (assigned to the aromatic protons of folate) in the spectrum of folate-sunflower polymer, and by an increase in UV absorbance on GPC (Figure S3.2). Each polymer was found to contain approximately 25-28 folate groups, a conjugation efficiency of 61-69% based on the theoretical polymer composition of 41 HEMA groups available for polymerization of petals and subsequent folate conjugation.

We next investigated FR-mediated uptake of the sunflower polymers in KB (FR+) and A549 (FR-) cells. Fluorescein was selected as a model drug due to its fluorescent and cell compatibility properties; in future work, aldehyde or ketone-containing drugs could be similarly conjugated to sunflowers for acid-triggered release at tumor sites. FA-SF-fluor was prepared by converting EGMA side chains in the polymer's cyclic core to hydrazide groups, followed by conjugation with the *N*-hydroxysuccinimide ester of fluorescein. An estimated 6-8 fluorescein molecules were conjugated per polymer, a conjugation efficiency of 59-78% based on the theoretical polymer composition of 12 EGMA groups and 85% conversion of EGMA to hydrazide groups for fluorescein incorporation.

Cells were then incubated with FA-SF-fluor at various concentrations, followed by flow cytometry analysis for binding. Although FA-SF-fluor uptake is dose-dependent in both cell lines, greater uptake was observed in the FR+ KB cells than in the A549 cells, as indicated by higher median fluorescence intensities of these cells at all polymer concentrations (Figure 3.8a). Minimal uptake of untargeted SF-fluor was observed in either cell line (Figure 3.8b). In competition studies, cells were treated with FA-SF-fluor in the presence of 2 mM free folate. Competition with free folate significantly reduced polymer uptake in KB cells but not in A549 cells. These results further support folate receptor-mediated endocytosis as a major uptake mechanism for FA-targeted sunflower polymers by FR+ KB cells.

Interestingly, when uptake of the comb-like linear analogue, FA-comb-fluor, was investigated, competition with free folate produced only a small decrease in polymer uptake in KB cells even at a low polymer concentration (Figure 3.8c). This may suggest higher levels of non-specific uptake of comb polymers relative to sunflower polymers. The effect of

56

polymer architecture on internalization mechanism will therefore be an interesting topic for future investigation.
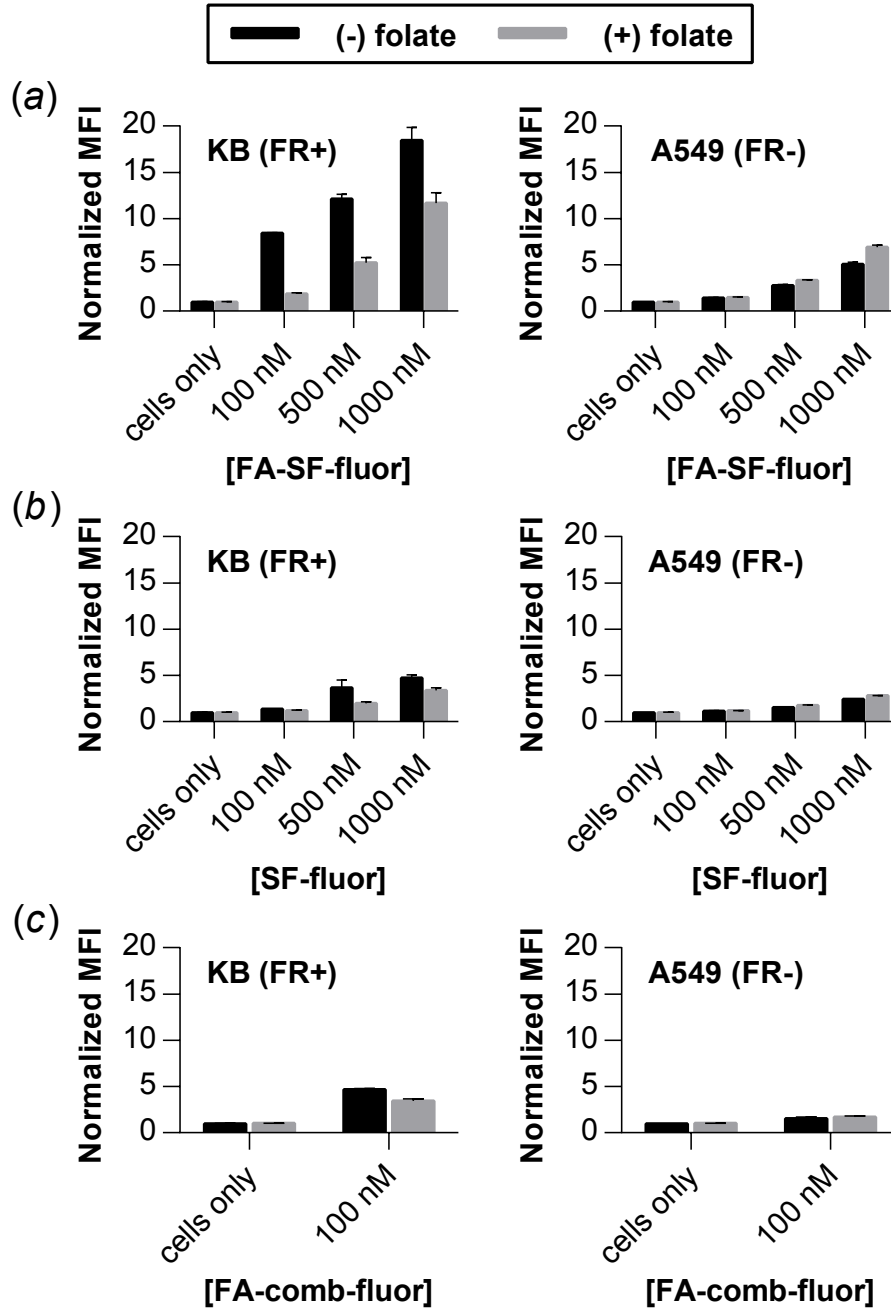
Figure 3.8 Uptake of (a) FA-SF-fluor, (b) untargeted SF-fluor, and (c) FA-comb-fluor polymers in FR+ KB cells and FR- A549 cells in the absence (black bars) and presence (grey bars) of 2 mM competing free folate.

57

3.3.3   *Cytotoxicity of sunflower polymers*

Because sunflower polymers demonstrate potential as drug carriers, we investigated the cytotoxicity of the materials using KB and A549 cells. An MTS metabolic activity assay was performed to determine cell viability. The base and FA-modified sunflower polymers were found to be minimally toxic in either cell line, with IC_{50}, or concentration for 50% cell killing, greater than 3.5 mg/mL in all cases.

3.4   *Conclusions*

In summary, this work introduces the sunflower polymer platform as a potential drug carrier. Using a combination of ATRP and click chemistry, sunflower polymers can be synthesized with control over hydrodynamic size based on polymerization time. The ability to tailor sizes within the relevant range for tumor delivery (5-50 nm), combined with the demonstrated advantage over comb-like polymers in targeted cellular uptake, support further investigation of these materials for tumor-targeted drug delivery and molecular imaging.

3.5   *Acknowledgements*

References

1. Laurent, B. A. & Grayson, S. M. Synthesis of cyclic dendronized polymers via divergent "graft-from" and convergent click 'graft-to' routes: preparation of modular toroidal macromolecules. *J. Am. Chem. Soc.* **133,** 13421–13429 (2011).
2. Laurent, B. A. & Grayson, S. M. Synthesis of cyclic amphiphilic homopolymers and their potential application as polymeric micelles. *Polym Chem* **3,** 1846–1855 (2012).
3. Liu, L., Parameswaran, S., Sharma, A., Grayson, S. M., Ashbaugh, H. S. & Rick, S. W. Molecular dynamics simulations of linear and cyclic amphiphilic polymers in aqueous and organic environments. *J Phys Chem B* **118,** 6491–6497 (2014).
4. Johnson, J. A., Lu, Y. Y., Burts, A. O., Lim, Y.-H., Finn, M. G., Koberstein, J. T.,

Turro, N. J., Tirrell, D. A. & Grubbs, R. H. Core-clickable PEG-branch-azide bivalent-bottle-brush polymers by ROMP: grafting-through and clicking-to. *J. Am. Chem. Soc.* **133,** 559–566 (2011).

5. Sheiko, S. S., Sumerlin, B. S. & Matyjaszewski, K. Cylindrical molecular brushes: Synthesis, characterization, and properties. *Progress in Polymer Science* **33,** 759–785 (2008).

6. Hawker, C. J., Fréchet, J. M. J., Grubbs, R. B. & Dao, J. Preparation of Hyperbranched and Star Polymers by a 'Living', Self-Condensing Free Radical Polymerization. *J. Am. Chem. Soc.* **117,** 10763–10764 (1995).

7. Trollsås, M. & Hedrick, J. L. Dendrimer-like Star Polymers. *J. Am. Chem. Soc.* 4644–4651 (1998). doi:10.1021/ja973678w

8. Lane, D. D., Chiu, D. Y., Su, F. Y., Srinivasan, S., Kern, H. B., Press, O. W., Stayton, P. S. & Convertine, A. J. Well-defined single polymer nanoparticles for the antibody-targeted delivery of chemotherapeutic agents. *Polym Chem* **6,** 1286–1299 (2015).

9. Smet, M. Biological and Medical Applications of Hyperbranched Polymers. *Hyperbranched Polymers: Synthesis, Properties, and Applications* 387–413 (2011).

10. Wang, C. E., Stayton, P. S., Pun, S. H. & Convertine, A. J. Polymer Nanostructures Synthesized by Controlled Living Polymerization for Tumor-Targeted Drug Delivery. *J Control Release* (2015). doi:10.1016/j.jconrel.2015.08.054

11. Chen, B., Jerger, K., Fréchet, J. M. J. & Szoka, F. C. The influence of polymer topology on pharmacokinetics: differences between cyclic and linear PEGylated poly(acrylic acid) comb polymers. *J Control Release* **140,** 203–209 (2009).

12. Nasongkla, N., Chen, B., Macaraeg, N., Fox, M. E., Fréchet, J. M. J. & Szoka, F. C. Dependence of Pharmacokinetics and Biodistribution on Polymer Architecture: Effect of Cyclic versus Linear Polymers. *J. Am. Chem. Soc.* **131,** 3842–3843 (2009).

13. Coulembier, O., Moins, S., De Winter, J., Gerbaux, P., Leclère, P., Lazzaroni, R. & Dubois, P. From Jellyfish Macromolecular Architectures to Nanodoughnut Self-Assembly. *Macromolecules* **43,** 575–579 (2010).

14. Xia, Y., Boydston, A. J. & Grubbs, R. H. Synthesis and Direct Imaging of Ultrahigh Molecular Weight Cyclic Brush Polymers. *Angew. Chem. Int. Ed. Engl.* **50,** 5882–5885 (2011).

15. Zhang, K. & Tew, G. N. Cyclic Brush Polymers by Combining Ring-Expansion Metathesis Polymerization and the 'Grafting from' Technique. *ACS Macro Lett.* **1,** 574–579 (2012).

16. Jia, Z. F. & Monteiro, M. J. Cyclic Polymers: Methods and Strategies. *J. Polym. Sci. A Polym. Chem.* **50,** 2085–2097 (2012).

17. Matyjaszewski, K. & Tsarevsky, N. V. Macromolecular engineering by atom transfer radical polymerization. *J. Am. Chem. Soc.* **136,** 6513–6533 (2014).

18. Wei, H., Chu, D. S., Zhao, J., Pahang, J. A. & Pun, S. H. Synthesis and evaluation of cyclic cationic polymers for nucleic acid delivery. *ACS Macro Lett.* **2,** 1047–1050 (2013).

19. Zhang, H., Cai, Z., Sun, Y., Yu, F., Chen, Y. & Sun, B. Folate-conjugated β-cyclodextrin from click chemistry strategy and for tumor-targeted drug delivery. *Journal of Biomedical Materials Research Part A* **100,** 2441–2449 (2012).

20. Etrych, T., Jelínková, M., Říhová, B. & Ulbrich, K. New HPMA copolymers containing doxorubicin bound via pH-sensitive linkage: synthesis and preliminary in vitro and in vivo biological properties. *J. Control. Release* **73,** 89–102 (2001).

21. Zhan, F., Chen, W., Wang, Z., Lu, W., Cheng, R., Deng, C., Meng, F., Liu, H. &

Zhong, Z. Acid-activatable prodrug nanogels for efficient intracellular doxorubicin release. *Biomacromolecules* **12,** 3612–3620 (2011).

22. Yang, P. & Armes, S. P. Preparation of Well-Defined Poly (2-hydroxyethyl methacrylate) Macromonomers via Atom Transfer Radical Polymerization. *Macromol. Rapid Commun.* **35,** 242–248 (2014).

23. Teodorescu, M. & Matyjaszewski, K. Atom transfer radical polymerization of (meth) acrylamides. *Macromolecules* **32,** 4826–4831 (1999).

24. Xu, F., Zheng, S. Z. & Luo, Y. L. Thermosensitive t-PLA-b-PNIPAAm tri-armed star block copolymer nanoscale micelles for camptothecin drug release. *J. Polym. Sci. A Polym. Chem.* **51,** 4429–4439 (2013).

25. Wang, J., Gao, P., Ye, L., Zhang, A.-Y. & Feng, Z.-G. Dual thermo-responsive polyrotaxane-based triblock copolymers synthesized via ATRP of N-isopropylacrylamide initiated with self-assemblies of Br end-capped Pluronic F127 with β-cyclodextrins. *Polym Chem* **2,** 931–940 (2011).

26. Xia, Y., Yin, X., Burke, N. A. & Stöver, H. D. Thermal response of narrow-disperse poly (N-isopropylacrylamide) prepared by atom transfer radical polymerization. *Macromolecules* **38,** 5937–5943 (2005).

27. Cai, T., Yang, W. J., Neoh, K.-G. & Kang, E.-T. Preparation of jellyfish-shaped amphiphilic block-graft copolymers consisting of a poly(?-caprolactone)-block-poly(pentafluorostyrene) ring and poly(ethylene glycol) lateral brushes. *Polym. Chem.* **3,** 1061–1068 (2012).

28. Chen, F., Liu, G. & Zhang, G. Synthesis of cyclic polyelectrolyte via direct copper(I)-catalyzed click cyclization. *J. Polym. Sci. A Polym. Chem.* **50,** 831–835 (2011).

29. Jiang, X., Shi, Y., Zhu, W., Chen, Y. & Xi, F. Synthesis of mikto-topology star polymer containing one cyclic arm. *J. Polym. Sci. A Polym. Chem.* **50,** 4239–4245 (2012).

30. Ren, J. M., Satoh, K., Goh, T. K., Blencowe, A., Nagai, K., Ishitake, K., Christofferson, A. J., Yiapanis, G., Yarovsky, I., Kamigaito, M. & Qiao, G. G. Stereospecific Cyclic Poly(methyl methacrylate) and Its Topology-Guided Hierarchically Controlled Supramolecular Assemblies. *Angew. Chem. Int. Ed. Engl.* **53,** 459–464 (2013).

31. Laurent, B. A. & Grayson, S. M. An efficient route to well-defined macrocyclic polymers via 'click' cyclization. *J. Am. Chem. Soc.* **128,** 4238–4239 (2006).

32. Wei, H., Chu, D. S., Zhao, J., Pahang, J. A. & Pun, S. H. Synthesis and evaluation of cyclic cationic polymers for nucleic acid delivery. *ACS Macro Lett.* **2,** 1047–1050 (2013).

33. Lee, S.-M., Chen, H., O'Halloran, T. V. & Nguyen, S. T. 'Clickable' polymer-caged nanobins as a modular drug delivery platform. *J. Am. Chem. Soc.* **131,** 9311–9320 (2009).

34. Low, P. S., Henne, W. A. & Doorneweerd, D. D. Discovery and development of folic-acid-based receptor targeting for imaging and therapy of cancer and inflammatory diseases. *Acc. Chem. Res.* **41,** 120–129 (2007).

35. Lu, Y. & Low, P. S. Folate-mediated delivery of macromolecular anticancer therapeutic agents. *Advanced Drug Delivery Reviews* **64,** 342–352 (2012).

36. Yang, X., Grailer, J. J., Pilla, S., Steeber, D. A. & Gong, S. Tumor-targeting, pH-responsive, and stable unimolecular micelles as drug nanocarriers for targeted cancer therapy. *Bioconjug. Chem.* **21,** 496–504 (2010).
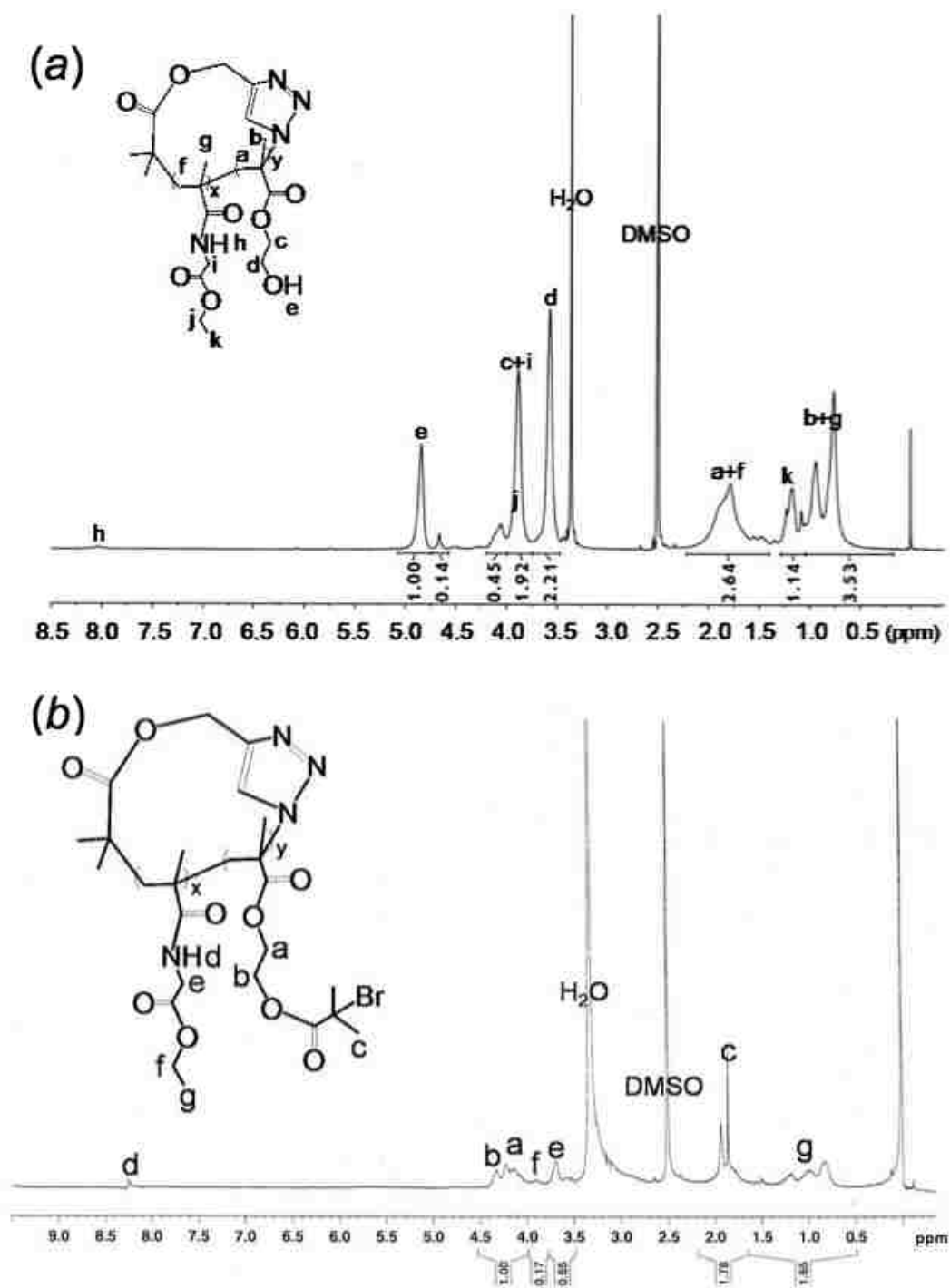
Figure S3.1 ¹H NMR spectra of (a) cyclic P(HEMA-*st*-EGMA) and (b) cyclic multimacroinitiator.

61
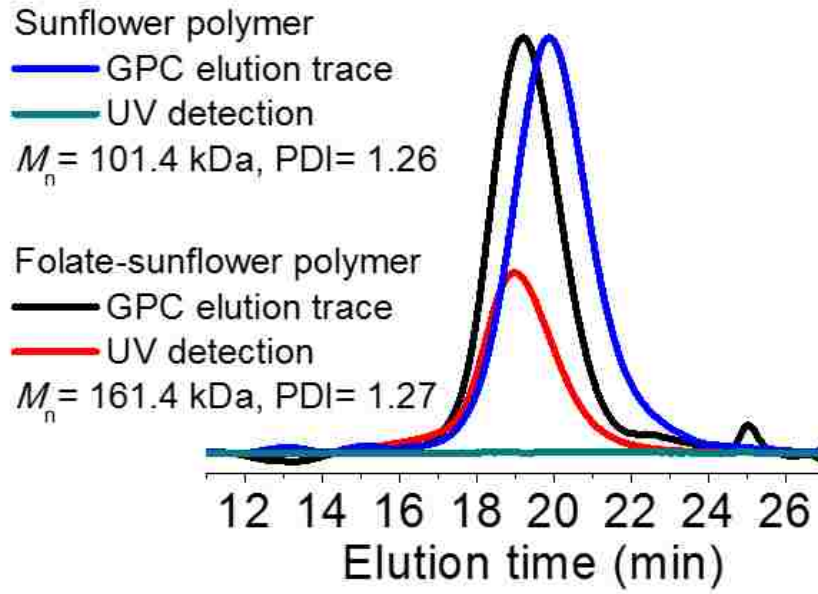
Figure S3.2 GPC elution traces and UV-detected signals of sunflower polymer and folate-conjugated sunflower polymer.

Chapter 4.

SUNFLOWER POLYMERS FOR FOLATE-MEDIATED DRUG DELIVERY

Christine E. Wang*, Hua Wei*, Nicholas Tan, Andrew J. Boydston, and Suzie H. Pun

Equally contributing authors

Abstract

Polymeric delivery vehicles can improve the safety and efficacy of chemotherapy drugs by facilitating preferential tumor delivery. Polymer-drug conjugates are especially attractive carriers because additional formulation steps are not required during manufacturing, and drug release profiles can be altered based on linker choice. For clinical translation, these vehicles should also be reproducibly and controllably synthesized. Recently, we reported the development of a class of materials called "sunflower polymers," synthesized by controlled radical polymerization of hydrophilic "petals" from a cyclic multimacroinitiator "core." This synthesis strategy afforded control over the size of the polymer nanostructures based on their petal polymerization time. In this work, we demonstrate that particle size can be further tuned by varying the degree of polymerization of the cyclic core in addition to that of the petals. Additionally, we investigate the application of these materials for tumor-targeted drug delivery. We demonstrate that folate-targeted, doxorubicin-conjugated sunflower polymers undergo receptor-mediated uptake into cancer cells and pH-triggered drug release leading to cytotoxicity. These materials are attractive as drug carriers due to their discrete and small size, shielded drug cargo that can be triggered for release, and relative ease of synthesis.†

4.1   Introduction

Cytotoxic chemotherapy remains the preferred frontline strategy for treatment against most types of cancer but is associated with significant side effects such as major organ

---

† Reprinted with permission from Wang, C. E., *et al. Biomacromolecules*, **17**, pp. 69-75. Copyright 2016 American Chemical Society.

damage, infertility, immunosuppression, and nausea/vomiting that severely compromise patient quality of life.[1,2] The development of improved chemotherapy formulations therefore remains an important research priority with significant medical impact. The adverse side effects associated with chemotherapy can be ameliorated by developing delivery formulations that rely on tumor localization via the "enhanced permeability and retention" (EPR) effect.[3] These formulations are large enough to be retained in the circulation after injection, avoiding tissue distribution and rapid renal clearance, but remain small enough to extravasate from abnormal tumor vasculature into tumors.[4,5] This paradigm is used by clinically-approved chemotherapy formulations such as liposomal anthracyclines (e.g., Doxil and Myocet) and albumin-bound paclitaxel (Abraxane) to offer improved safety profiles over equivalent solution formulations.

Still, drawbacks to these formulations remain. Multiple formulation steps are often required in manufacturing, increasing scale-up complexity.[6] Interstitial tumor penetration is also reduced due to the larger size of these formulations (50-150 nm) compared to free drug.[7-9] Finally, drug leakage from the vehicle prior to tumor localization can result in off-target effects.[10,11]

Polymer-drug conjugates are an alternative delivery technology in the development pipeline.[12,13] The smaller size of these constructs compared to liposomal carriers and drug attachment via labile linkages allow for improved tumor penetration and controlled drug release. In contrast to polymeric carriers such as micelles or nanoencapsulates,[14,15] polymer-drug conjugates do not require formulation steps during manufacturing. Dendrimers, star polymers, and cyclic polymers have prolonged circulation *in vivo* compared to linear polymers, an important property in tumor accumulation via EPR.[16-18] Therefore, polymers with advanced architectures that can be reproducibly and controllably synthesized are of great interest as drug carriers.

We have recently described a strategy for synthesizing macrocyclic brush or "sunflower" (SF) polymers[19] using atom transfer radical polymerization (ATRP) and a "grafting-from" approach.[20,21] We demonstrated that sunflower polymers could be synthesized with relatively low polydispersity and with control over their hydrodynamic size based on the polymerization time of their radiating "petals." Because the folate receptor (FR) is commonly overexpressed on various cancer cell types,[22,23] we also conjugated the petal termini with folate (FA) as a targeting ligand and the polymer "core" with fluorescein as a model drug to demonstrate receptor-mediated uptake in FR-positive

cells. These sunflower polymers appeared to have an advantage over their linear analogues (comb-like polymers), which were shown to be taken up by non-specific mechanisms.

In this work, we have expanded on our platform by synthesizing sunflower polymers with two different core sizes and then applied these materials for targeted drug delivery through conjugation of FA to the sunflower petals and doxorubicin to the sunflower cores. Together with the petal polymerization time, controlling core size allows for greater control over the hydrodynamic size of the polymers. We investigate the uptake properties as compared to the previously reported small-core sunflowers. We further demonstrate that sunflower polymers can be used for targeted, intracellular drug delivery by conjugating the chemotherapy drug doxorubicin (Dox) via hydrazone bonds that release drug under acidic conditions (Figure 4.1). Finally, we investigate the cytotoxicity of the various polymer-Dox constructs synthesized.
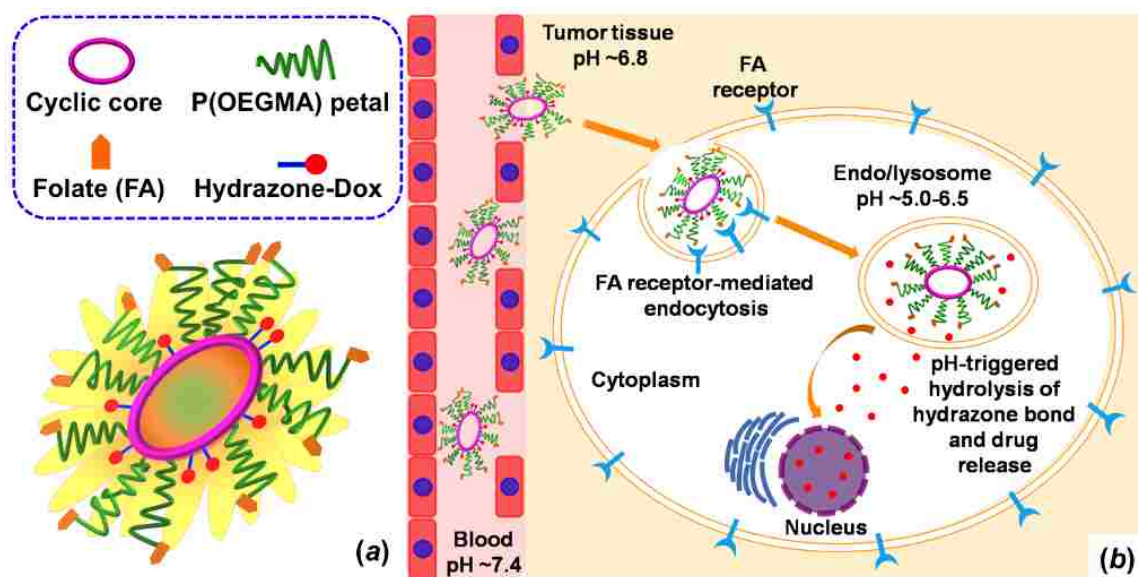
Figure 4.1 Schematic illustrations of (a) sunflower polymer containing FA targeting ligands and Dox drug and (b) proposed delivery mechanism: extravasation into tumor tissue by EPR effect, internalization by FR-expressing cancer cells, and intracellular, pH-triggered Dox release.

65

4.2 Materials and methods

4.2.1 Materials

All chemicals were purchased from Sigma-Aldrich and used without further purification unless otherwise noted.

4.2.2 Polymer synthesis and Dox conjugation

Preparation of P((HEMA-sunflower-OEGMA-folate)-st-(GMA-hydrazide)) (FA-SF-hydrazide)

All steps for the synthesis of the folate-targeted, hydrazide-containing sunflower polymer were performed as reported previously,[19] but using a HEMA:initiator molar ratio of 100:1 in the synthesis of the linear P(HEMA-*st*-EGMA) precursor to yield sunflower polymers with a larger core.

Preparation of P((HEMA-sf-OEGMA-folate)-st-(GMA-fluorescein)) (FA-SF-fluor)

A 50 mL falcon tube equipped with a magnetic stirrer was charged with the polymer precursor P((HEMA-*sf*-OEGMA-folate)-*st*-(GMA-hydrazide)) (146.0 mg, 14.5 μmol of hydrazide), NHS-Fluorescein (Thermo Scientific, 13.7 mg, 29.0 μmol), and anhydrous methanol (4 mL). The tube was sealed, and the reaction mixture was placed in the dark at room temperature for 48 h. The resultant fluorescein-labeled sunflower polymer, P((HEMA-*sf*-OEGMA-folate)-*st*-(GMA-fluorescein)), was purified by extensive dialysis against distilled water (4 L) for 24 h and collected by freeze-drying. Yield: 67.0% (97.8 mg). The amount of fluorescein conjugated to the sunflower polymer was determined by ^{1}H NMR analysis as described previously.[19]

Preparation of P((HEMA-sf-OEGMA-folate)-st-(GMA-Dox)) (FA-SF-Dox)

A 50 mL falcon tube equipped with a magnetic stirrer was charged with the polymer precursor P((HEMA-*sf*-OEGMA-folate)-*st*-(GMA-hydrazide)) (180.0 mg, 29.2 μmol of hydrazide), doxorubicin hydrochloride (Dox•HCl, LC Laboratories, Woburn, MA) (33.8 mg, 58.4 μmol), a drop of acetic acid, and anhydrous methanol (6 mL). The tube was sealed, and

66

the reaction mixture was placed in the dark at room temperature for 48 h. The resultant sunflower polymeric prodrug, P((HEMA-*sf*-OEGMA-folate)-*st*-(GMA-Dox)), was purified by extensive dialysis against anhydrous methanol (2 L) for 24 h, followed by dialysis against distilled water (4 L) for another 24 h, and collected by freeze-drying. Yield: 78.7% (155 mg). The amount of Dox conjugated to the sunflower polymer was determined by absorbance at 480 nm based on a standard curve obtained from free Dox•HCl in water.

4.2.3   Polymer characterization

^{1}H NMR spectra were recorded on a Bruker AV 500 nuclear magnetic resonance (NMR) instrument using DMSO-d_6 as the solvent.

Fourier transform infrared (FT-IR) spectra were recorded on a Bruker Vector 33 FT-IR spectrometer. Samples were pressed into potassium bromide (KBr) pellets for measurements.

Gel permeation chromatography (GPC) was used to determine molecular weight and polydispersity (M_w/M_n, PDI) of polymer samples prepared. SEC Tosoh TSK-GEL R-3000 and R-4000 columns (Tosoh Bioscience, Montgomeryville, PA) were connected in series to an Agilent 1200 Series System (Agilent Technologies, Santa Clara, CA), Optilab-rEX refractometer, and miniDAWN TREOS triple-angle static light scattering detector (Wyatt Technology, Santa Barbara, CA). HPLC-grade DMF containing 0.1 wt% LiBr at 60°C was used as the mobile phase at a flow rate of 1 mL/min. Absolute molecular weight averages and dn/dc were calculated using ASTRA software (Wyatt).

Average dimensions of sunflower polymers in an aqueous phase were measured by dynamic light scattering (DLS) with a ZetaPALS (Brookhaven Instruments Corp.) at a detection angle of 90°. The measurements were performed in triplicate. The aqueous solution was passed through a 0.22 μm pore-sized syringe filter before measurements.

4.2.4   Quantification of Dox release

FA-SF-Dox polymer was dissolved in release buffer at different pHs (PBS at pH 7.4, phosphate buffer at pH 6.8, or citrate buffer at pH 5.5) at a concentration of 1 mg/mL. Spectra/Por Float-A-Lyzer G2 Dialysis Devices (MWCO: 8-10 kDa, Spectrum Laboratories)

were pre-soaked in release buffer for 30 min, then loaded with 1 mL of polymer solution each. Each device was immersed in a 50 mL conical containing 12 mL of the same release buffer and incubated in the dark at 37°C with shaking at 125 rpm. At predetermined times, 1 mL of the dialysate was sampled and replaced with an equal volume of fresh buffer. Dialysate samples were stored at -20°C for later analysis. After all time points were collected, dialysate samples were analyzed for Dox fluorescence (excitation: 480 nm, emission: 580 nm) on a Tecan Safire2 plate reader (Männedorf, Switzerland). The concentration of released Dox in each sample was calculated based on standard curves obtained from free Dox•HCl in the respective release buffer.

4.2.5   Cell culture

KB cells (ATCC CCL-17) and A549 cells (ATCC CCL-185) were maintained in folate-free RPMI 1640 (Life Technologies) and F-12K (Corning cellgro) media, respectively. Media was supplemented with 10% fetal bovine serum (FBS, HyClone) and 1% penicillin/streptomycin (HyClone). Cells were cultured as a monolayer in a 37°C, 5% CO_2 environment. Medium was replaced every 2-3 days. Cells were passaged at ~70-80% confluence by incubation with Trypsin-EDTA, followed by resuspension in complete growth medium.

4.2.6   Serum stability studies

Sunflower polymers were incubated in cell culture medium (MEM supplemented with 10% FBS) for 4 h at 37°C. The resultant polymer was recovered by extraction using dichloromethane (DCM), vacuum dried, and analyzed by GPC.

4.2.7   In vitro uptake and competition studies

Cells were seeded in 24-well plates at a density of 40,000 cells per well in 1 mL of complete growth medium and incubated in a 37°C, 5% CO_2 environment for 24 h. Cells were rinsed once with PBS and incubated in 1 mL of supplemented folate-free RPMI 1640 medium +/- 2 mM folate competition for 1 h at room temperature. Polymer samples at varying concentrations were prepared in serial dilutions in water and then diluted 10-fold in

68

supplemented folate-free RPMI 1640 medium +/- 2 mM folate. The media was aspirated from each well, and cells were incubated with 200 µL of polymer solution for 20 min at 37°C. After incubation, the polymer solutions were aspirated, and the cells were rinsed twice with PBS/1% BSA. Cells were then harvested by incubation with 200 µL of Trypsin-EDTA, followed by resuspension with 1 mL of complete growth medium. Cells were transferred to 1.5 mL microcentrifuge tubes and pelleted at 300 g for 5 min at 4°C. The supernatant was aspirated, and the cell pellets were resuspended in 200 µL of PBS/1% BSA containing 2 µg/mL propidium iodide (PI) as a marker for cell viability. Cells were analyzed for uptake of fluorescent polymer using a MACSQuant Analyzer flow cytometer (Miltenyi).

4.2.8   Confocal imaging

KB cells were seeded on poly-D-lysine-coated glass coverslips in 24-well plates at a density of 80,000 cells per well in 1 mL of complete growth medium and incubated in a 37°C, 5% CO_2 environment for 12 h. Solutions of FA-SF-Dox polymer and free Dox were prepared in complete growth medium at concentrations equal to 25% of their respective IC_{50} values. Cells were treated with 400 µL of FA-SF-Dox or free Dox for 12 h at 37°C. Cells were rinsed 3 times with HBSS/1% BSA, fixed with 300 µL of 4% paraformaldehyde (PFA) solution for 15 min at room temperature, and rinsed twice with HBSS/1% BSA. Finally, cells were counterstained with 300 µL of 5 µg/mL 4',6-diamidino-2-phenylindole (DAPI) in HBSS/1% BSA for 5 min at room temperature and rinsed twice more. Coverslips were mounted onto glass slides with Fluoromount-G (eBioscience) and imaged using a Leica TCS SP8X confocal microscope.

4.2.9   In vitro cytotoxicity studies

The cytotoxicities of various formulations were evaluated *in vitro* using the MTS assay. The cells were seeded in 96-well plates at a density of 2500 cells per well in 100 µL of complete growth medium and incubated in a 37°C, 5% CO_2 environment for 24 h. Samples were prepared in serial dilutions in water and then diluted 10-fold in OptiMEM medium (Invitrogen). The cells were then rinsed once with PBS and incubated with 40 µL of the sample solutions with different polymer or Dox concentrations at 37°C for 4 h. Cells were

69

then rinsed with PBS, and the medium was replaced with 100 µL of culture medium. At 48 h, 20 µL of 3-(4,5-dimethylthiazol-2-yl)-5-(3-carboxymethoxyphenyl)-2-(4-sulfophenyl)-2H-tetrazolium (MTS, Promega) reagent was added to each well. Cells were then incubated at 37°C, 5% CO_2 for 3 h. The absorbance of each well was measured at 490 nm on a Tecan Safire2 plate reader (Männedorf, Switzerland). Cell viability for each treatment condition was determined by normalizing to the cells only signal.

4.2.10   Animals

Female NCr nude mice (4-5 weeks) were purchased from Taconic. All experimental procedures were performed in accordance with protocols approved by the University of Washington Institutional Animal Care and Use Committee.

4.2.11   Tumor inhibition studies

NCr nude mice were placed on a folic acid-deficient diet (Harlan Laboratories, Indianapolis, IN) for at least one week before tumor inoculation and were maintained on the special feed throughout the study. To develop xenograft tumors, mice were inoculated subcutaneously in the right hind flank with 5×10^6 KB cells in 100 µL of folate-free RPMI 1640 medium without serum.

After tumor inoculation, mice were randomly distributed into treatment groups of 7 mice each. Mice receiving a single treatment (on day 7 after tumor inoculation) were injected with free Dox or FA-SF-Dox at a dose of 6 mg Dox/kg mouse, or FA-SF at an equivalent polymer concentration. Mice receiving three treatments (on days 7, 10, and 13 after tumor inoculation) were injected with free Dox or FA-SF-Dox at a dose of 4 mg Dox/kg mouse per treatment, or FA-SF at an equivalent polymer concentration. Each formulation was administered intravenously by retroorbital injection in 5% glucose and in a volume of less than 150 µL. In addition, control mice were given a single injection of 5% glucose solution.

Tumor volume was calculated by measuring the tumor with calipers and using the formula *volume = 0.5 × a × b²*, where *a* is the longer of the two dimensions. Tumor measurements and mouse weights were recorded every 2-3 days for the duration of the

study. Mice were euthanized if tumor volume exceeded 10% of body weight, tumor ulceration was observed, or body weight decreased by 20%.
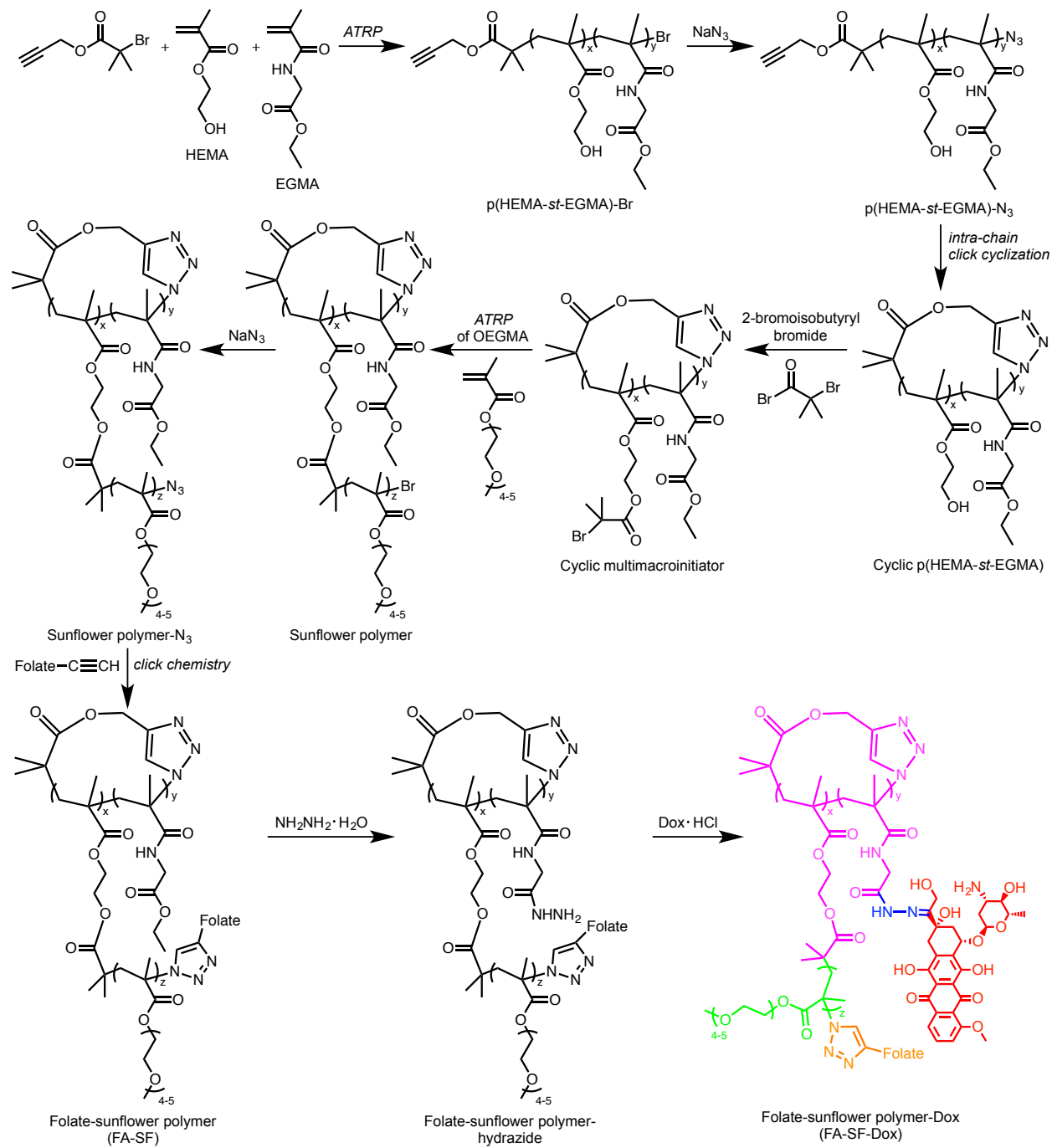
Figure 4.2 Synthesis of folate-sunflower polymer-Dox.

4.3 Results and discussion

4.3.1 Synthesis and characterization of sunflower polymers with different core sizes

We have previously reported a strategy for synthesizing sunflower polymers using a combination of ATRP and click chemistry.[19] The general steps of the synthesis are (i) synthesis of linear statistical copolymers of hydroxyethyl methacrylate (HEMA) and ethyl glycinate methacrylamide (EGMA), (ii) cyclization of the polymers by intra-chain coupling of the chain ends under highly diluted conditions, (iii) conversion of HEMA groups in the polymer core to alkyl halide ATRP initiators, and (iv) ATRP of oligoethylene glycol methacrylate (OEGMA) to generate petals that radiate from the polymer's cyclic core (Figure 4.2).

In this report, we synthesize sunflower polymers with two different core sizes and then investigate these materials for targeted anti-cancer drug delivery to cultured cells. Sunflower polymers with smaller cores were prepared as described previously; these polymers were determined to have, on average, a core composition of 53 monomers (~41 HEMA and ~12 EGMA) and are therefore referred to as core 50 polymers.[19] Sunflower polymers with larger cores were prepared by first synthesizing the linear P(HEMA-*st*-EGMA) precursor using an alkyne-containing ATRP initiator and a target DP of 100 for HEMA units. A 16 h polymerization time was used to achieve a conversion of 80% and an actual DP of ~80. Gel permeation chromatography (GPC) indicates that the resulting copolymer has a number-average molar mass (M_n) of 8.37 kDa and relatively low dispersity (PDI) of 1.33, demonstrating good control over the polymerization (Figure 4.3a). The molar ratio of HEMA and EGMA in the copolymer was determined to be 3.3:1 by ^{1}H NMR spectroscopy, the same as for the linear P(HEMA-*st*-EGMA) precursor with a target DP of 50. The resulting copolymer was thus denoted P(HEMA$_{80}$-*st*-EGMA$_{24}$) and used to prepare core 100 sunflower polymers.

Following conversion of the terminal bromine of the polymer to an azide, the linear precursor was cyclized by an intra-chain copper-catalyzed azide-alkyne cycloaddition (CuAAC) reaction[24] between the polymer chain ends.[25-27] Cyclization was confirmed by a shift toward longer retention times on GPC relative to the linear precursor and by the disappearance of the characteristic azide signal (2100 cm^{-1}) from the Fourier transform-infrared (FT-IR) spectrum (Figure 4.3).
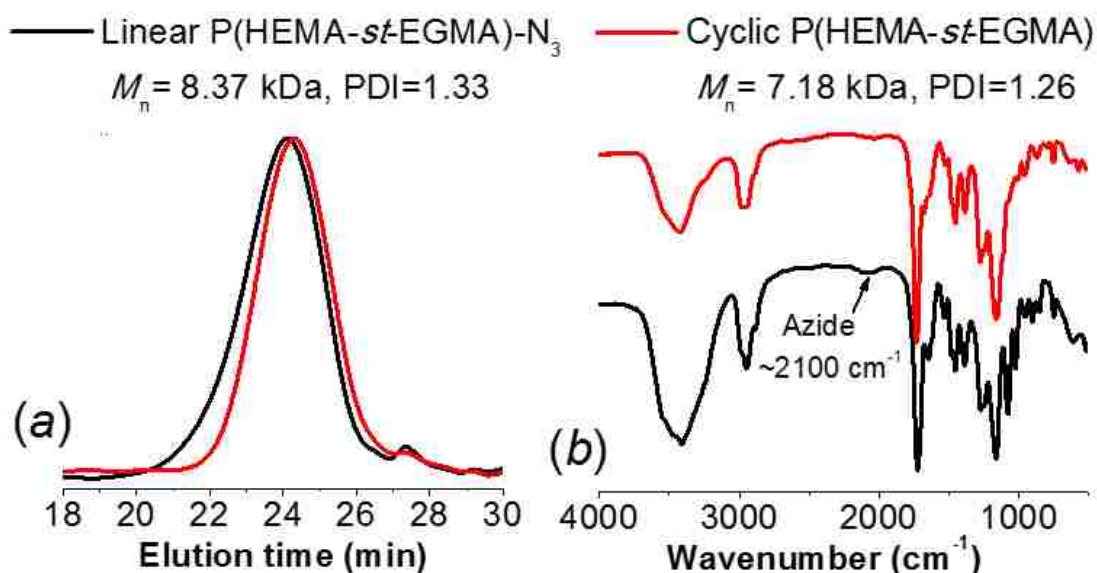
Figure 4.3 (a) GPC elution traces and (b) FT-IR spectra of linear and cyclic P(HEMA$_{80}$-st-EGMA$_{24}$).

Cyclic multimacroinitiators were prepared by esterifying the HEMA units of cyclic P(HEMA-st-EGMA) with the reagent 2-bromoisobutyryl bromide as described previously.[19] Finally, polymerization of OEGMA from the cyclic multimacroinitiator yielded large core sunflowers. As with the small core sunflowers from our earlier work, a kinetic study indicates an increase in molecular weight with petal polymerization time, pseudo-first-order kinetics of the polymerization process, and relatively low PDI (~1.2 when conversion is limited to ~10%) (Figure 4.4).
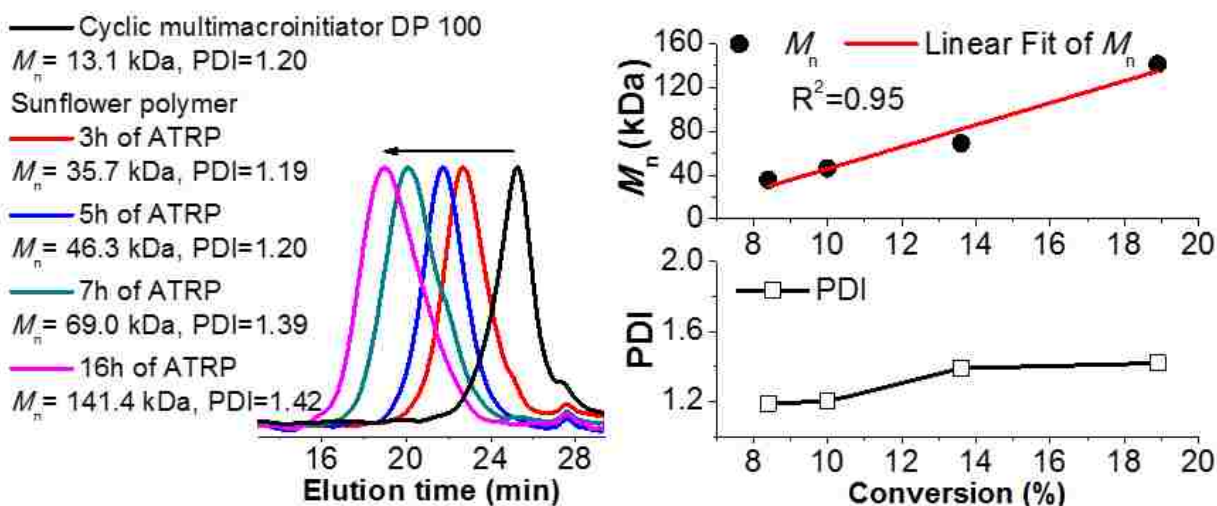
Figure 4.4 ATRP kinetics of sunflower polymers prepared using cyclic multimacroinitiator of DP 100, with a target DP of 100 for each petal.

73

The Z-average hydrodynamic diameters of the large core sunflower polymers as determined by dynamic light scattering were shown to increase with petal polymerization time and ranged from 39.7 to 65.6 nm for the panel (Figure 4.5). Particle size is a particularly important factor in tumor delivery applications. Prolonged circulation is achieved by increasing polymer size above the threshold for renal filtration and extravasation into normal tissue (>5 nm[28] and >2-6 nm[29], respectively), but the optimal particle size for maximizing tumor penetration is generally less than ~50 nm in diameter.[30-32] The sizes of these sunflower polymers are therefore relevant for tumor targeted delivery.
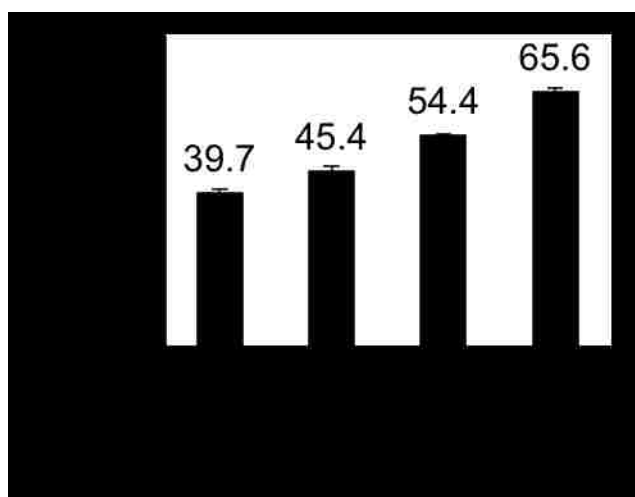
Figure 4.5 Z-average diameters of sunflower polymers with cyclic core of DP 100 and petals polymerized for different lengths of time.

4.3.2   *Uptake of large core sunflower polymers in FR+ cells*

Core 100 sunflower polymers with petals synthesized by 3 h ATRP of OEGMA were selected for biological evaluation. We first confirmed that sunflower polymers retain their structure in the presence of serum-containing cell culture media. Polymers were incubated with complete media for 4 h, recovered by extraction, and analyzed by size exclusion chromatography. Chromatography traces reveal that serum-treated polymers have elution times similar to those of untreated polymers (data not shown), indicating that molecular weight and structure are not significantly changed by serum enzymes, which could potentially hydrolyze polymers during the course of the experiment. Therefore, polymers were conjugated with FA-alkyne targeting ligands at petal terminal azides (59% efficiency,

determined by absorbance at 360 nm) and NHS-fluorescein at core hydrazides (49% efficiency, determined by ^{1}H NMR). These constructs, named FA-SF-fluor, were investigated for FR-mediated uptake in KB (FR+) and A549 (FR-) cells. Although KB cells demonstrated higher normalized median fluorescence intensities (MFIs) than A549 cells at the same polymer concentrations, competition with free FA surprisingly did not reduce polymer uptake in either cell line. This indicates that substantial uptake of these large core sunflowers can occur by non-FR-mediated mechanisms (Figure 4.6). This is in contrast to the results observed for their small core counterparts, which undergo FR-mediated endocytosis specifically in KB cells.[19] On the basis of this finding, we decided to focus on the small (DP 50) core sunflower polymers for targeted drug delivery applications.
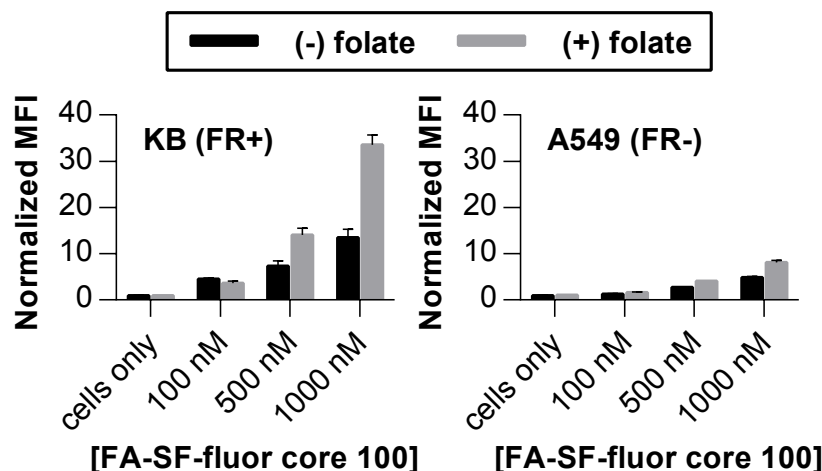
Figure 4.6 Uptake of FA-SF-fluor with DP 100 core in FR+ KB cells and FR- A549 cells in the absence (black bars) and presence (grey bars) of 2 mM competing free folate.

4.3.3   Dox release kinetics

Ideally, polymer-drug conjugates for cancer therapy should remain stable during circulation and release drug in the tumor environment or after tumor cell uptake in order to minimize off-site exposure and toxicity. Dox hydrochloride was therefore conjugated to the FA-targeted sunflower polymer (FA-SF) via an acyl hydrazone bond, shown previously to provide preferred *in vivo* release kinetics at tumor sites.[33,34] Following conversion of the EGMA side chains in the polymer core from ethyl esters to hydrazides (85% efficiency, determined by trinitrobenzenesulfonic acid [TNBS] assay), Dox was covalently linked via

75

its hydroxyl ketone group (38% efficiency, determined by absorbance at 480 nm; ~2.5 w/w%). Dox conjugation was also confirmed by an increased signal at 8.0 ppm in the ^{1}H NMR spectrum of the targeted, drug-loaded sunflower polymers, and DLS sizing indicated minimal polymer aggregation (Figure S4.1).

To investigate the pH-dependent kinetics of Dox release, FA-sunflower-Dox polymer (FA-SF-Dox) was incubated in PBS (pH 7.4), phosphate buffer (pH 6.8), or citrate buffer (pH 5.5) at 37°C, and Dox release was quantified by dialysis method (Figure 4.7).[35] The conjugates were highly stable under physiological conditions, with only 6.5% of the Dox being released over 4 d at pH 7.4. In contrast, incubation of the FA-SF-Dox at pH 5.5 (comparable to the pH of late endosomes and lysosomes) resulted in over 74% Dox release from the polymer after 24 h. Incubation at pH 6.8 (the pH of the tumor microenvironment)[36] resulted in intermediate levels of hydrolysis, with 33% Dox release after 24 h.
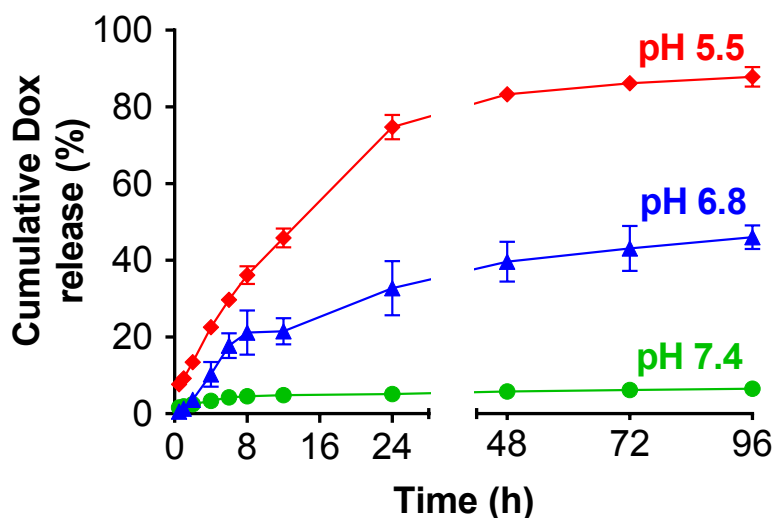
Figure 4.7 Release kinetics of Dox from FA-SF-Dox polymer at pH 7.4, 6.8, and 5.5.

4.3.4   *Confocal imaging of intracellular drug delivery*

The intracellular trafficking of FA-SF-Dox in KB cells was then examined by confocal microscopy. Dox fluorescence was clearly seen in the nuclei of cells incubated with either FA-SF-Dox or free Dox for 12 h, suggesting that drug is released from the polymer and localizes to the nucleus, or that the entire polymer construct undergoes intracellular

76

trafficking and nuclear localization in a pattern consistent with the free drug (Figure 4.8). Some punctate staining throughout the cytoplasm could also be observed in the FA-SF-Dox-treated cells, but not cells treated with free Dox, suggesting that the polymer traffics through an endocytic pathway, consistent with the internalization mechanism of other FA-conjugated carriers.[23]
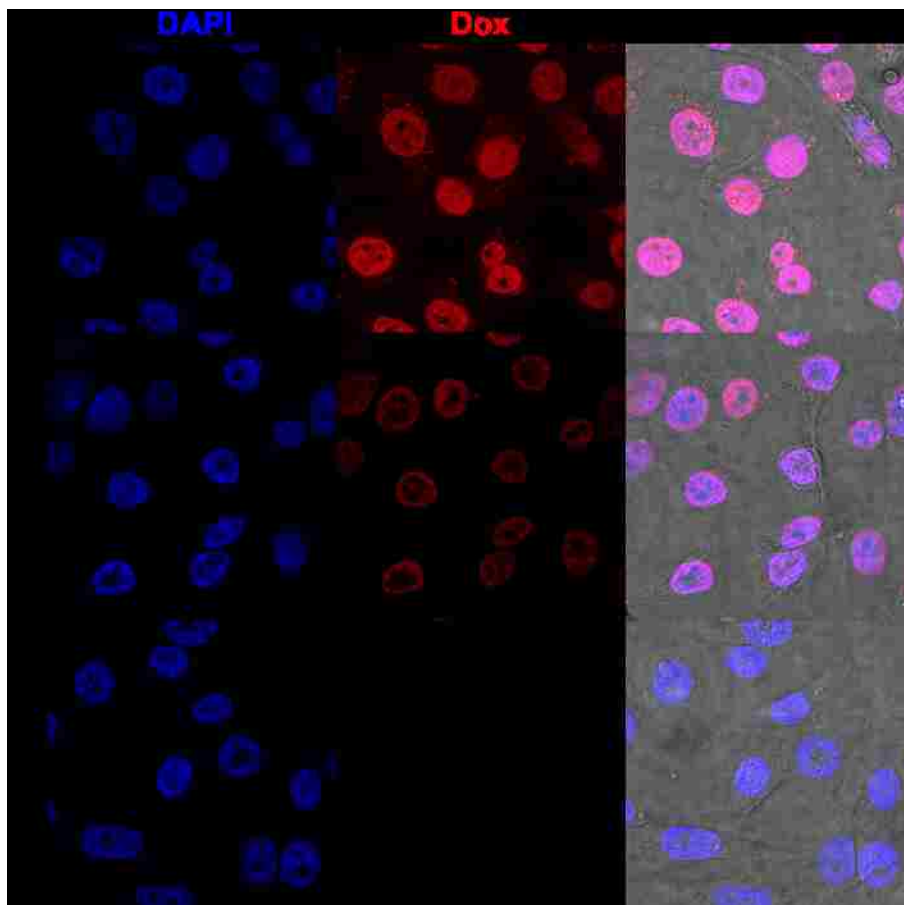
Figure 4.8 Confocal imaging of FA-SF-Dox and Dox (red) uptake in KB cells (nuclei stained blue with DAPI). Cells were treated with polymer or free drug at 25% of their respective IC_{50} values to minimize cell death. (BF: brightfield image.)

4.3.5   *Cytotoxicity of sunflower polymers*

The cytotoxicity of sunflower polymer constructs to FR+ KB and FR- A549 cells was assessed by MTS cell viability studies (Table 4.1). The base sunflower (SF) and FA-modified SF (FA-SF) polymers were minimally toxic to cells (IC_{50}, or concentration for 50% cell killing, at least 1 mg/mL), although cytotoxicity of polymers is increased by conjugation of FA, likely due to higher levels of polymer internalization mediated by the targeting ligand.

77

Table 4.1 IC_{50} values and 95% confidence intervals for Dox and polymer formulations in KB (FR+) and A549 (FR-) cell lines.

			IC_{50} in Dox equivalents (µg/mL) (95% CI)			
Cell line	SF	FA-SF	Free Dox	SF-Dox	FA-SF-Dox	FA-comb-Dox
KB	N/A* (>5.5 mg/mL)	3.59 mg/mL (3.40, 3.79)	0.918 (0.866, 0.972)	4.15 (3.93, 4.38)	2.47 (2.22, 2.75)	2.42 (2.22, 2.64)
A549	N/A* (>5.5 mg/mL)	N/A* (>5.5 mg/mL)	1.65 (1.47, 1.84)	7.23 (6.79, 7.70)	8.14 (7.64, 8.67)	3.40 (3.07, 3.75)

*Cell survival >90% at the highest tested concentration.

In KB cells, the IC_{50} of free Dox and FA-SF-Dox were 0.92 and 2.47 µg/mL in Dox equivalents, respectively. The increased IC_{50} of FA-SF-Dox compared to free Dox is likely due to slower internalization mechanism (endocytosis vs. direct membrane permeation) and the release kinetics of free drug from polymer. In A549 cells, the IC_{50} of the FA-SF-Dox formulation is increased to an even greater extent relative to free Dox and is not significantly different from the untargeted SF-Dox formulation.

The cytotoxicity results also confirm trends in uptake based on polymer architecture. FA-SF-Dox polymer, which was previously shown to undergo FR-dependent uptake, exhibited the best selectivity in cell killing for KB cells over A549 cells. Meanwhile, the analogous linear comb-like polymer, FA-comb-Dox, was similarly cytotoxic in both KB cells and non-target A549 cells. This non-specific cytotoxicity correlates well with the previous uptake data suggesting non-FR-mediated uptake of the comb polymer.[19] It is possible that the constrained architecture of the sunflower polymer facilitates display of the FA targeting ligand and subsequent interaction with cell surface receptors; the mechanistic basis for this difference in uptake warrants further study.

4.3.6   Anti-tumor efficacy in vivo

The efficacy of the FA-SF-Dox formulation *in vivo* was tested using a KB xenograft tumor model. Tumor-bearing mice were treated according to one of two dosing strategies: a single injection of free Dox or FA-SF-Dox at a dose of 6 mg Dox/kg mouse, or three injections of 4 mg Dox/kg mouse over the course of one week. FA-SF polymer without Dox was also tested

as a negative control. Tumor volumes and mouse weights were monitored for 38 days as indicators of drug efficacy and toxicity, respectively.
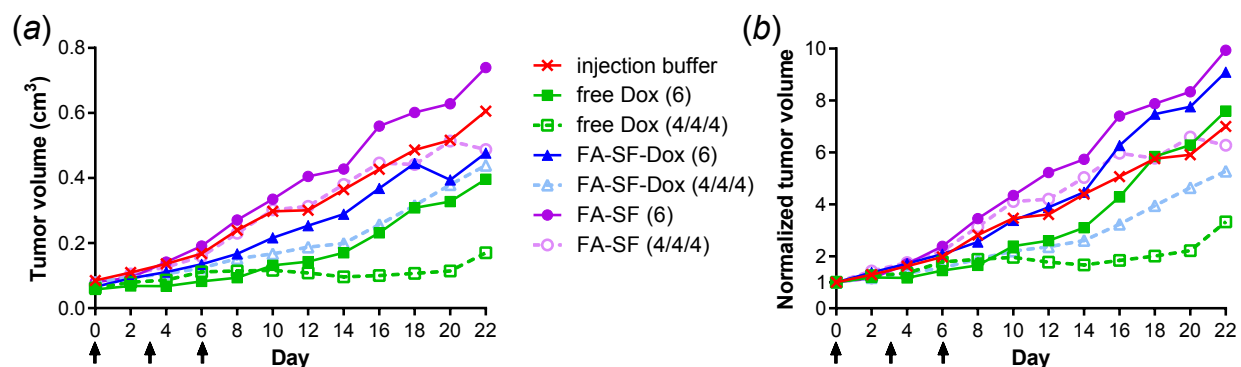
Figure 4.9 *In vivo* tumor growth in tumor-bearing mice dosed with free Dox or FA-SF-Dox at 6 mg Dox/kg mouse on day 0, or with multiple doses each at 4 mg/kg on days 0, 3, and 6. (a) Raw tumor volumes and (b) tumor volumes normalized to day 0.

Rapid tumor growth was observed for mice receiving injection buffer or FA-SF controls (Figure 4.9). Three doses of free Dox were extremely effective for suppressing tumor growth over the initial 2-3 weeks, while a single larger dose of Dox showed initial inhibition for about 1 week after injection. Some promising activity was observed with three doses of FA-SF-Dox, which appeared to have an effect comparable to a single dose of free Dox; however, FA-SF-Dox was not effective if administered as a single dose. This is likely due to differences in pharmacokinetics and drug release for free drug vs. the polymer-drug formulation. In addition, after normalization to initial tumor volume (Figure 4.9b), the efficacy of a single dose of Dox was less pronounced (the mice in this group had somewhat smaller tumors initially), while multiple doses of FA-SF-Dox resulted in slightly sustained tumor inhibition.

Overall, large variability in tumor growth was observed, and the differences in tumor volumes between the groups were not statistically significant. This variability underscores the need for a robust and consistent tumor model or a model that allows more accurate quantification of tumor burden (e.g. luciferase-expressing tumor cells).

Tumor volumes were not plotted after day 22; these trends became skewed as animals reached their endpoints. Therefore, tumor burden was also evaluated using a Kaplan-Meier survival curve. In this study, mice were euthanized if tumor volume exceeded 10% of body weight, tumor ulceration was observed, or body weight decreased by 20%. Because this is a

79

relatively slow-growing tumor model, most euthanasia events were the result of tumor ulceration. However, tumor ulceration did not necessarily correlate with tumor size. Therefore, the endpoints for survival were defined as (1) an event resulting in euthanasia or (2) a tumor volume exceeding 0.5 cm^3. Using these criteria, both Dox and FA-SF-Dox appeared to extend survival over the 38-day period when administered in multiple doses (Figure 4.10). However, differences in survival were statistically significant only for mice treated with three doses of free Dox.
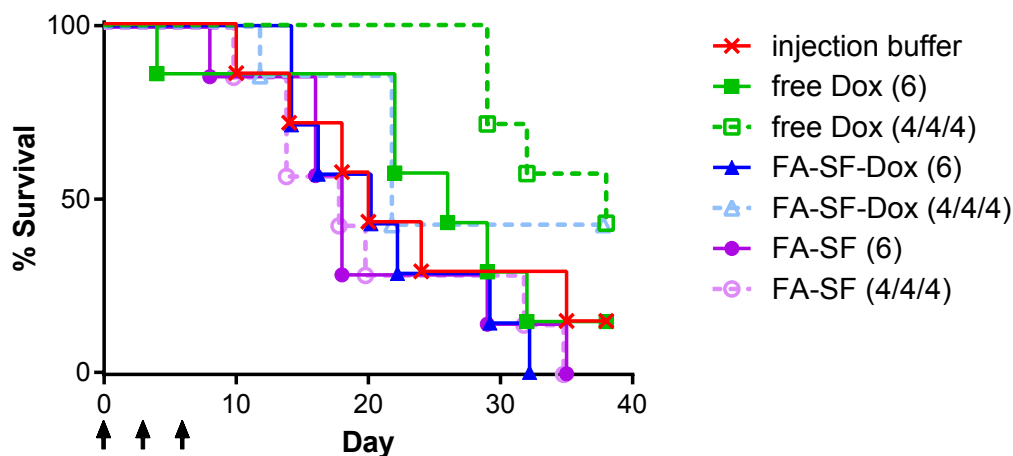
Figure 4.10 Survival curve for tumor-bearing mice. Endpoint criteria were: tumor volume exceeding 0.5 cm^3 or 10% of body weight, tumor ulceration, or 20% decrease in body weight.

Polymeric drug formulations have previously been shown to reduce the toxicity that can result from chemotherapy treatment.[37,38] The weights of treated mice were monitored as an indication of systemic toxicity (Figure 4.11). Normalized weights indicate that multiple doses of free Dox resulted in sustained and gradual weight loss over the initial treatment period. Mice receiving only a single Dox treatment did not demonstrate significant weight loss (the apparent weight loss in this group on day 4 after injection is attributed to an adverse reaction to the injection in a single mouse, resulting in significant weight loss and euthanasia). Interestingly, some weight loss was observed in mice treated with control polymer but not in mice treated with FA-SF-Dox, even when multiple doses were used. Overall, this indicates that the polymer-drug formulation is well tolerated and could potentially increase the maximum tolerated dose over the free Dox equivalent, while mitigating systemic toxicity and adverse side effects.

80
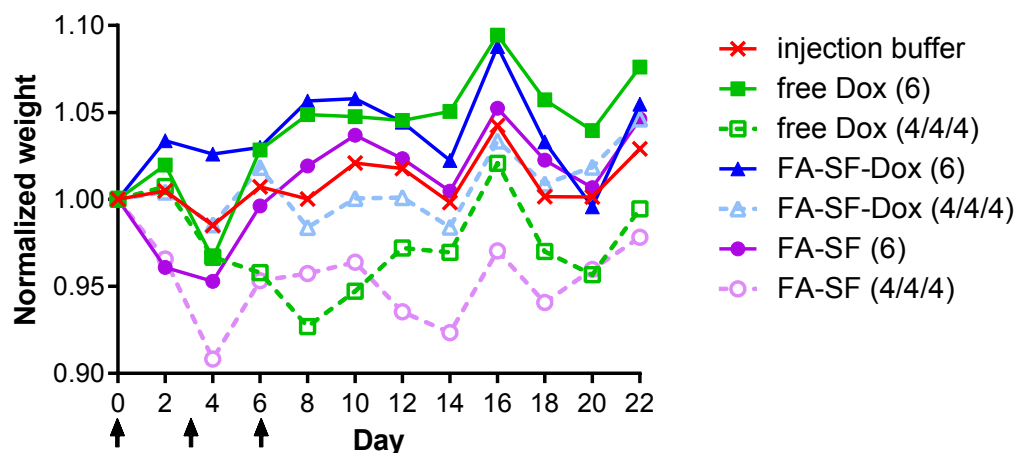
Figure 4.11 Normalized body weights of tumor-bearing mice receiving a single or multiple chemotherapy treatments.

4.4   Conclusions

In this work, we have extended the sunflower polymer platform by investigating the degree of polymerization of the core as an additional tunable parameter for synthesizing polymers with precise hydrodynamic sizes. Preliminary findings indicate that polymers of different core sizes have significantly different uptake behaviors; the mechanisms underlying this phenomenon may be interesting for further investigation. We have also demonstrated that drugs can be conjugated to the cyclic core buried within the polymer petals, thereby reducing polymer aggregation that has been observed in dendrimer-drug conjugates induced by hydrophobic drug-drug interactions.[39] Using this platform, doxorubicin can be incorporated via a pH-sensitive linker and triggered for intracellular release of active drug. *In vivo* studies indicate that the FA-SF-Dox formulation avoids the systemic toxicity associated with free Dox treatment, although limited efficacy was shown. This effect may be attributed to incomplete Dox release, as well as the low drug content of the polymer overall. In future work, drug loading (currently 2-5 w/w%) might be increased by altering sunflower polymer structure, for example, conjugating drugs onto petals instead of cores or encapsulating drugs by hydrophobic or ionic interactions, methods that have been shown to improve drug loading (15-50 w/w%).[40,41]

In summary, sunflower polymers represent a unique platform for targeted drug delivery. Sunflower polymers combine the structural complexity and nano-size of dendrimers with the relative ease of synthesis of traditional linear polymers. These

81

polymers integrate multiple characteristics to address the challenges of drug delivery to tumors – such as appropriate size for tumor penetration, preferential drug release in the tumor microenvironment, and cell-specific delivery – into a single material.

4.5   Acknowledgements

References

1.   Meirow, D. & Nugent, D. The effects of radiotherapy and chemotherapy on female reproduction. *Hum. Reprod. Update* **7,** 535–543 (2001).
2.   Singal, P. K. & Iliskovic, N. Doxorubicin-induced cardiomyopathy. *N. Engl. J. Med.* **339,** 900–905 (1998).
3.   Matsumura, Y. & Maeda, H. A new concept for macromolecular therapeutics in cancer chemotherapy: mechanism of tumoritropic accumulation of proteins and the antitumor agent smancs. *Cancer Res.* **46,** 6387–6392 (1986).
4.   Davis, M. E., Chen, Z. G. & Shin, D. M. Nanoparticle therapeutics: an emerging treatment modality for cancer. *Nat Rev Drug Discov* **7,** 771–782 (2008).
5.   Peer, D., Karp, J. M., Hong, S., Farokhzad, O. C., Margalit, R. & Langer, R. Nanocarriers as an emerging platform for cancer therapy. *Nat Nanotechnol* **2,** 751–760 (2007).
6.   Desai, N. Challenges in Development of Nanoparticle-Based Therapeutics. *AAPS J* **14,** 282–295 (2012).
7.   Beyer, I., Cao, H., Persson, J., Song, H., Richter, M., Feng, Q., Yumul, R., van Rensburg, R., Li, Z., Berenson, R., Carter, D., Roffler, S., Drescher, C. & Lieber, A. Coadministration of epithelial junction opener JO-1 improves the efficacy and safety of chemotherapeutic drugs. *Clin. Cancer Res.* **18,** 3340–3351 (2012).
8.   Moghimi, S. M. & Szebeni, J. Stealth liposomes and long circulating nanoparticles: critical issues in pharmacokinetics, opsonization and protein-binding properties. *Prog. Lipid Res.* **42,** 463–478 (2003).
9.   Sun, X., Yan, Y., Liu, S., Cao, Q., Yang, M., Neamati, N., Shen, B., Niu, G. & Chen, X. 18F-FPPRGD2 and 18F-FDG PET of response to Abraxane therapy. *J. Nucl. Med.* **52,** 140–146 (2011).
10.   Elzoghby, A. O., Samy, W. M. & Elgindy, N. A. Albumin-based nanoparticles as

potential controlled release drug delivery systems. *J Control Release* **157,** 168–182 (2012).

11. Gabizon, A., Shmeeda, H. & Barenholz, Y. Pharmacokinetics of Pegylated Liposomal Doxorubicin. *Clin Pharmacokinet* **42,** 419–436 (2003).

12. Du, J.-Z., Du, X.-J., Mao, C.-Q. & Wang, J. Tailor-made dual pH-sensitive polymer-doxorubicin nanoparticles for efficient anticancer drug delivery. *J. Am. Chem. Soc.* **133,** 17560–17563 (2011).

13. Tong, R. & Cheng, J. Ring-opening polymerization-mediated controlled formulation of polylactide-drug nanoparticles. *J. Am. Chem. Soc.* **131,** 4744–4754 (2009).

14. Kataoka, K., Harada, A. & Nagasaki, Y. Block copolymer micelles for drug delivery: design, characterization and biological significance. *Advanced Drug Delivery Reviews* **47,** 113–131 (2001).

15. Tong, R. & Cheng, J. Paclitaxel-Initiated, Controlled Polymerization of Lactide for the Formulation of Polymeric Nanoparticulate Delivery Vehicles. *Angew. Chem.* **120,** 4908–4912 (2008).

16. Fox, M. E., Guillaudeu, S., Fréchet, J. M. J., Jerger, K., Macaraeg, N. & Szoka, F. C. Synthesis and in vivo antitumor efficacy of PEGylated poly(l-lysine) dendrimer-camptothecin conjugates. *Mol. Pharm.* **6,** 1562–1572 (2009).

17. Kaminskas, L. M., Boyd, B. J., Karellas, P., Henderson, S. A., Giannis, M. P., Krippner, G. Y. & Porter, C. J. H. Impact of surface derivatization of poly-L-lysine dendrimers with anionic arylsulfonate or succinate groups on intravenous pharmacokinetics and disposition. *Mol. Pharm.* **4,** 949–961 (2007).

18. Nasongkla, N., Chen, B., Macaraeg, N., Fox, M. E., Fréchet, J. M. J. & Szoka, F. C. Dependence of Pharmacokinetics and Biodistribution on Polymer Architecture: Effect of Cyclic versus Linear Polymers. *J. Am. Chem. Soc.* **131,** 3842–3843 (2009).

19. Wei, H., Wang, C. E., Tan, N., Boydston, A. J. & Pun, S. H. ATRP Synthesis of Sunflower Polymers Using Cyclic Multimacroinitiators. *ACS Macro Lett.* 938–941 (2015). doi:10.1021/acsmacrolett.5b00565

20. Matyjaszewski, K. & Tsarevsky, N. V. Macromolecular engineering by atom transfer radical polymerization. *J. Am. Chem. Soc.* **136,** 6513–6533 (2014).

21. Neugebauer, D., Zhang, Y., Pakula, T., Sheiko, S. S. & Matyjaszewski, K. Densely-Grafted and Double-Grafted PEO Brushes via ATRP. A Route to Soft Elastomers. *Macromolecules* **36,** 6746–6755 (2003).

22. Low, P. S., Henne, W. A. & Doorneweerd, D. D. Discovery and development of folic-acid-based receptor targeting for imaging and therapy of cancer and inflammatory diseases. *Acc. Chem. Res.* **41,** 120–129 (2008).

23. Lu, Y. & Low, P. S. Folate-mediated delivery of macromolecular anticancer therapeutic agents. *Advanced Drug Delivery Reviews* **64,** 342–352 (2012).

24. Kolb, H. C., Finn, M. G. & Sharpless, K. B. Click Chemistry: Diverse Chemical Function from a Few Good Reactions. *Angew. Chem. Int. Ed. Engl.* **40,** 2004–2021 (2001).

25. Laurent, B. A. & Grayson, S. M. An efficient route to well-defined macrocyclic polymers via 'click' cyclization. *J. Am. Chem. Soc.* **128,** 4238–4239 (2006).

26. Laurent, B. A. & Grayson, S. M. Synthesis of cyclic dendronized polymers via divergent "graft-from" and convergent click 'graft-to' routes: preparation of modular toroidal macromolecules. *J. Am. Chem. Soc.* **133,** 13421–13429 (2011).

27. Laurent, B. A. & Grayson, S. M. Synthesis of cyclic amphiphilic homopolymers and their potential application as polymeric micelles. *Polym Chem* **3,** 1846–1855 (2012).

28. Duncan, R. The dawning era of polymer therapeutics. *Nat Rev Drug Discov* **2,** 347–

360 (2003).

29. Jain, R. K. Transport of molecules across tumor vasculature. *Cancer Metastasis Rev* **6,** 559–593 (1987).

30. Goodman, T. T., Olive, P. L. & Pun, S. H. Increased nanoparticle penetration in collagenase-treated multicellular spheroids. *Int J Nanomedicine* **2,** 265–274 (2007).

31. Ng, C. P. & Pun, S. H. A perfusable 3D cell-matrix tissue culture chamber for in situ evaluation of nanoparticle vehicle penetration and transport. *Biotechnol. Bioeng.* **99,** 1490–1501 (2008).

32. Perrault, S. D., Walkey, C., Jennings, T., Fischer, H. C. & Chan, W. C. W. Mediating tumor targeting efficiency of nanoparticles through design. *Nano Lett* **9,** 1909–1915 (2009).

33. Lee, C. C., Gillies, E. R., Fox, M. E., Guillaudeu, S. J., Fréchet, J. M. J., Dy, E. E. & Szoka, F. C. A single dose of doxorubicin-functionalized bow-tie dendrimer cures mice bearing C-26 colon carcinomas. *Proc. Natl. Acad. Sci. U.S.A.* **103,** 16649–16654 (2006).

34. Padilla De Jesús, O. L., Ihre, H. R., Gagne, L., Fréchet, J. M. J. & Szoka, F. C. Polyester Dendritic Systems for Drug Delivery Applications: In Vitro and In Vivo Evaluation. *Bioconjug. Chem.* **13,** 453–461 (2002).

35. Kim, D., Lee, E. S., Oh, K. T., Gao, Z. G. & Bae, Y. H. Doxorubicin-loaded polymeric micelle overcomes multidrug resistance of cancer by double-targeting folate receptor and early endosomal pH. *Small* **4,** 2043–2050 (2008).

36. Gerweck, L. E. & Seetharaman, K. Cellular pH gradient in tumor versus normal tissue: potential exploitation for the treatment of cancer. *Cancer Res.* **56,** 1194–1198 (1996).

37. Kim, T. H., Mount, C. W., Gombotz, W. R. & Pun, S. H. The delivery of doxorubicin to 3-D multicellular spheroids and tumors in a murine xenograft model using tumor-penetrating triblock polymeric micelles. *Biomaterials* **31,** 7386–7397 (2010).

38. Chen, C.-Y., Kim, T. H., Wu, W.-C., Huang, C.-M., Wei, H., Mount, C. W., Tian, Y., Jang, S.-H., Pun, S. H. & Jen, A. K.-Y. pH-dependent, thermosensitive polymeric nanocarriers for drug delivery to solid tumors. *Biomaterials* (2013).

39. Pu, Y., Chang, S., Yuan, H., Wang, G., He, B. & Gu, Z. The anti-tumor efficiency of poly(L-glutamic acid) dendrimers with polyhedral oligomeric silsesquioxane cores. *Biomaterials* **34,** 3658–3666 (2013).

40. Kataoka, K., Matsumoto, T., Yokoyama, M., Okano, T., Sakurai, Y., Fukushima, S., Okamoto, K. & Kwon, G. S. Doxorubicin-loaded poly(ethylene glycol)-poly(beta-benzyl-L-aspartate) copolymer micelles: their pharmaceutical characteristics and biological significance. *J Control Release* **64,** 143–153 (2000).

41. Kim, J. O., Kabanov, A. V. & Bronich, T. K. Polymer micelles with cross-linked polyanion core for delivery of a cationic drug doxorubicin. *J Control Release* **138,** 197–204 (2009).

Results

		Size (d.nm):	% Volume	Width (d.nm):
Z-Average (d.nm): 80.38	Peak 1:	98.89	3.9	58.70
Pdl: 0.447	Peak 2:	12.86	96.1	4.730
Intercept: 0.926	Peak 3:	0.000	0.0	0.000
Result quality : Good				
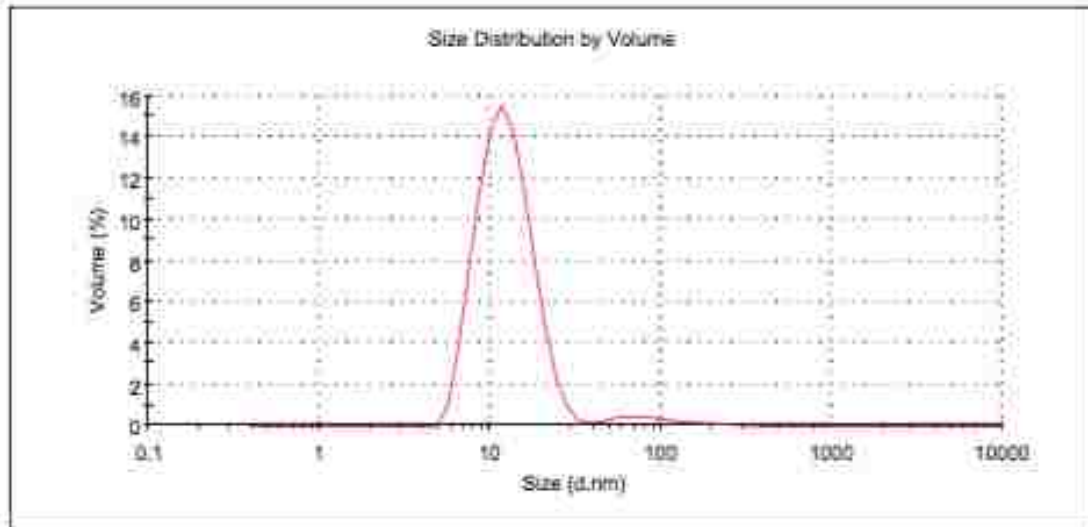
Figure S4.1 Raw particle size distribution by volume of FA-SF-Dox with DP 50 core and OEGMA petals polymerized for 3 h.

Part III.

Modifications Enabling Systemic

Administration of Adenovirus

Chapter 5.

ADENOVIRAL VECTORS FOR CANCER GENE THERAPY: PHARMACOLOGY AND STRATEGIES FOR MODIFICATION

5.1   Introduction

Gene therapy involves the introduction of nucleic acids into cells in order to replace mutated genes or to alter cellular phenotypes. As a result, gene therapy has the potential to treat a wide variety of hereditary and acquired diseases. In the context of cancer, gene therapy encompasses diverse treatment strategies including the delivery of suicide genes or anti-angiogenic genes, as well as immunotherapy approaches, whereby cancer cells are induced to express highly antigenic proteins or immunostimulatory cytokines to encourage recognition by the host immune system.[1,2]

Gene delivery has traditionally been approached with either viral[3] or non-viral[4] vectors. Viruses are particularly well suited as gene carriers because they are highly evolved for gene transfer, often carrying various proteins to navigate the cell interior; this typically results in very efficient transduction and robust or long-term transgene expression. Furthermore, genetically engineered viruses known as oncolytic viruses have the unique ability to preferentially infect and lyse cancer cells while leaving normal cells intact.[5] Clinical application of viral gene delivery vectors is primarily limited by safety concerns. Viruses are inherently immunogenic, which can lead to undesirable immune reactions and even resistance after repeat administrations. To date, only two gene therapy products have been clinically approved. Oncorine (H101), an oncolytic adenovirus targeting p53-deficient tumor cells,[6] was approved by China's State Food and Drug Administration in 2005 for the treatment of head and neck cancer.[7] In 2015, Imlygic, a herpes simplex virus for the treatment of melanoma lesions, became the first oncolytic virus to be approved by the U.S. Food and Drug Administration. Notably, both products are administered by direct injection into the tumors or lesions; studies have demonstrated dramatically reduced anti-tumor efficacy for viruses administered systemically rather than intratumorally.[6,8]

In contrast to viral vectors, synthetic gene delivery vectors, such as those based on cationic lipids and polymers, can be synthesized with relatively good biocompatibility and limited immunogenicity *in vivo*, even after systemic administration. However, non-viral vectors generally achieve much lower levels of gene transfer efficiency than their viral counterparts. As a result, research is turning toward "hybrid" vectors, which combine both viral and synthetic components to maximize safety and efficacy.[9]

In this work, we investigate the use of polymers to mitigate the immunogenicity of adenoviruses after systemic administration. This chapter provides a broad overview of adenoviral vector biology, pharmacology, and current strategies for re-engineering adenoviruses to provide contextual background for the research described in Part III of this thesis.

5.2   *Adenoviral vectors*

Adenoviruses (Ads) are one of the most commonly used delivery vectors in gene therapy clinical trials to date.[10] Ads are a family of non-enveloped viruses carrying double-stranded DNA and have several advantages as a delivery platform: they can be easily produced to high titer, efficiently transduce both dividing and non-dividing cells, have a large coding capacity for transgenes (genome size of ~36 kilobase pairs), and do not integrate into the host genome. However, Ad also suffer from significant safety issues which have limited their clinical translation, as we will describe in Section 5.3.

Ads have an icosahedral capsid structure with a diameter of approximately 100 nm. The major capsid proteins are the hexon, penton, and fiber (Figure 5.1). Each of the icosahedron's 20 triangular faces is composed of 12 hexon homotrimers, a total of 240 trimers or 720 individual hexon proteins per virion.[11] Each of the 12 vertices of the icosahedron consists of a pentameric penton base (60 monomers total) and a trimeric fiber (36 monomers).
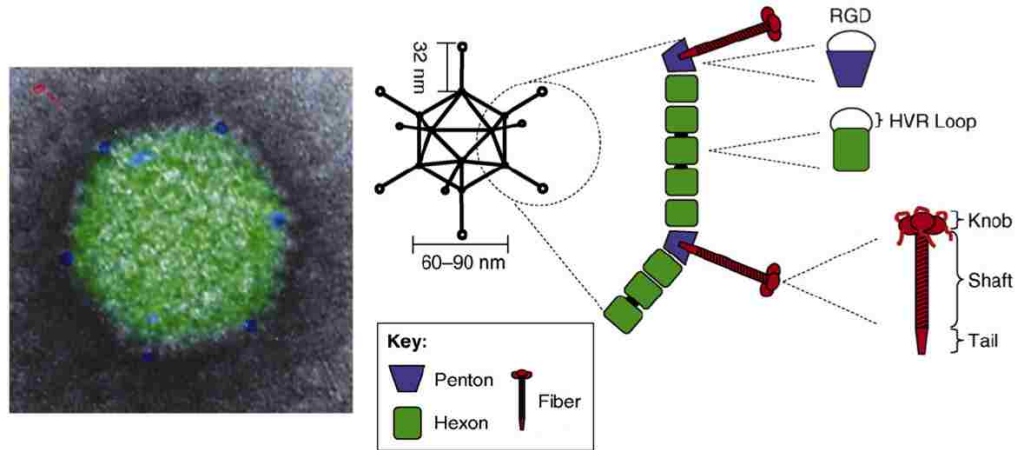
Figure 5.1 False-colored electron micrograph and schematic representation of the icosahedral structure of adenovirus, depicting the major capsid proteins: hexon (green), penton (blue) and fiber (red). Adapted with permission from Ref. 12.

There are more than 50 different Ad serotypes known, classified into 7 different species from A to G based on genetic similarity.[13] Different species may vary in the lengths of their fiber shafts. In addition, the knob domain of the fiber determines specificity for cellular receptors. Most species of adenoviruses, including the species C Ads (Ads 1, 2, 5, and 6), are known to bind the coxsackievirus and adenovirus receptor (CAR),[14] while several species B viruses use human CD46 as their receptor.[15] In this work, we have focused specifically on Ad of serotype 5 (Ad5), the most studied and most utilized member of the adenovirus family.

5.3   *Adenovirus pharmacology*

5.3.1   *CAR paradigm of adenovirus infection*

Ad5 infection *in vitro* occurs efficiently through CAR. Ad5 first binds CAR via its fiber knob with high affinity. Ad5 has a relatively long and flexible fiber shaft;[16] after binding, the shaft flexes to allow interaction between RGD (arginine-glycine-aspartic acid) motifs in the penton base and cell surface integrins $\alpha_v\beta_1$, $\alpha_v\beta_3$, $\alpha_v\beta_5$, or $\alpha_3\beta_1$.[17] RGD-integrin binding subsequently triggers receptor-mediated endocytosis of the virus. If cells lack CAR or CAR binding is ablated on the fiber knob, infection can occur slowly by direct (but lower-affinity) interaction of the penton base and integrins.[18] Cells lacking both CAR and integrins are therefore relatively nonpermissive to transduction.

91

Upon systemic administration, adenoviruses are subject to a host of interactions with various blood and cell components and do not follow the simple CAR infection paradigm. Moreover, in an *in vivo* context, CAR is found as a component of intercellular tight junctions and therefore is not accessible for Ad binding without the disruption of tight junctions.[19]

The first major barrier to Ad use is that a large percentage of the population has pre-existing adaptive immunity to Ad5, with neutralizing antibodies (NAbs) that inactivate virus, while naïve individuals rapidly develop NAbs that prevent repeated vector administration.[18] As the most abundant capsid protein, most anti-Ad NAbs are directed against the hexon.[20]

Intravenously delivered Ad are primarily sequestered in the liver and spleen and also trigger a potent innate immune response. Up to 90% of viral particles are quickly scavenged by Kupffer cells (KCs), the liver resident macrophages, which clear Ad from the bloodstream without being productively transduced.[21] Phagocytic uptake by KCs is accompanied by the release of pro-inflammatory cytokines such as TNF and IL-6, leading to hepatotoxicity.[22] The primary mechanism of Ad sequestration in the liver is interaction of the KC scavenger receptor SRA-II with anionic surfaces such as hexon. Specifically, hypervariable regions (HVRs) 1, 2, 5, and 7 of the Ad5 hexon have been implicated in scavenger receptor recognition;[23] these HVRs are clustered on the surface of the hexon trimer and may lead to KC binding at either a depression at the center of each hexon trimer or a depression at the center of three hexon trimers. In the spleen, Ad particles accumulate in MARCO- and CD169-positive marginal zone macrophages, leading to an IL-1α-mediated innate immune response.[24] Liver sinusoidal endothelial cells (LSECs) are also capable of scavenging Ad from the bloodstream, and as seen with KCs, Ad uptake by LSECs does not lead to efficient transduction.[25]

At doses surpassing saturation of KCs and LSECs, transduction is primarily observed in hepatocytes.[26] Liver transduction is mediated by the high-affinity (229 pM) binding of blood coagulation factor X (FX) to the Ad5 hexon.[27] Binding of the γ-carboxyglutamic acid (Gla) domain of FX[28] to hexon subsequently "bridges" the virus to heparan sulfate proteoglycans expressed on the surface of hepatocytes.[29] The Ad5-FX interaction has been localized to HVRs 5 and 7[30] at the center depression of the hexon trimer, although data

92

suggest that FX and scavenger receptor do not bind the same surface on Ad5 hexon.[23] Critically, Ad5 vectors with hexon mutations that prevent FX binding fail to transduce hepatocytes *in vivo*.[27] Recent studies also found that innate immune sensors respond to the misplacement of FX from blood into intracellular compartments during Ad5 infection, and that preventing the formation of the Ad5-FX complex may be key to minimizing the innate immune response against Ad.[31]

5.4 Strategies for adenovirus modification

Efforts to improve adenoviral vectors have focused on engineering Ad with reduced immunogenicity, evasion of NAbs, and/or altered *in vivo* tropism. Current strategies for Ad modification include genetic modification, polymer conjugation, and non-covalent coating of vectors.

5.4.1 Genetic modification

Ad vectors have been genetically engineered to eliminate undesirable interactions, typically by substitution with domains from other Ad serotypes or by modification of specific capsid motifs. However, this approach typically does little to modulate viral immunogenicity. For example, hexon mutations that prevent FX binding to Ad5 vectors have been shown to reduce liver transduction but with no change to systemic inflammatory profiles.[32] Recent work also found that FX binding has the unexpected ability to protect Ad5 from attack by natural IgM antibodies and the classical complement pathway.[33] Consequently, engineering Ad5 for ablated FX binding may render these vectors more susceptible to inactivation *in vivo*.

Furthermore, studies by Di Paolo *et al.* suggest that ablating liver sequestration of Ad requires simultaneous inactivation of three major mechanisms: 1) Kupffer cell scavenging, 2) hepatocyte transduction mediated by FX binding, and 3) Ad5 penton RGD motif-mediated interactions with LSECs and hepatocytes, which cause virus retention in the space of Disse.[34] Extensive genetic modifications may be poorly tolerated because they often prevent self-assembly of the viral capsid, resulting in reduced or ablated virus production. Consequently, rather than systematically engineering Ad to eliminate each of the

93

numerous potential interactions, strategies which focus on masking viruses have come to the forefront.

5.4.2   Polymer conjugation

Covalent chemical modifications of Ad capsids using synthetic polymers such as polyethylene glycol (PEG) and poly-*N*-(2-hydroxypropyl) methacrylamide (HPMA) have yielded some of the most promising results thus far.[35] Polymer-conjugated Ad have been shown to evade pre-existing NAbs and KC scavenging, in addition to detargeting from the liver and blunted innate immune responses.[36-40] However, repeated dosing remains problematic because antibodies are generated against the sites of polymer attachment to the virus.[41] Studies also suggest that polymer conjugation, particularly with low molecular weight PEGs, provides incomplete shielding of the virus.[39] Still, it may be difficult to achieve high-density conjugation of large PEGs to viral capsids due to steric hindrance between PEG molecules. Furthermore, a high degree of covalent modification can significantly inhibit viral transduction efficiency, potentially by interfering with the intracellular trafficking of vector particles.[37,39] Viral inactivation resulting from heavy modification must be carefully balanced with the need to mask the virus effectively.

5.4.3   Non-covalent coating

Various materials have been investigated for the non-covalent modification of Ad vectors. Because the Ad hexon is negatively charged, cationic lipids, polymers, and polypeptides have been electrostatically complexed with the Ad capsid.[42-44] Some groups have taken advantage of the high-affinity Ad5 hexon-FX interaction by coating Ad5 with fusion proteins containing the Gla domain of FX,[45] and with PEGylated FX.[46] In contrast to the covalent modifications described previously, these self-assembly approaches have the advantage of being reversible, allowing for native virus trafficking in the intracellular environment. Unfortunately, promising *in vitro* results such as resistance to NAbs and reduced hepatocyte transduction failed to translate to *in vivo* experiments in most cases. It is likely that non-covalent coatings are prematurely displaced *in vivo* as a result of

94

interactions with charged molecules or endogenous coagulation factors that are present in the blood at high concentrations.

5.5   Future perspectives

Overall, clinical translation of adenoviral gene delivery vectors has been limited as a result of high seroprevalence in the general population and sequestration of the majority of intravenously injected adenovirus by Kupffer cells and hepatocytes. Reducing immunogenicity and detargeting virus away from the liver are therefore critical challenges in developing more effective Ad-based vectors that can be administered systemically for cancers that are not amenable to intratumoral injections or for metastatic cancer. Although modification of viruses with polymers has yielded some promising results thus far, many of the complex *in vivo* interactions between virus and host are still poorly understood. As these interactions are elucidated, further modifications can be made to significantly improve the safety and biodistribution profiles of these vectors. In addition, advances in polymer synthesis can be harnessed to develop sophisticated new materials for use in adenovirus-polymer hybrid vectors.

References

1.   Cross, D. & Burmester, J. K. Gene therapy for cancer treatment: past, present and future. *Clin Med Res* **4,** 218–227 (2006).
2.   Amer, M. H. Gene therapy for cancer: present status and future perspective. *Mol Cell Ther* **2,** 27 (2014).
3.   Warnock, J. N., Daigre, C. & Al-Rubeai, M. Introduction to viral vectors. *Viral Vectors for Gene Therapy* (2011).
4.   Pack, D. W., Hoffman, A. S., Pun, S. H. & Stayton, P. S. Design and development of polymers for gene delivery. *Nat Rev Drug Discov* **4,** 581–593 (2005).
5.   Liu, T.-C. & Kirn, D. Gene therapy progress and prospects cancer: oncolytic viruses. *Gene Ther.* **15,** 877–884 (2008).
6.   Ries, S. & Korn, W. M. ONYX-015: mechanisms of action and clinical potential of a replication-selective adenovirus. *Br. J. Cancer* **86,** 5–11 (2002).
7.   Garber, K. China approves world's first oncolytic virus therapy for cancer treatment. *J Natl Cancer Inst* **98,** 298–300 (2006).
8.   Demers, G. W., Johnson, D. E., Tsai, V., Wen, S.-F., Quijano, E., Machemer, T., Philopena, J., Ramachandra, M., Howe, J. A., Shabram, P., Ralston, R. & Engler, H. Pharmacologic indicators of antitumor efficacy for oncolytic virotherapy. *Cancer Res.* **63,** 4003–4008 (2003).

9. Ramsey, J. D., Vu, H. N. & Pack, D. W. A top-down approach for construction of hybrid polymer-virus gene delivery vectors. *J Control Release* **144,** 39–45 (2010).

10. *J. Gene Med. Gene Therapy Clinical Trials Worldwide.* at <http://www.wiley.com/legacy/wileychi/genmed/clinical/>

11. Campos, S. K. & Barry, M. A. Current advances and future challenges in Adenoviral vector biology and targeting. *Curr Gene Ther* **7,** 189–204 (2007).

12. Singh, R. & Kostarelos, K. Designer adenoviruses for nanomedicine and nanodiagnostics. *Trends Biotechnol.* **27,** 220–229 (2009).

13. Arnberg, N. Adenovirus receptors: implications for tropism, treatment and targeting. *Rev. Med. Virol.* **19,** 165–178 (2009).

14. Roelvink, P. W., Lizonova, A., Lee, J. G., Li, Y., Bergelson, J. M., Finberg, R. W., Brough, D. E., Kovesdi, I. & Wickham, T. J. The coxsackievirus-adenovirus receptor protein can function as a cellular attachment protein for adenovirus serotypes from subgroups A, C, D, E, and F. *J. Virol.* **72,** 7909–7915 (1998).

15. Gaggar, A., Shayakhmetov, D. M. & Lieber, A. CD46 is a cellular receptor for group B adenoviruses. *Nat. Med.* **9,** 1408–1412 (2003).

16. Wu, E. & Nemerow, G. R. Virus yoga: the role of flexibility in virus host cell recognition. *Trends Microbiol* **12,** 162–169 (2004).

17. Wickham, T. J., Mathias, P., Cheresh, D. A. & Nemerow, G. R. Integrins αvβ3 and αvβ5 promote adenovirus internalization but not virus attachment. *Cell* **73,** 309–319 (1993).

18. Khare, R., Chen, C. Y., Weaver, E. A. & Barry, M. A. Advances and future challenges in adenoviral vector pharmacology and targeting. *Curr Gene Ther* **11,** 241–258 (2011).

19. Cohen, C. J., Shieh, J. T., Pickles, R. J., Okegawa, T., Hsieh, J. T. & Bergelson, J. M. The coxsackievirus and adenovirus receptor is a transmembrane component of the tight junction. *Proc. Natl. Acad. Sci. U.S.A.* **98,** 15191–15196 (2001).

20. Sumida, S. M., Truitt, D. M., Lemckert, A. A. C., Vogels, R., Custers, J. H. H. V., Addo, M. M., Lockman, S., Peter, T., Peyerl, F. W., Kishko, M. G., Jackson, S. S., Gorgone, D. A., Lifton, M. A., Essex, M., Walker, B. D., Goudsmit, J., Havenga, M. J. E. & Barouch, D. H. Neutralizing antibodies to adenovirus serotype 5 vaccine vectors are directed primarily against the adenovirus hexon protein. *J. Immunol.* **174,** 7179–7185 (2005).

21. Alemany, R., Suzuki, K. & Curiel, D. T. Blood clearance rates of adenovirus type 5 in mice. *J. Gen. Virol.* **81,** 2605–2609 (2000).

22. Lieber, A., He, C. Y., Meuse, L., Schowalter, D., Kirillova, I., Winther, B. & Kay, M. A. The role of Kupffer cell activation and viral gene expression in early liver toxicity after infusion of recombinant adenovirus vectors. *J. Virol.* **71,** 8798–8807 (1997).

23. Khare, R., Reddy, V. S., Nemerow, G. R. & Barry, M. A. Identification of adenovirus serotype 5 hexon regions that interact with scavenger receptors. *J. Virol.* **86,** 2293–2301 (2012).

24. Di Paolo, N. C., Miao, E. A., Iwakura, Y., Murali-Krishna, K., Aderem, A., Flavell, R. A., Papayannopoulou, T. & Shayakhmetov, D. M. Virus binding to a plasma membrane receptor triggers interleukin-1 alpha-mediated proinflammatory macrophage response in vivo. *Immunity* **31,** 110–121 (2009).

25. Hegenbarth, S., Gerolami, R., Protzer, U., Tran, P. L., Brechot, C., Gerken, G. & Knolle, P. A. Liver sinusoidal endothelial cells are not permissive for adenovirus type 5. *Hum. Gene Ther.* **11,** 481–486 (2000).

26. Tao, N., Gao, G. P., Parr, M., Johnston, J., Baradet, T., Wilson, J. M., Barsoum, J. & Fawell, S. E. Sequestration of adenoviral vector by Kupffer cells leads to a nonlinear

dose response of transduction in liver. *Mol. Ther.* **3,** 28–35 (2001).

27. Kalyuzhniy, O., Di Paolo, N. C., Silvestry, M., Hofherr, S. E., Barry, M. A., Stewart, P. L. & Shayakhmetov, D. M. Adenovirus serotype 5 hexon is critical for virus infection of hepatocytes in vivo. *Proc. Natl. Acad. Sci. U.S.A.* **105,** 5483–5488 (2008).

28. Waddington, S. N., McVey, J. H., Bhella, D., Parker, A. L., Barker, K., Atoda, H., Pink, R., Buckley, S. M. K., Greig, J. A., Denby, L., Custers, J., Morita, T., Francischetti, I. M. B., Monteiro, R. Q., Barouch, D. H., van Rooijen, N., Napoli, C., Havenga, M. J. E., Nicklin, S. A. & Baker, A. H. Adenovirus serotype 5 hexon mediates liver gene transfer. *Cell* **132,** 397–409 (2008).

29. Bradshaw, A. C., Parker, A. L., Duffy, M. R., Coughlan, L., van Rooijen, N., Kähäri, V.-M., Nicklin, S. A. & Baker, A. H. Requirements for receptor engagement during infection by adenovirus complexed with blood coagulation factor X. *PLoS Pathog.* **6,** – (2010).

30. Alba, R., Bradshaw, A. C., Parker, A. L., Bhella, D., Waddington, S. N., Nicklin, S. A., van Rooijen, N., Custers, J., Goudsmit, J., Barouch, D. H., McVey, J. H. & Baker, A. H. Identification of coagulation factor (F)X binding sites on the adenovirus serotype 5 hexon: effect of mutagenesis on FX interactions and gene transfer. *Blood* **114,** 965–971 (2009).

31. Doronin, K., Flatt, J. W., Di Paolo, N. C., Khare, R., Kalyuzhniy, O., Acchione, M., Sumida, J. P., Ohto, U., Shimizu, T., Akashi-Takamura, S., Miyake, K., Macdonald, J. W., Bammler, T. K., Beyer, R. P., Farin, F. M., Stewart, P. L. & Shayakhmetov, D. M. Coagulation factor X activates innate immunity to human species C adenovirus. *Science* **338,** 795–798 (2012).

32. Alba, R., Bradshaw, A. C., Coughlan, L., Denby, L., McDonald, R. A., Waddington, S. N., Buckley, S. M. K., Greig, J. A., Parker, A. L., Miller, A. M., Wang, H., Lieber, A., van Rooijen, N., McVey, J. H., Nicklin, S. A. & Baker, A. H. Biodistribution and retargeting of FX-binding ablated adenovirus serotype 5 vectors. *Blood* **116,** 2656–2664 (2010).

33. Xu, Z., Qiu, Q., Tian, J., Smith, J. S., Conenello, G. M., Morita, T. & Byrnes, A. P. Coagulation factor X shields adenovirus type 5 from attack by natural antibodies and complement. *Nat. Med.* **19,** 452–457 (2013).

34. Di Paolo, N. C., van Rooijen, N. & Shayakhmetov, D. M. Redundant and synergistic mechanisms control the sequestration of blood-born adenovirus in the liver. *Mol. Ther.* **17,** 675–684 (2009).

35. Kreppel, F. & Kochanek, S. Modification of adenovirus gene transfer vectors with synthetic polymers: a scientific review and technical guide. *Mol. Ther.* **16,** 16–29 (2008).

36. O'Riordan, C. R., Lachapelle, A., Delgado, C., Parkes, V., Wadsworth, S. C., Smith, A. E. & Francis, G. E. PEGylation of adenovirus with retention of infectivity and protection from neutralizing antibody in vitro and in vivo. *Hum. Gene Ther.* **10,** 1349–1358 (1999).

37. Doronin, K., Shashkova, E. V., May, S. M., Hofherr, S. E. & Barry, M. A. Chemical modification with high molecular weight polyethylene glycol reduces transduction of hepatocytes and increases efficacy of intravenously delivered oncolytic adenovirus. *Hum. Gene Ther.* **20,** 975–988 (2009).

38. Prill, J.-M., Espenlaub, S., Samen, U., Engler, T., Schmidt, E., Vetrini, F., Rosewell, A., Grove, N., Palmer, D., Ng, P., Kochanek, S. & Kreppel, F. Modifications of adenovirus hexon allow for either hepatocyte detargeting or targeting with potential evasion from Kupffer cells. *Mol. Ther.* **19,** 83–92 (2011).

97

39. Mok, H., Palmer, D. J., Ng, P. & Barry, M. A. Evaluation of polyethylene glycol modification of first-generation and helper-dependent adenoviral vectors to reduce innate immune responses. *Mol. Ther.* **11,** 66–79 (2005).
40. Croyle, M. A., Le, H. T., Linse, K. D., Cerullo, V., Toietta, G., Beaudet, A. & Pastore, L. PEGylated helper-dependent adenoviral vectors: highly efficient vectors with an enhanced safety profile. *Gene Ther.* **12,** 579–587 (2005).
41. Croyle, M. A., Chirmule, N., Zhang, Y. & Wilson, J. M. 'Stealth' adenoviruses blunt cell-mediated and humoral immune responses against the virus and allow for significant gene expression upon readministration in the lung. *J. Virol.* **75,** 4792–4801 (2001).
42. Fasbender, A., Zabner, J., Chillón, M., Moninger, T. O., Puga, A. P., Davidson, B. L. & Welsh, M. J. Complexes of adenovirus with polycationic polymers and cationic lipids increase the efficiency of gene transfer in vitro and in vivo. *J Biol Chem* **272,** 6479–6489 (1997).
43. Wang, C.-H. K., Chan, L. W., Johnson, R. N., Chu, D. S. H., Shi, J., Schellinger, J. G., Lieber, A. & Pun, S. H. The transduction of Coxsackie and Adenovirus Receptor-negative cells and protection against neutralizing antibodies by HPMA-co-oligolysine copolymer-coated adenovirus. *Biomaterials* **32,** 9536–9545 (2011).
44. Jiang, Z. K., Koh, S. B. S., Sato, M., Atanasov, I. C., Johnson, M., Zhou, Z. H., Deming, T. J. & Wu, L. Engineering polypeptide coatings to augment gene transduction and in vivo stability of adenoviruses. *J Control Release* **166,** 75–85 (2013).
45. Chen, C. Y., May, S. M. & Barry, M. A. Targeting adenoviruses with factor x-single-chain antibody fusion proteins. *Hum. Gene Ther.* **21,** 739–749 (2010).
46. Matsui, H., Sakurai, F., Katayama, K., Yamaguchi, T., Okamoto, S., Takahira, K., Tachibana, M., Nakagawa, S. & Mizuguchi, H. A hexon-specific PEGylated adenovirus vector utilizing blood coagulation factor X. *Biomaterials* **33,** 3743–3755 (2012).

<div align="center">Chapter 6.</div>

IDENTIFICATION OF ADENOVIRUS-BINDING PEPTIDES FOR USE IN SELF-ASSEMBLING POLYMER SHIELDS

<div align="center">Christine E. Wang, Hua Wei, André Lieber, Dmitry Shayakhmetov, and Suzie H. Pun</div>

Abstract

Clinical translation of adenovirus (Ad)-based gene delivery vectors remains challenging due to innate and adaptive immune responses triggered by the virus, as well as significant liver sequestration of viral particles preventing delivery to peripheral disease sites such as tumors. We hypothesized that a self-assembling, non-covalent polymeric coating could be used to shield Ad vectors against undesirable interactions *in vivo* while maintaining the activity of the native virus. In this work, phage display was used to screen for novel peptide sequences with affinity for the major Ad capsid protein. Although several promising peptide candidates were isolated from panning experiments and demonstrated binding to Ad when expressed in phage, binding was not observed for purified peptide.

6.1   Introduction

Adenoviruses, particularly Ad serotype 5 (Ad5), are the most common vectors used in clinical gene therapy trials because of their efficient transduction of many cell types and ease of production.[1] However, broad clinical utility of adenoviral vectors has been limited by safety issues such as the induction of potent innate immune responses after systemic Ad administration,[2] the strong liver tropism of Ad5 *in vivo*,[3,4] and a high prevalence of pre-existing anti-Ad5 immunity in the population. Genetic and chemical modifications that can allow Ad vectors to overcome these hurdles are therefore of great interest.

Recent work in our lab demonstrated that copolymers of *N*-(2-hydroxypropyl) methacrylamide (HPMA) and cationic oligolysine peptides can complex with negatively-charged Ad capsids through electrostatic interactions.[5] *In vitro* transductions performed in the presence of neutralizing antibodies (NAbs) against Ad5 demonstrated that these

<div align="center">99</div>

polymer-coated viruses were substantially resistant to NAb inactivation. Unfortunately, subsequent testing in mice pre-immunized against Ad5 indicated that the coating did not confer resistance to NAbs *in vivo* (unpublished data). This finding is thought to be the result of premature displacement of the polymer coating *in vivo*.

We hypothesized that a novel self-assembling polymer coating based on peptides with specificity and affinity for adenovirus would be more stable *in vivo* than the previous coating based on charge interactions. To this end, the goals of this work were to (1) identify Ad-binding peptides and (2) synthesize and evaluate Ad-coating polymers *in vitro*. Several promising peptide candidates were identified through phage display and demonstrated binding to Ad in the context of isolated phage; however, no binding was observed for the purified peptide alone. Interestingly, complexation of viral particles with peptide-polymer conjugates led to an unexpected increase in viral transduction *in vitro*.

6.2   Materials and methods

6.2.1   Phage panning

Phage display was used to screen for peptide sequences that bind specifically to the hexon protein of Ad5 through a competitive displacement panning technique (Figure 6.1). 6×10^{10} vp of Ad5 in 0.1 M $NaHCO_3$ (pH 8.6) buffer were adsorbed to a polystyrene plate overnight at 4°C, followed by blocking with a solution of 0.5% bovine serum albumin (BSA) in $NaHCO_3$ buffer for 1 h at 4°C. In the first round of panning, surface-immobilized Ad5 were incubated with 2×10^{11} plaque forming units (pfu) of phage from the Ph.D-12 library (New England Biolabs, NEB) for 1 h at room temperature with gentle shaking. The plate was then washed 5 times with TBST (Tris-buffered saline containing 0.1% Tween-20 detergent) to remove unbound or weakly bound phage. Capitalizing on the fact that the blood protein coagulation factor X (FX) binds a known site on the Ad5 hexon with picomolar affinity,[3] the remaining phage were eluted via competitive displacement by the FX protein. The sample was incubated with a 50-fold excess of FX protein (over the number of immobilized virus hexon trimers) in TBS containing 2 mM $CaCl_2$ and 2 mM $MgCl_2$ for 1.5 h at room temperature with gentle shaking, and the supernatant containing eluted phage was then collected.

100
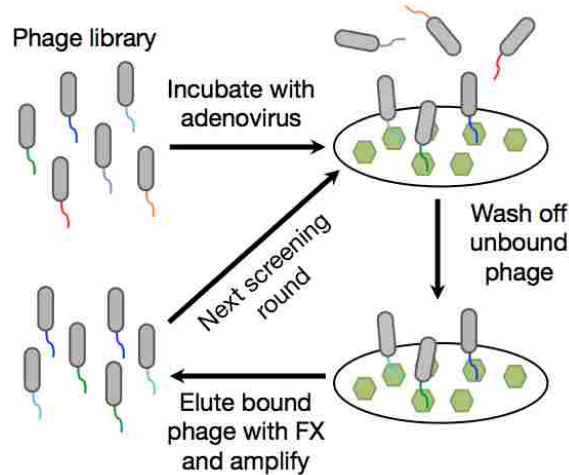
Figure 6.1 Phage panning strategy using competitive displacement with FX protein to elute adenovirus-binding phage.

Eluted phage were titered and amplified following standard protocols from NEB. 2×10^{11} pfu of the amplified library were then used as the input library for the subsequent panning round; a total of 4 rounds of panning were performed in this manner. To increase the stringency of each successive round, the phage library incubation time was decreased (to 45 min, 30 min, and 20 min for the second, third, and fourth rounds, respectively) while the concentration of Tween-20 in the wash buffer was increased (to 0.5%, 1%, and 1%) in order to favor retention of high-affinity binders. A 1 h elution was used for the second through fourth rounds.

Following the third and fourth rounds of panning, individual phage clones were amplified, and their DNA was purified using a QIAprep Spin M13 Kit (Qiagen). Samples containing 300-350 ng of DNA and 25 pmol of -96 gIII primer were submitted to GENEWIZ for sequencing.

6.2.2   Phage binding studies

Selected phage clones were tested for binding to Ad5 in an elution and titering-based assay mirroring the format and conditions of the fourth round of panning. 3×10^{10} vp of Ad5 in NaHCO$_3$ buffer were adsorbed to each well of a 96-well polystyrene plate overnight at 4°C, followed by blocking with 0.5% BSA in NaHCO$_3$ buffer for 1 h at 4°C. 10^{11} pfu of each isolated phage clone were then added to different virus-coated wells and incubated for 20 min at room temperature with gentle shaking. Wells were washed 5 times with 1% TBST to

101

remove unbound phage. Bound phage were eluted by incubating wells with FX solution for 1 h at room temperature with gentle shaking and then collecting the supernatants. Finally, samples were titered according to NEB protocols to determine the number of phage eluted from each well. As a negative control, each phage clone was also tested for binding to blocked, uncoated wells. M13KE, an "insertless" phage displaying no peptide, was also tested.

6.2.3   Peptide synthesis

The 2-04 peptide and a scrambled version of the peptide (scr2-04) were synthesized on solid support by standard Fmoc solid phase peptide synthesis (SPPS) using an automated PS3 Peptide Synthesizer (Protein Technologies, Phoenix, AZ). Peptides were synthesized with C-terminal Gly_3-Ser spacers, using the Biotin-PEG NovaTag resin (Novabiochem) to yield a biotin at the C-termini of the peptides or Fmoc-Cys(Trt)-Wang resin (Novabiochem) to add a thiol residue at the C-terminal for conjugation to polymer. The resulting sequences are as follows: 2-04-biotin (EHTPRLSWLEPSGGGS-PEG$_3$-biotin), 2-04-Cys (EHTPRLSWLEPSGGGSC), scr2-04-biotin (HRSPESTWELLPGGGS-PEG$_3$-biotin), and scr2-04-Cys (HRSPESTWELLPGGGSC).

Peptides were cleaved from resin using a cocktail of trifluoroacetic acid (TFA)/triisopropylsilane (TIPS)/H_2O (95:2.5:2.5, v/v/v) for biotin-terminated peptides or TFA/TIPS/dichloromethane (DCM)/1,2-ethanedithiol (EDT) (92.5/2.5/2.5/2.5, v/v/v/v) for cysteine-terminated peptides. Cleaved peptides were precipitated in cold ether, dissolved in methanol, and reprecipitated in cold ether. Peptides were purified to >90% purity using reverse-phase high performance liquid chromatography (RP-HPLC) and verified by matrix-assisted laser desorption/ionization time-of-flight mass spectrometry (MALDI-TOF MS).

6.2.4   Peptide binding studies

Binding of the 2-04 and scr2-04 peptides to Ad5 was measured using an Octet Red96 (ForteBio). Biotinylated peptides (100 nM) in binding buffer (PBS containing 1% BSA and 0.05% Tween-20) were immobilized to streptavidin biosensors (ForteBio) for 300 s.

Biosensors were dipped in solutions of 10^9 vp of Ad5 in binding buffer to measure association and then transferred back to fresh binding buffer to monitor dissociation.

6.2.5   *Polymer synthesis and characterization*

A diblock copolymer containing an oligoethylene glycol methacrylate (OEGMA, MW 300) block and a hydroxyethylmethacrylate (HEMA)/pyridyl disulfide methacrylate (PDSMA) block was synthesized by atom transfer radical polymerization (ATRP). Polymerization of the P(OEGMA) block was first conducted in tetrahydrofuran (THF), using ethyl-2-bromoisobutyrate as the initiator and *N,N,N',N'',N''*-pentamethyldiethylenetriamine (PMDETA)/Cu(I)Br as the catalyst (relative molar ratios of initiator:CuBr:PMDETA = 1:1:1). The monomer:initiator ratio used was 50:1, and the initial monomer concentration was 1.5 M. Polymerization was allowed to proceed for 15 min at 45°C. The reaction mixture was dialyzed against distilled water to remove unreacted monomers and copper catalyst. The product was collected by lyophilization.

The diblock copolymer was synthesized using the P(OEGMA)-Br block as the macroinitiator and PMDETA/CuBr at the catalyst. The relative molar ratios of initiator:CuBr:PMDETA were 1:1:1. The feed ratios of HEMA:PDSMA:initiator were 300:36:1 and the total monomer concentration was 3 M in dimethylsulfoxide (DMSO). Polymerization was allowed to proceed for 24 h at 65°C. The reaction mixture was dialyzed against distilled water to remove unreacted monomers and copper catalyst. The product was collected by lyophilization.

^{1}H NMR spectra were recorded on a Bruker AV 500 nuclear magnetic resonance (NMR) instrument using DMF-d_7 as the solvent to determine polymer composition. Gel permeation chromatography (GPC) was used to determine molecular weight and polydispersity. SEC Tosoh TSK-GEL R-3000 and R-4000 columns (Tosoh Bioscience, Montgomeryville, PA) were connected in series to an Agilent 1200 Series System (Agilent Technologies, Santa Clara, CA), Optilab-rEX refractometer, and miniDAWN TREOS triple-angle static light scattering detector (Wyatt Technology, Santa Barbara, CA). HPLC-grade DMF containing 0.1 wt% LiBr at 60°C was used as the mobile phase at a flow rate of 1 mL/min. Absolute molecular weight averages and dn/dc were calculated using ASTRA software (Wyatt). The final composition of the copolymer was P(OEGMA)$_{33}$-*b*-P(HEMA$_{55}$-*st*-PDSMA$_8$).

103

6.2.6   Preparation of peptide-grafted polymers poly(2-04) and poly(scr2-04)

Peptide conjugation to the diblock copolymer was performed as described previously with slight modification.[6] 8 mg of P(OEGMA)$_{33}$-*b*-P(HEMA$_{55}$-*st*-PSDMA$_8$) polymer (0.36 μmol polymer, 2.91 μmol PDS groups) was dissolved in 1 mL of a 1:1 mixture of 0.5 M NaCl/20 mM HEPES buffer at pH 7.1 and *N,N*-dimethylformamide (DMF) in a 5 mL pear-shaped flask. 10.6 mg of 2-04-Cys or scr2-04-Cys peptide (5.82 μmol, 2 equivalents relative to diblock copolymer PDS groups) was dissolved in 0.2 mL of buffer/DMF, added into the flask, and allowed to stir under argon at room temperature. After overnight reaction, the absorbance of released 2-pyridinethione was measured at 343 nm to determine the extent of the disulfide exchange reaction. The reaction mixture was dialyzed against distilled water to remove DMF and unconjugated peptide. The product was collected by lyophilization.

6.2.7   Cell culture

HeLa cells (ATCC CCL-2) were maintained in MEM medium (Corning cellgro) supplemented with 10% fetal bovine serum (HyClone) and 1% antibiotic-antimycotic solution (HyClone). Cells were cultured as a monolayer in a 37°C, 5% CO_2 environment. Medium was replaced every 2-3 days. Cells were passaged at ~70-80% confluence by incubation with Trypsin-EDTA, followed by resuspension in complete growth medium.

6.2.8   Cell transduction

Cell transduction studies with polymer-coated viruses were performed as described previously with some modifications.[5] Cells were seeded in 24-well plates at a density of 20,000 cells per well in 1 mL of complete growth medium and incubated in a 37°C, 5% CO_2 environment for 24 h prior to transduction.

Polymer solutions (dissolved in sterile dH_2O) were added to Ad5-GFP virus solutions (University of Michigan Vector Core) to achieve the desired polymer to viral particle mole ratios. Solutions were then incubated at room temperature for 30 min (or at 37°C for 3 days for long-term stability studies) to allow polymer-virus complexes to form.

After incubation, adenovirus or polymer-coated virus solutions were diluted 10-fold in growth medium without serum. Cells were rinsed once with PBS, and 200 μL of virus or polymer-coated virus solution was added to each well. A particle multiplicity of infection (pMOI, viral particles per cell) of 5000 was used for viral transduction. Cells were incubated with virus at 37°C for pre-determined amounts of time and then rinsed once with PBS. 1 mL of complete growth medium with serum was added to each well and cells were returned to the incubator.

24 h after transduction, cells were prepared for flow cytometry analysis. Cells were rinsed once with PBS and then harvested by incubation with 200 μL of Trypsin-EDTA, followed by resuspension with 1 mL of complete growth medium. Cells were transferred to 1.5 mL microcentrifuge tubes and pelleted at 1000 g for 5 min at 4°C. The supernatant was aspirated, and the cell pellets were resuspended in complete growth medium containing 2 μg/mL propidium iodide (PI) and incubated at 4°C for 5 min. Cells were pelleted, resuspended in fresh growth medium, and analyzed for GFP expression using a MACSQuant Analyzer flow cytometer (Miltenyi).

6.3   Results and discussion

6.3.1   Identification of Ad-binding phage candidates

$2{\times}10^{11}$ pfu of phage were used as input in each round of panning. The results demonstrated an increase in the titer of phage eluted with each successive round (Figure 6.2). This suggests progressive enrichment of the phage pool with phage bearing specificity for the Ad5 target.
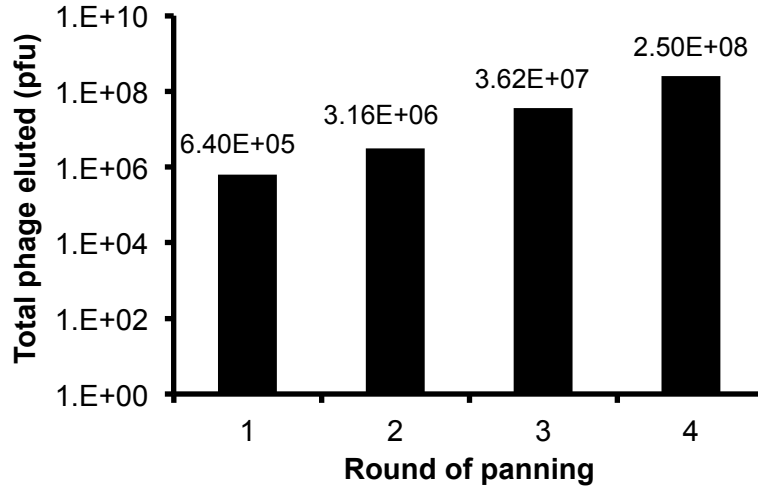
Figure 6.2 Titers of eluted phage over 4 rounds of panning.

Following the third and fourth rounds of panning, individual phage clones were isolated and sequenced to identify the displayed peptides. From the sequencing results, a number of possible consensus sequences were identified based on the frequency of their occurrence and/or similarities to other sequences (Table 6.1). The remaining phage clones not represented in the table (13 other clones after the third round and 6 others after the fourth round) had unique sequences with no overlapping motifs and were not considered to be consensus sequences.

Three potential binding sequences were identified following the fourth round of panning. Two homologous sequences, clones 2-04 and 2-13, were found to overlap at 8 out of 12 amino acid positions and together accounted for 26% and 42% of the clones sequenced after the third and fourth rounds, respectively. A third, non-homologous sequence (2-15) occurred in 9% and 21% of the clones sequenced after the third and fourth rounds, respectively.

Table 6.1 Possible consensus peptide sequences and their frequencies after the third and fourth rounds of panning. Sequence overlaps between clones 2-04/2-13 and 2-05/2-10 are underlined.

Clone name	Peptide sequence	Frequency after 3rd round	Frequency after 4th round
2-04	EHTPRLSWLEPS	**21.7%** (5/23)	**10.5%** (2/19)
2-13	EHTAALSWLPPL	**4.3%** (1/23)	**31.6%** (6/19)
2-15	NHWPFIIRYDSL	**8.7%** (2/23)	**21.1%** (4/19)

106

| 2-05 | KLWDYKLSYTPV | **4.3%** (1/23) | **5.3%** (1/19) |
| 2-10 | KIWDISLSPPFT | **4.3%** (1/23) | **0.0%** (0/19) |

Interestingly, two other clones, 2-05 and 2-10, were identified after the third round of panning and overlapped one another at 5 out of 12 amino acids (and also contained the "LS" motif present in the 2-04/2-13 sequences). However, these two clones had low overall occurrence among the sequenced phage, particularly after the fourth round.

6.3.2   Phage binding studies

Because they were highly represented among the sequences obtained from the third and fourth rounds of panning, phage clones 2-04, 2-13, and 2-15 were tested for binding to Ad5. Overall, all three phage clones demonstrated specificity for Ad5, with 2- to 11-fold higher bound phage titers over the M13KE insertless control phage (Figure 6.3). Therefore, binding was believed to be mediated by the displayed peptide and not by another portion of the bacteriophage coat. A low and consistent level of phage binding to uncoated polystyrene wells was observed for all clones, suggesting that binding was predominantly virus-dependent.
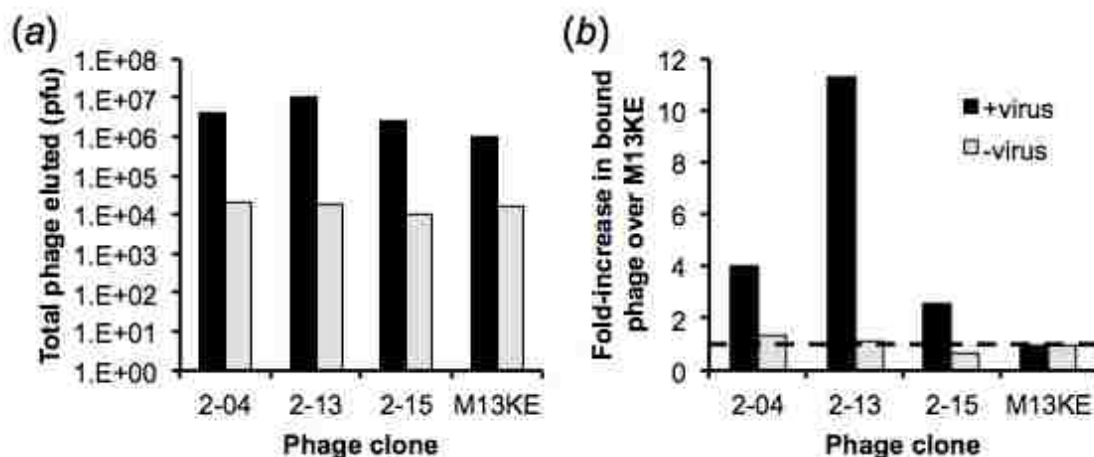

Figure 6.3 Selected phage clones demonstrate specificity for Ad5 by an elution and titering assay. (a) Raw eluate titers of phage clones bound to Ad5-coated polystyrene (black bars) and uncoated polystyrene (grey bars). (b) Peptide-mediated increase in binding, calculated by normalizing the eluate titer for each clone to the corresponding titer for the M13KE control phage.

107

6.3.3   Peptide binding studies

Having demonstrated Ad5 binding by the phage-displayed peptides, the isolated peptides were synthesized for further characterization. Although phage clone 2-13 demonstrated the most promising phage binding data (in addition to being the most prevalent clone found in sequencing after the fourth round of panning), its displayed peptide is highly hydrophobic and was predicted to have poor water solubility. Thus, we chose to investigate the 2-04 peptide due to its promising phage binding, relative hydrophilicity, and sequence similarity to 2-13. The 2-04 peptide and a scrambled version of the peptide (scr2-04) were synthesized to contain C-terminal biotin tags.

Biolayer interferometry (BLI) was used to assess binding interactions between the 2-04 peptide and Ad5. Biotinylated peptides were immobilized to streptavidin-coated biosensor tips before immersing the tips in virus solution. However, only non-specific binding was observed, as the greatest signal was seen for Ad5 binding to unloaded tips (without any peptide immobilized), and the signal-to-noise ratio was low overall (Figure 6.4). This result suggests that the 2-04 peptide does not bind the target or binds with extremely low affinity.

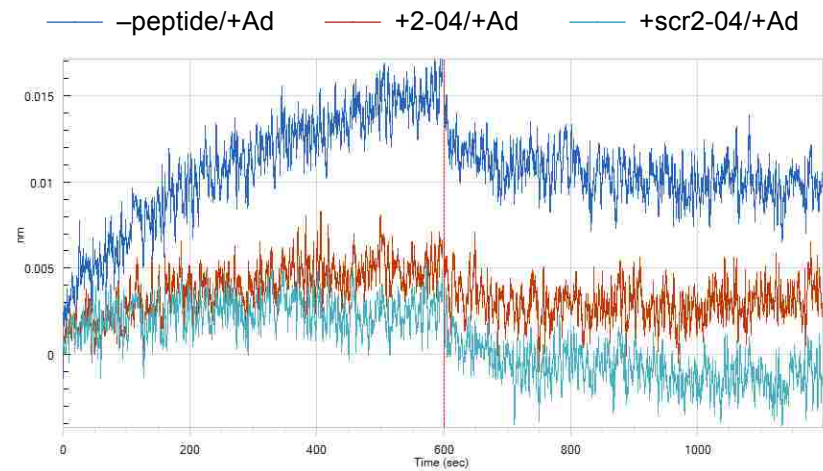**Figure 6.4** BLI sensorgram of Ad5 binding to immobilized peptides.

6.3.4   Transduction of HeLa cells with poly(2-04)-"coated" viruses

Because each phage virion displays 5 copies of its peptide variant, avidity effects could explain the discrepancy in binding between the phage clone and the synthesized peptide. We therefore sought to synthesize peptide-polymer conjugates for multivalent display of the

www.manaraa.com

peptides. A copolymer of oligoethylene glycol methacrylate (OEGMA), hydroxylethylmethacrylate (HEMA), and pyridyl disulfide methacrylate (PDSMA) was synthesized for preliminary studies. 2-04-Cys and scr2-04-Cys peptides were conjugated via the PDSMA groups of the polymer to yield poly(2-04) and poly(scr2-04), respectively. UV absorbance measurements indicate that approximately 5 peptides were conjugated per polymer chain, consistent with the efficiency reported in the literature.[6]

Because the virus-binding peptides were localized to one block of the polymer, we believed that interactions of poly(2-04) with the Ad5 surface would produce a virus that was effectively masked by the polymer's OEGMA block. We hypothesized that this neutral, hydrophilic OEGMA shield would decrease viral interaction with (and therefore decrease transduction of) HeLa cells, a cell line permissive for Ad5 infection. Surprisingly, the use of poly(2-04) to coat Ad5-GFP was found to increase the percentage of cells that were GFP-positive after a 1 h transduction (Figure 6.5a). These results were statistically significant for two different molar ratios of polymer to viral particle tested, 1000:1 and 5000:1, relative to their virus only, base polymer, and poly(scr2-04) controls. These trends were further confirmed in a duplicate study with similar results.
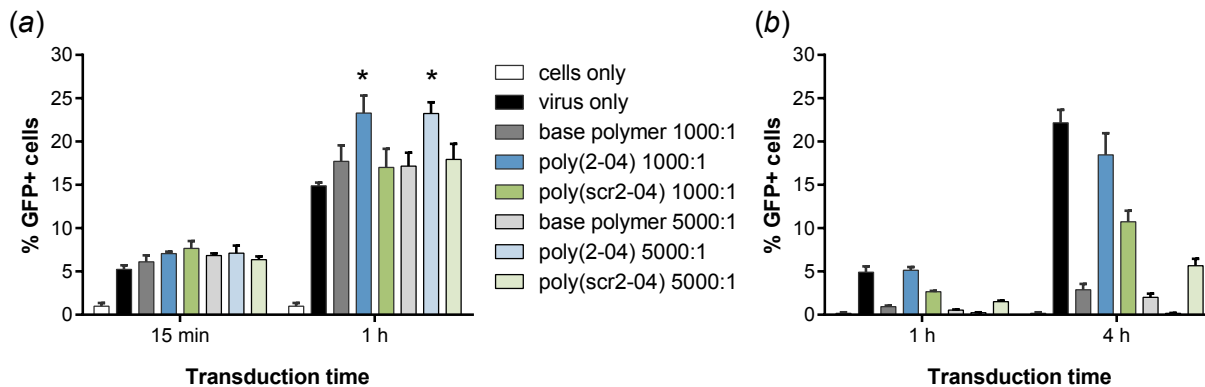
Figure 6.5 HeLa transduction efficiency of uncoated Ad5-GFP and Ad5-GFP complexed with poly(2-04) or control polymers at polymer:viral particle ratios of 1000:1 and 5000:1. Complexes were incubated for (a) 30 min at room temperature or (b) 3 days at 37°C prior to transduction. Data are reported as the mean ± S.D., $n = 3$. *$p < 0.05$ compared to virus only, base polymer, and poly(scr2-04) at the same polymer:virus ratio.

Based on these trends, we hypothesized that the increased transduction efficiency of poly(2-04)-coated viruses might be due to polymer-mediated stabilization of the virus, as has been demonstrated for adenovirus nanocapsule formulations.[7] To test this hypothesis, naked virus and polymer-virus complexes were incubated for 3 days at 37°C prior to cell

transduction. The transduction efficiency of naked virus was significantly reduced following 3 day incubation, and transduction was not improved by the addition of poly(2-04) coating (Figure 6.5b). Meanwhile, infection with an equal pMOI of fresh virus resulted in ~40% and 90% GFP+ cells for 1 h and 4 h transductions, respectively (data not shown). Overall, these results indicate that the polymer does not stabilize the virus to inactivation over long periods of time.

6.4   Conclusions and future studies

The goal of this research was to identify peptides with specificity for Ad5 hexon to be incorporated into self-assembling polymer shields. As the first step toward developing rationally designed polymer-adenovirus hybrids, this study demonstrated the identification of several potential adenovirus-binding peptide sequences, using phage display panning against surface-immobilized Ad5 with FX-based phage elution. The specificity of the candidate phage clones for adenovirus was demonstrated via a phage titering assay. However, binding affinity was negligible for the synthesized 2-04 peptide alone. Moreover, preliminary studies with multivalent peptide-polymer conjugates indicated a surprising ability of polymers containing the 2-04 peptide to *increase* rather than mask viral transduction in HeLa cells. Additional studies can be performed to investigate the mechanisms underlying increased transduction by poly(2-04)-coated viruses.

Several alternative approaches toward the development of Ad-binding polymer shields are possible. Phage panning can be repeated using a different strategy, such as by using solution-phase panning rather than surface panning to reduce the likelihood of selecting for plastic-binding phage, by incorporating negative selection steps (subtractive panning) with non-FX-binding virus mutants, or by panning against isolated Ad5 hexon protein rather than the intact virion. Additionally, rather than identifying novel Ad-binding peptides through phage display, the hexon-binding portion of the FX protein can be synthesized for incorporation into polymer shields. Fender and coworkers have reported the synthesis of a FX Gla domain-derived 40-mer peptide (termed Gla^{mim}).[8] However, despite binding to hexon with nanomolar affinity, Gla^{mim} was not able to compete with FX for hexon binding and in fact appeared to have a different binding site than the full-length FX protein. Multivalent

110

display of the Gla^mim peptide on a hydrophilic polymer backbone could potentially provide sufficient avidity and steric hindrance to compete with the FX protein.

6.5 Acknowledgements

References

1. Khare, R., Chen, C. Y., Weaver, E. A. & Barry, M. A. Advances and future challenges in adenoviral vector pharmacology and targeting. *Curr Gene Ther* **11,** 241–258 (2011).
2. Lieber, A., He, C. Y., Meuse, L., Schowalter, D., Kirillova, I., Winther, B. & Kay, M. A. The role of Kupffer cell activation and viral gene expression in early liver toxicity after infusion of recombinant adenovirus vectors. *J. Virol.* **71,** 8798–8807 (1997).
3. Kalyuzhniy, O., Di Paolo, N. C., Silvestry, M., Hofherr, S. E., Barry, M. A., Stewart, P. L. & Shayakhmetov, D. M. Adenovirus serotype 5 hexon is critical for virus infection of hepatocytes in vivo. *Proc. Natl. Acad. Sci. U.S.A.* **105,** 5483–5488 (2008).
4. Waddington, S. N., McVey, J. H., Bhella, D., Parker, A. L., Barker, K., Atoda, H., Pink, R., Buckley, S. M. K., Greig, J. A., Denby, L., Custers, J., Morita, T., Francischetti, I. M. B., Monteiro, R. Q., Barouch, D. H., van Rooijen, N., Napoli, C., Havenga, M. J. E., Nicklin, S. A. & Baker, A. H. Adenovirus serotype 5 hexon mediates liver gene transfer. *Cell* **132,** 397–409 (2008).
5. Wang, C.-H. K., Chan, L. W., Johnson, R. N., Chu, D. S. H., Shi, J., Schellinger, J. G., Lieber, A. & Pun, S. H. The transduction of Coxsackie and Adenovirus Receptor-negative cells and protection against neutralizing antibodies by HPMA-co-oligolysine copolymer-coated adenovirus. *Biomaterials* **32,** 9536–9545 (2011).
6. Schellinger, J. G., Pahang, J. A., Johnson, R. N., Chu, D. S., Sellers, D. L., Maris, D. O., Convertine, A. J., Stayton, P. S., Horner, P. J. & Pun, S. H. Melittin-grafted HPMA-Oligolysine Based Copolymers for Improved Gene Delivery. *Biomaterials* **34,** 2318–2326 (2013).
7. Weng, D., Jiang, Z. K., Jin, J., Wu, L. & Lu, Y. Enhanced structural stability of adenovirus nanocapsule. *Progress in Natural Science: Materials International* **24,** 171–174 (2014).
8. Sumarheni, S., Hong, S.-S., Josserand, V., Coll, J.-L., Boulanger, P., Schoehn, G. & Fender, P. Human full-length coagulation factor X and a GLA domain-derived 40-mer polypeptide bind to different regions of the adenovirus serotype 5 hexon capsomer. *Hum. Gene Ther.* **25,** 339–349 (2014).

112

Part IV.

Future Perspectives

Chapter 7.

SUMMARY OF MAJOR FINDINGS AND RECOMMENDATIONS FOR FUTURE WORK

7.1   Summary of major findings

7.1.1   Junction opener proteins for enhancing nanoparticle delivery to solid tumors

Proteins that disrupt intercellular tight junctions can be used to enhance the diffusion of chemotherapeutic agents into epithelial tumors. In Chapter 1, PEGylated gold nanoparticles (AuNPs) were synthesized and injected in mice to investigate the size-dependent effect of the junction opener protein JO-4 on particle biodistribution. JO-4 pretreatment significantly increased tumor accumulation of 35 nm AuNPs but had no effect on larger particles of 120 nm. In addition to increasing the overall number of AuNPs localized to the tumor, JO-4 increased nanoparticle penetration into the tumor. These findings are important to further the design and development of drug carriers that utilize this delivery mechanism.

7.1.2   Sunflower polymers for tumor-targeted drug delivery

Polymer-drug conjugates with advanced architectures were investigated as an alternative to traditional drug carriers such as liposomes and micelles, which require formulation steps during manufacturing and can release drug prematurely *in vivo*. Chapter 2 summarizes the major considerations when designing anti-cancer drug delivery vehicles and highlights controlled living polymerization techniques enabling the synthesis of increasingly complex polymer nanostructures. In Chapter 3, atom transfer radical polymerization was used to synthesize polymers with a sunflower-like architecture. Sunflower polymers were synthesized with low polydispersity and good control over particle size based on polymerization time. Polymers were targeted to cancer cells by conjugation of folate to radiating "petals." These targeted sunflower polymers demonstrated receptor-mediated uptake by folate receptor-positive KB cells, while their linear analogues (comb polymers)

were taken up by non-specific mechanisms. In Chapter 4, this platform was extended by conjugating doxorubicin (Dox) to the polymer core via a pH-sensitive linker; targeted, Dox-loaded sunflower polymers demonstrated intracellular release of active drug leading to cytotoxicity in KB cells. However, *in vivo* efficacy of these polymers was limited due to low drug loading.

7.1.3 Self-assembling materials for cloaking adenoviral vectors

Polymeric coatings have the potential to improve the safety and efficacy of adenoviral gene delivery vectors *in vivo*. Chapter 5 reviews the challenges in translating adenoviruses to the clinic and current strategies for virus modification. In Chapter 6, phage display was used to screen for novel peptide ligands that bind specifically to the hexon protein of adenovirus serotype 5 (Ad5), with the ultimate goal of incorporating these peptides into self-assembling polymer shields for the virus. Multiple consensus sequences were identified, and several phage clones were found to bind specifically to adenovirus. However, binding affinity to adenovirus was negligible for the purified peptide alone.

7.2 Recommendations for future work

7.2.1 JO-conjugated sunflower polymers for tumor-targeted drug delivery

Background and significance

In previous work by Lieber and coworkers[1,2] and in Chapter 1 of this thesis, junction opener (JO) proteins were administered one hour prior to injection with a therapeutic compound or model drug. JO proteins have not yet been conjugated directly to drugs, nanoparticles, or other systems; however, given that the junction opening effect appears to be specific to tumors (DSG2 is generally not accessible for JO binding in normal tissues[3]), JO conjugation may be a useful strategy for enhancing the tumor localization, penetration, and therapeutic efficacy of anti-cancer drug delivery vehicles.

Aim 1: Synthesis of JO-conjugated AuNPs and quantification of biodistribution

JO proteins containing a C-terminal cysteine will be provided by PAI Life Sciences (Seattle, WA) and used to surface modify 5 nm AuNPs via thiol-gold reaction. After reaction, AuNPs

116

will be pelleted by centrifugation and washed, and unbound protein will be removed with the supernatant. JO-conjugated AuNPs (JO-AuNPs) will be characterized by dynamic light scattering. The biodistribution and intratumoral penetration of JO-AuNPs in A549 tumor-bearing mice will be analyzed following the methods described in Chapter 1. Results will be compared to those obtained with the traditional administration strategy (injection of JO protein followed by a separate injection of AuNPs one hour later). Furthermore, JO content on the AuNPs can be varied to determine if there is a JO surface density for which tumor accumulation is maximized.

Aim 2: Synthesis of JO-conjugated sunflower polymers

JO proteins containing a C-terminal cysteine will be labeled with a dibenzocyclooctyne (DBCO)-PEG$_4$-maleimide crosslinker (Click Chemistry Tools, Scottsdale, AZ) to introduce cyclooctyne functionality. Labeled protein will be purified using a PD-10 desalting column to remove unreacted crosslinker. The resulting JO-DBCO protein will be conjugated to the sunflower polymers synthesized in Chapters 3 and 4 by strain-promoted copper-free click reaction between the cyclooctyne and the azide termini of sunflower petals. The final JO-sunflower conjugates will be purified by size exclusion chromatography and characterized by dynamic light scattering, SDS-PAGE, and Western blot analysis.

The ability of the JO-sunflower conjugates to bind and open tight junctions will be verified using PEG permeability assays as described previously.[1] In addition, cytotoxicity studies will be performed as described in Chapter 4 to ensure that JO conjugation does not affect the potency of the sunflower-Dox formulation.

Aim 3: In vivo evaluation of JO-conjugated sunflower polymers

JO-sunflower conjugates will be tested for anti-tumor efficacy using DSG2 transgenic mice.[3] Mice will be inoculated subcutaneously with ID8-DSG2 cells, a murine ovarian cancer cell line that has been engineered to express human DSG2. After tumors are established, the following treatment groups will be tested: free Dox, free JO protein, sunflower-Dox formulation, JO-sunflower-Dox formulation, or a noncovalent mixture of JO protein and sunflower-Dox formulation. Tumor volumes and mouse weights will be measured every 2-3 days for the duration of the study. In initial studies, mice will receive a single treatment; if no anti-tumor efficacy is observed, the study may be repeated using a multiple-dose strategy. If promising efficacy is observed, JO-sunflower conjugates bearing a fluorescent

117

label can also be synthesized to analyze biodistribution and intratumoral penetration of the polymers.

Preliminary results

In preliminary studies, the sunflower polymers described in Chapter 3 were conjugated with two different JO-derived protein constructs, named GB3_JO1 and GB7_JO1, by copper-free click chemistry. Anti-JO1 Western blot analysis of the crude reaction mixtures indicated that GB3_JO1-sunflower conjugates were successfully generated and that conjugates were stable under reducing conditions (**A** in Figure 7.1). However, GB7_JO1 conjugation appeared to be unsuccessful (no shift in protein migration at **B** in Figure 7.1); this may be the result of poor labeling of GB7_JO1 protein with the DBCO-PEG$_4$-maleimide crosslinker.
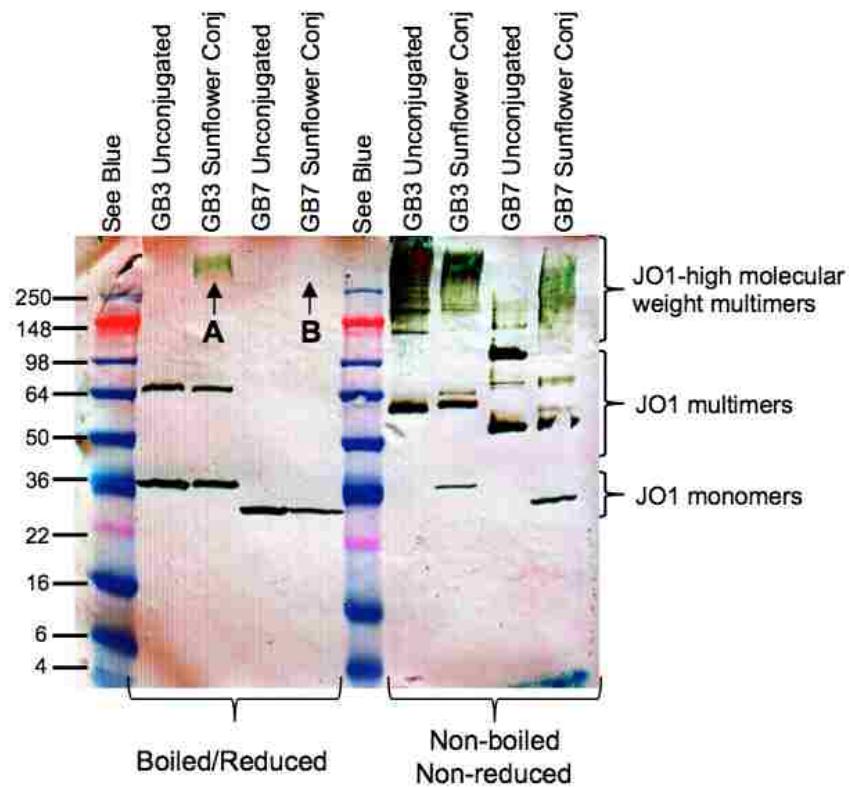

Figure 7.1 Anti-JO1 Western blot of GB3_JO1 and GB7_JO1 proteins before and after click conjugation to sunflower polymers.

118

7.2.2 Sunflower polymers with increased drug loading

Background and significance

In Chapters 3 and 4, we reported the synthesis of sunflower polymers containing ethyl glycinate methacrylamide (EGMA) monomers in the polymer core. The EGMA sidechains were then converted from ethyl esters to hydrazides to allow for direct conjugation of doxorubicin (Dox). However, these polymers suffered from a low level of drug loading (<5 w/w%). In order to increase the drug content of the sunflower polymer formulation, a second generation of sunflower polymers can be synthesized with carboxylic acid groups in the polymer core. These functional groups can be used for electrostatic complexation of Dox (which is cationic at neutral pH).[4,5]

Aim 1: Synthesis of sunflower polymers for electrostatic Dox loading

Modified sunflower polymers will be synthesized and characterized as described in Chapters 3 and 4 with slight variation. The protected monomer *tert*-butyl methacrylate (*t*BMA) will be used in place of the EGMA monomer in the sunflower polymer core. After completing the sunflower polymer synthesis, an excess of trifluoroacetic acid (TFA) will be used to deprotect *t*BMA monomers, yielding carboxylic acid groups (Figure 7.2).[6,7] The final sunflower polymer composition will therefore be P[(HEMA-*sunflower*-P(OEGMA))-*st*-methacrylic acid]. Sunflower polymers will then be drug-loaded by noncovalent complexation with Dox.
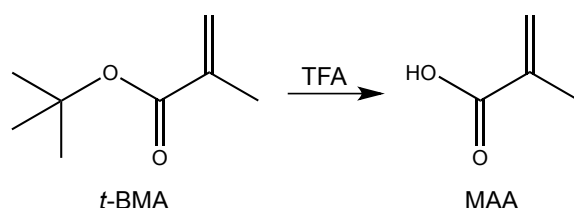
Figure 7.2 Hydrolysis of *tert*-butyl methacrylate (*t*BMA) to methacrylic acid (MAA).

As an alternative strategy to increase the number of sites available for drug loading, each "petal" of the sunflower polymer can be synthesized as a diblock copolymer, such that the block adjacent to the polymer core is composed of *t*BMA while the outer block of the petal is composed of a hydrophilic monomer such as oligoethylene glycol methacrylate (OEGMA) to shield the drug cargo.

Background and significance

One strategy for engineering adenoviral vectors with reduced immunogenicity and altered biodistribution *in vivo* involves conjugating polymers such as polyethylene glycol (PEG) and poly-*N*-(2-hydroxypropyl) methacrylamide (HPMA) to the Ad capsid.[8] Covalent modifications have shown great promise for circumventing the major hurdles to *in vivo* delivery but can also lead to decreased infectivity of the viruses.[9-11] Bioresponsive linkers including reducible disulfide bonds[11,12] and pH-sensitive hydrazone bonds[12] can allow for "re-activation" of the virus upon uncoating. Even so, these bioresponsive polymers are typically conjugated to the Ad capsid via surface amine groups, and it has been suggested that residual linker groups left behind at the site of attachment could increase particle immunogenicity.[13] Indeed, studies with non-responsive PEG modification have demonstrated that the neutralizing antibody response may be directed against the site of PEG conjugation.[14]

Recently, Kreppel and co-workers reported the development of AdHexCys, an Ad5-based vector which was genetically modified to contain a cysteine residue in hypervariable region 5 (HVR5) of the hexon.[13] Using this vector, "traceless" bioresponsive shielding could be achieved using HPMA-based polymers incorporating pyridyl-dithio groups for reaction with the introduced cysteines. As compared to non-responsive shielding based on irreversible maleimide conjugations, bioresponsive shields maintained high transduction efficiency both *in vitro* and *in vivo*. However, *in vivo* data suggested that these polymers provided incomplete shielding against IgM binding.

Covalent modification of vectors using pre-synthesized polymers (the "grafting-to" approach) is limited in its ability to achieve a high density of surface conjugation due to steric hindrance between bulky polymer molecules. In contrast, a "grafting-from" approach, in which polymer chains are grown directly from the Ad capsid, may allow for the generation of a more uniform coating. Although previous results demonstrate that conjugation of large PEG moieties of at least 20 kDa is necessary for efficient Ad detargeting away from hepatocytes *in vivo*,[15] it is possible that a denser layer of shorter polymer chains may afford the same protection.

We propose to synthesize polymer-modified adenoviruses using a grafting-from approach, in which AdHexCys is conjugated with chain transfer agents (CTAs) for

120

reversible addition-fragmentation chain-transfer (RAFT) polymerization. Grafting-from RAFT polymerization using protein-based macroCTAs has been demonstrated previously,[16,17] although it has not yet been applied to biologically active proteins such as viruses. This strategy can potentially enable high-density covalent (yet bioresponsive) coating of adenovirus, thereby maximizing shielding while maintaining the activity of the native virus.

Aim 1: Synthesis and characterization of pOEGMA-Ad vectors

A RAFT CTA containing a pyridyl disulfide functional group, trithiocarbonic acid 1-cyano-1-methyl-3-[2-(pyridin-2-yldisulfanyl)-ethylcarbamoyl]-propyl ester ethyl ester (PyrECT),[18] will be reacted to free thiols on the AdHexCys surface via disulfide exchange. PyrECT conjugation will be performed under physiological conditions as described previously.[18,19]

PyrECT-conjugated AdHexCys will be used as "multi-macroCTAs" in RAFT polymerization to generate polymer-virus conjugates. RAFT polymerization will be conducted in aqueous buffer at 35°C to minimize inactivation of the virus, using OEGMA as the monomer and VA-044 as the initiator. Free ethyl cyanovaleric trithiocarbonate (ECT) will also be included as sacrificial CTA due to the relatively low quantities of virus used. The ratio of monomer to ECT/PyrECT can be varied to produce viruses with different lengths of their polymer shield. This can be used to identify a polymer length that is optimal for downstream virus activity. The final polymer-modified virus, referred to as pOEGMA-Ad, will be purified using an Amicon Ultra Centrifugal Filter device with 100 kDa MWCO (Millipore).

Successful modification of the virus will be assessed by SDS-PAGE. pOEGMA-Ad will be incubated at 100°C for 5 min in reducing or non-reducing Laemmli sample buffer and run on a 10% Mini-PROTEAN TGX gel (Bio-Rad), followed by staining with a SilverQuest Silver Staining Kit (Invitrogen). Under non-reducing conditions, the electrophoretic mobility of hexon proteins is expected to be retarded by covalent polymer modification; the addition of reducing agent should release the polymer and allow for hexon migration into the gel.[11]

The pOEGMA chains grown from sacrificial ECT will be used as a proxy to characterize the polymer chains grown from the virus surface. Free pOEGMA will be separated from virus using an Amicon Ultra Centrifugal Filter device, followed by gel permeation chromatography (GPC) to determine molecular weight and polydispersity.

121

Finally, dynamic light scattering (DLS) will be used to measure pOEGMA-Ad particle size and zeta potential. Relative to naked Ad, pOEGMA modification is expected to produce a slight increase in size and in zeta potential (from negative to near-neutral) depending on the length of polymer chains.[20]

Aim 2: In vitro evaluation of pOEGMA-Ad vectors

CAR-positive HeLa cells will be infected with pOEGMA-Ad encoding GFP or naked Ad-GFP and analyzed for GFP expression as described in Chapter 6. Because Ad5 transduces HeLa cells efficiently via CAR (through interactions with the Ad5 fiber protein), transduction efficiency is expected to be similar between the naked and polymer-modified vectors. However, if polymer modification compromises transduction efficiency, activity should be restored with the addition of a reducing agent such as tris(2-carboxyethyl) phosphine (TCEP).

CAR-negative SKOV3 (human ovarian carcinoma) cells will be infected with pOEGMA-Ad or naked Ad in the absence or presence of a physiological concentration (8 µg/mL) of human FX protein (Haematologic Technologies). The addition of FX is expected to significantly enhance the transduction efficiency of unmodified Ad, as others have shown;[21] however, FX addition should have minimal effect on transduction efficiency of pOEGMA-Ad, as these should be resistant to FX binding.

pOEGMA-Ad and naked Ad will be incubated with serum containing anti-Ad5 neutralizing antibodies for 20 min at 37°C and then used to infect HeLa cells.[20] The addition of NAbs is expected to severely compromise the transduction efficiency of naked Ad5 while pOEGMA-Ad will be resistant to inactivation by NAbs.

Preliminary results

Conditions for aqueous RAFT polymerization of OEGMA were optimized in the absence of virus. Polymerizations were conducted in 0.1 M phosphate buffer (pH 6.5) using ECT as the RAFT CTA and VA-044 as the initiator (I). The initial OEGMA monomer concentration was 0.25 M, and the molar ratios of monomer:CTA:I at the start of polymerization were 150:1:1. Polymerizations were carried out in a 35°C oil bath. A study of the polymerization kinetics indicated that 25% conversion (corresponding to a theoretical polymer molecular weight of approximately 11.3 kDa) was achieved by 1 h (Figure 7.3).
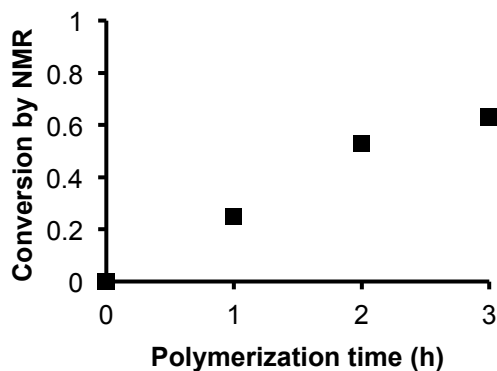
122

Figure 7.3 RAFT kinetics of aqueous, low temperature polymerization of P(OEGMA) as determined by NMR.

References

1. Beyer, I., van Rensburg, R., Strauss, R., Li, Z., Wang, H., Persson, J., Yumul, R., Feng, Q., Song, H., Bartek, J., Fender, P. & Lieber, A. Epithelial junction opener JO-1 improves monoclonal antibody therapy of cancer. *Cancer Res.* **71,** 7080–7090 (2011).
2. Beyer, I., Cao, H., Persson, J., Song, H., Richter, M., Feng, Q., Yumul, R., van Rensburg, R., Li, Z., Berenson, R., Carter, D., Roffler, S., Drescher, C. & Lieber, A. Coadministration of epithelial junction opener JO-1 improves the efficacy and safety of chemotherapeutic drugs. *Clin. Cancer Res.* **18,** 3340–3351 (2012).
3. Wang, H., Beyer, I., Persson, J., Song, H., Li, Z., Richter, M., Cao, H., van Rensburg, R., Yao, X., Hudkins, K., Yumul, R., Zhang, X.-B., Yu, M., Fender, P., Hemminki, A. & Lieber, A. A new human DSG2-transgenic mouse model for studying the tropism and pathology of human adenoviruses. *J. Virol.* **86,** 6286–6302 (2012).
4. Yuan, L., Tang, Q., Yang, D., Zhang, J. Z., Zhang, F. & Hu, J. Preparation of pH-Responsive Mesoporous Silica Nanoparticles and Their Application in Controlled Drug Delivery. *J. Phys. Chem. C* **115,** 9926–9932 (2011).
5. Shi, F., Ding, J., Xiao, C., Zhuang, X., He, C., Chen, L. & Chen, X. Intracellular microenvironment responsive PEGylated polypeptide nanogels with ionizable cores for efficient doxorubicin loading and triggered release. *J. Mater. Chem.* **22,** 14168 (2012).
6. Ma, Q. & Wooley, K. L. The preparation of t-butyl acrylate, methyl acrylate, and styrene block copolymers by atom transfer radical polymerization: Precursors to amphiphilic and hydrophilic block copolymers and conversion to complex nanostructured materials. *J. Polym. Sci. A Polym. Chem.* **38,** 4805–4820 (2000).
7. Tian, Y., Bromberg, L., Lin, S. N., Alan Hatton, T. & Tam, K. C. Complexation and release of doxorubicin from its complexes with pluronic P85-b-poly(acrylic acid) block copolymers. *J. Control. Release* **121,** 137–145 (2007).
8. Kreppel, F. & Kochanek, S. Modification of adenovirus gene transfer vectors with synthetic polymers: a scientific review and technical guide. *Mol. Ther.* **16,** 16–29 (2008).

9. Mok, H., Palmer, D. J., Ng, P. & Barry, M. A. Evaluation of polyethylene glycol modification of first-generation and helper-dependent adenoviral vectors to reduce innate immune responses. *Mol. Ther.* **11,** 66–79 (2005).

10. Wortmann, A., Vöhringer, S., Engler, T., Corjon, S., Schirmbeck, R., Reimann, J., Kochanek, S. & Kreppel, F. Fully detargeted polyethylene glycol-coated adenovirus vectors are potent genetic vaccines and escape from pre-existing anti-adenovirus antibodies. *Mol. Ther.* **16,** 154–162 (2008).

11. Subr, V., Kostka, L., Selby-Milic, T., Fisher, K. D., Ulbrich, K., Seymour, L. W. & Carlisle, R. C. Coating of adenovirus type 5 with polymers containing quaternary amines prevents binding to blood components. *J Control Release* **135,** 152–158 (2009).

12. Espenlaub, S., Corjon, S., Engler, T., Fella, C., Ogris, M., Wagner, E., Kochanek, S. & Kreppel, F. Capsomer-specific fluorescent labeling of adenoviral vector particles allows for detailed analysis of intracellular particle trafficking and the performance of bioresponsive bonds for vector capsid modifications. *Hum. Gene Ther.* **21,** 1155–1167 (2010).

13. Prill, J.-M., Subr, V., Pasquarelli, N., Engler, T., Hoffmeister, A., Kochanek, S., Ulbrich, K. & Kreppel, F. Traceless Bioresponsive Shielding of Adenovirus Hexon with HPMA Copolymers Maintains Transduction Capacity In Vitro and In Vivo. *PLoS ONE* **9,** e82716 (2014).

14. Croyle, M. A., Chirmule, N., Zhang, Y. & Wilson, J. M. 'Stealth' adenoviruses blunt cell-mediated and humoral immune responses against the virus and allow for significant gene expression upon readministration in the lung. *J. Virol.* **75,** 4792–4801 (2001).

15. Prill, J.-M., Espenlaub, S., Samen, U., Engler, T., Schmidt, E., Vetrini, F., Rosewell, A., Grove, N., Palmer, D., Ng, P., Kochanek, S. & Kreppel, F. Modifications of adenovirus hexon allow for either hepatocyte detargeting or targeting with potential evasion from Kupffer cells. *Mol. Ther.* **19,** 83–92 (2011).

16. Boyer, C., Bulmus, V., Liu, J., Davis, T. P., Stenzel, M. H. & Barner-Kowollik, C. Well-defined protein-polymer conjugates via in situ RAFT polymerization. *J. Am. Chem. Soc.* **129,** 7145–7154 (2007).

17. Li, H., Li, M., Yu, X., Bapat, A. P. & Sumerlin, B. S. Block copolymer conjugates prepared by sequentially grafting from proteins via RAFT. *Polym Chem* (2011).

18. Duvall, C. L., Convertine, A. J., Benoit, D. S. W., Hoffman, A. S. & Stayton, P. S. Intracellular delivery of a proapoptotic peptide via conjugation to a RAFT synthesized endosomolytic polymer. *Mol. Pharm.* **7,** 468–476 (2010).

19. Schellinger, J. G., Pahang, J. A., Johnson, R. N., Chu, D. S., Sellers, D. L., Maris, D. O., Convertine, A. J., Stayton, P. S., Horner, P. J. & Pun, S. H. Melittin-grafted HPMA-Oligolysine Based Copolymers for Improved Gene Delivery. *Biomaterials* **34,** 2318–2326 (2013).

20. Wang, C.-H. K., Chan, L. W., Johnson, R. N., Chu, D. S. H., Shi, J., Schellinger, J. G., Lieber, A. & Pun, S. H. The transduction of Coxsackie and Adenovirus Receptor-negative cells and protection against neutralizing antibodies by HPMA-co-oligolysine copolymer-coated adenovirus. *Biomaterials* **32,** 9536–9545 (2011).

21. Alba, R., Bradshaw, A. C., Parker, A. L., Bhella, D., Waddington, S. N., Nicklin, S. A., van Rooijen, N., Custers, J., Goudsmit, J., Barouch, D. H., McVey, J. H. & Baker, A. H. Identification of coagulation factor (F)X binding sites on the adenovirus serotype 5 hexon: effect of mutagenesis on FX interactions and gene transfer. *Blood* **114,** 965–971 (2009).

124

125

APPENDIX

MATLAB code for AuNP penetration analysis

Sample code to calculate penetration distances for a collection of thresholded brightfield and fluorescence image pairs:

```matlab
% mouse ID: 583 (JO/35 nm)
filepath =
'\\studentfile.student.bioeng.washington.edu\usr$\cewang\Desktop\NP
analysis\Thresholded\JO-35\583'; % path to folder containing pairs of
thresholded brightfield and fluorescence images (e.g., 1B.tif, 1F.tif,
2B.tif, 2F.tif,...)
savepath =
'\\studentfile.student.bioeng.washington.edu\usr$\cewang\Desktop\NP
analysis\Output\583_'; % path for output

distance_data_aggregate = [];
N_aggregate = [];

cd(filepath);
filelist = dir;

for ii = 3:length(filelist)
    if strcmp(filelist(ii).name(end-4:end),'B.tif')
        % import a pair of brightfield and fluorescence images
        bf = imread(filelist(ii).name);
        fl = imread(strcat(filelist(ii).name(1:end-5),'F.tif'));
    else
        continue
    end

    % find all regions of fluorescence (thresholded as white on black)
    [fl_L ~] = bwlabel(fl);
    fl_stats = regionprops(fl_L);
    for zz = 1:length(fl_stats)
        object_size = fl_stats(zz).Area;
        % remove fluorescent regions with areas smaller than 9 pixels
        % (assumed to be noise)
        if object_size<=9
            [r,c] = find(fl_L==zz);
            fl_L(r,c)=0;
        end
    end
    fl_L(fl_L>0)=255;
    fl = uint8(fl_L);

    % obtain coordinates for all fluorescent pixels
    [fl_y fl_x] = find(fl > 0);

    % find all AuNPs in brightfield image (thresholded as white on black)
    [L N] = bwlabel(bf);
```

```matlab
    stats = regionprops(L);
    centroids_x = [];
    centroids_y = [];
    % calculate centroid of each AuNP
    for jj = 1:length(stats)
        centroids_x = [centroids_x stats(jj).Centroid(1)];
        centroids_y = [centroids_y stats(jj).Centroid(2)];
    end

    centroids_x_length = length(centroids_x);
    fl_x_length = length(fl_x);
    centroids_x_tiled = repmat(centroids_x,fl_x_length,1);
    fl_x_tiled = repmat(fl_x,1,centroids_x_length);

    centroids_y_length = length(centroids_y);
    fl_y_length = length(fl_y);
    centroids_y_tiled = repmat(centroids_y,fl_y_length,1);
    fl_y_tiled = repmat(fl_y,1,centroids_y_length);

    % calculate minimum pixel distance from each AuNP centroid to a
    % fluorescent pixel
    distances = sqrt((centroids_x_tiled-fl_x_tiled).^2 + ...
        (centroids_y_tiled-fl_y_tiled).^2);
    [distance_data,index]=min(distances);

    % overlay brightfield/fluorescence images
    figure
    im = cat(3,zeros(size(bf)),fl, bf);
    imshow(im);
    hold on
    % draw lines to indicate penetration distances
    for jj = 1:length(centroids_x)
        plot([centroids_x(jj),fl_x(index(jj))], ...
            [centroids_y(jj),fl_y(index(jj))],'r')
    end
    title(filelist(ii).name);
    savefig(strcat(savepath,filelist(ii).name(1:end-5)));

    % save distances and # of nanoparticles for this image pair to data file
    save(strcat(savepath,filelist(ii).name(1:end-5)),'N','distance_data');
    pause(2);
    hold off
    close

    distance_data_aggregate = [distance_data_aggregate distance_data];
    N_aggregate = [N_aggregate N];
end

% aggregate distances and # of nanoparticles for all images analyzed
save(strcat(savepath,'aggregate'),'distance_data_aggregate','N_aggregate');
```

127

www.manaraa.com

Sample code to generate histograms and statistics for penetration distance data:

```matlab
filepath = ...
'\\studentfile.student.bioeng.washington.edu\usr$\cewang\Desktop\NP
analysis\Output'; % path to folder containing aggregated distance data
cd(filepath);

% load distance data and convert to microns according to an image scale of
% 0.15 um/pixel
dat583 = load('583_aggregate.mat');
dist583 = dat583.distance_data_aggregate .* 0.15;
N583 = dat583.N_aggregate;

dat593 = load('593_aggregate.mat');
dist593 = dat593.distance_data_aggregate .* 0.15;
N593 = dat593.N_aggregate;

% remove distances <= 5 um
dist583_2 = dist583(find(dist583>5));
dist593_2 = dist593(find(dist593>5));


% plot histograms of penetration distances
figure
hist583_2 = histogram(dist583_2, 'Normalization', 'probability');
hist583_2.BinWidth = 5;
xlim([5 135])

hold on
hist593_2 = histogram(dist593_2, 'Normalization', 'probability', ...
    'BinEdges', hist583_2.BinEdges);

legend('583: JO-4 / 35 nm','593: Untreated / 35 nm')
xlabel('Penetration distance (\mum)')
ylabel('Fraction')


% return statistics on number of NPs analyzed
fprintf('Total nanoparticles analyzed\n\n')
fprintf('583: ')
disp(sum(N583))

fprintf('593: ')
disp(sum(N593))


% return statistics on average number of nanoparticles per image
fprintf('\n\nAverage and SD of nanoparticles per image\n\n')
fprintf('583: ')
disp(mean(N583))
disp(std(N583))

fprintf('593: ')
disp(mean(N593))
```

```matlab
disp(std(N593))


% return statistics on percent of NPs <= 5 um from blood vessel
fprintf('\n\nFraction of NPs within 5 um of blood vessel\n\n')
fprintf('583: ')
disp(1-(length(dist583_2)/length(dist583)))

fprintf('593: ')
disp(1-(length(dist593_2)/length(dist593)))


% return statistics on median penetration distance
fprintf('\n\nMedian penetration distance in um (excluding values below 5 um)
\n\n')
fprintf('583: ')
disp(median(dist583_2))

fprintf('593: ')
disp(median(dist593_2))
```